

# Design and Development of the Class E RF Power Amplifier Prototype by Using a Power MOSFET

Tiaotiao Xie



University of Kansas  
2335 Irving Hill Road  
Lawrence, KS 66045-7612  
<http://crexis.ku.edu>

Technical Report  
CReSIS TR 129

July 23, 2007

*This work was supported by a grant from the  
National Science Foundation  
(#ANT-0424589).*

## **Acknowledgement**

I would like to thank Dr. Prasad Gogineni for giving me the opportunities to work on this project, which I did not complete for my senior design at KU in 2005, to learn what I did not do right and what could be done better in order to make it work. I am deeply indebted to professor for it and for the opportunities to learn from him the good work ethic, dedication, commitment, and perseverance necessary not only for researcher but also for success in anything I will be doing.

I am extremely thankful to Dr. Fernando Rodriguez-Morales who took over the mentor role of me from Professor Gogineni when he got very busy with the running of CReSIS. I very appreciate Dr. Rodriguez-Morales' instruction and technical help in my design, especially teaching me how to do hardware testing at the laboratory. I learned the good quality of patience and meticulousness in research from him.

I would like to extend my sincere and utmost gratitude to Dr. Chris Allen and Dr. David Braaten for being the members of my defense committee. I acquired considerable amount of knowledge and training for my degrees from Dr. Allen both for my undergraduate and graduate studies at KU. Thus, I very appreciate Dr. Allen for it. My education with him is very pleasant and memorable. I thank Dr. Braaten for taking time to edit my thesis.

In addition, I would like to acknowledge the help received from CReSIS staff. Special thanks to Mr. Dennis Sundermeyer for his help in the milling process,

making the heat sinks and other mechanical issues; to Mr. Tory Akins for helping me with the questions about Altium Designer software; to Ms. Keron Hopkins for taking care of my payroll and purchase orders; to Ms. Tommie Cassen and Ms. Ferdouz Vuilliomenet Cochran for help in processing purchase orders whenever Ms. Hopkins is not available and for getting professors' signatures for my important school paperwork and for help in other daily life issues; to Dr. Kelly Mason and Dr. Gary Webber for significant amount of help in my research trip to Australia last summer. They made my life there problem-free, very pleasant and memorable; to Mr. Steve Ingalls who taught me how to be competent for the job and how to work hard; and last to Mr. Thorbjorn Axelsson and all other people at CReSIS IT Help Desk. Without the help and support from you guys, I just do not know how to get half of my thesis work done by using the required software.

I also would like use this opportunity to express my gratitude to every friend of mine at CReSIS, who made my time and life there very enjoyable and memorable.

This work would not have been possible without the endless love, encouragement and support from my parents Xiaoping Chen and Qingmu Xie, my twin sister Yaoyao and my husband Andy Wang.

I thank my friends at KU and everyone in CReSIS for making my stay here a memorable one.

## **Abstract**

The continuous rise of global sea level demands better and more accurate models of the ice sheets and glaciers in polar regions for better understanding and prediction so that we can minimize the resulting damages to the world. This requires more sophisticated and miniaturized systems, such as radar systems, so that they can be carried to perform tasks without human attendance in the dangerous areas. A class E RF power amplifier prototype with the physical size of 2.9 in x 1.6 in operating at 150 MHz was designed and developed as the first step of the miniaturization process of radar systems developed at the Center for Remote Sensing of Ice Sheets at the University of Kansas. Simulated results and laboratory measurements were used to document the prototype's performance. It employs the single-ended configuration with MOSFET transistor MRF134. The drain DC supply used is 22.5 V and the gate bias is 3.5 V. The highest drain efficiency observed at the lab is 69.55% with 8.379 dB power gain. When the drain efficiency drops to 65.31%, the power gain obtained is 10.09 dB.

## Table of Contents

<b>CHAPTER 1 .....</b>	<b>1</b>
<b>INTRODUCTION.....</b>	<b>1</b>
1.1 MOTIVATIONS .....	1
1.2 REASONS FOR NEED OF HIGH EFFICIENCY POWER AMPLIFIERS .....	2
1.3 REASONS FOR CLASS E POWER AMPLIFIERS .....	3
1.3.1 PA Classifications.....	3
1.3.2 Transconductance Amplifiers for Linearity.....	4
1.3.3 Switch Mode Operation for High Efficiency.....	6
1.3.4 Class E and Its Advantages over other Classes of Power Amplifiers.....	7
1.4 ORGANIZATION .....	8
<b>CHAPTER 2 .....</b>	<b>9</b>
<b>BASIC CLASS E IDEAS .....</b>	<b>9</b>
2.1 COMMON CLASS E RF POWRE AMPLIFIER CONFIGURATIONS .....	9
2.2 OPTIMUM AND SUBOPTIMUM CLASS E OPERATIONS .....	10
2.3 BASIC CIRCUIT SCHEMATIC .....	15
2.4 CLASS E CIRCUIT COMPOSITION AND FUNCTION.....	15
2.4.1 Driver.....	15
2.4.2 Input Matching.....	17
2.4.3 Gate Bias.....	17
2.4.4 Switch.....	18
2.4.5 DC Supply.....	19
2.4.6 RF Chocks.....	19
2.4.7 Load Network.....	19
2.4.8 Load.....	25
<b>CHAPTER 3 .....</b>	<b>27</b>
<b>CLASS E PA CIRCUIT DESIGN ANALYSIS WITH LINEAR DRAIN SHUNT OUTPUT CAPACITANCE.....</b>	<b>27</b>
3.1 LINEAR DESIGN ANALYSIS FOR CLASS E PA OPERATIONS.....	27
3.2 CIRCUIT DESIGN BY USING LINEAR METHOD .....	30
3.2.1 General Circuit Parameter Selections for Theoretical Design in ADS.....	30
3.2.2 Performance Evaluating Parameters for Class E RF Power Amplifiers....	40
3.2.3 ADS Simulation for 17 Cases with Calculated Circuit Elements Using Linear Design Method.....	43
3.2.4 Design Optimization.....	46
3.2.5 Results from Optimization Using Linear Method.....	50

<b>CHAPTER 4</b> .....	<b>54</b>
<b>CLASS E PA CIRCUIT DESIGN ANALYSIS WITH NONLINEAR DRAIN SHUNT OUTPUT CAPACITANCE</b> .....	<b>54</b>
4.1 ANALYSIS EQUATIONS FOR CLASS E NONLINEAR DESIGN USING MRF134 .....	54
4.2 CIRCUIT DESIGN BY USING NONLINEAR METHOD .....	60
4.3 OPTIMIZATION FOR 15 CAES BY USING NONLINEAR METHOD .....	62
<b>CHAPTER 5</b> .....	<b>66</b>
<b>DESIGN IMPLEMENTATION AND TESTING</b> .....	<b>66</b>
5.1 COMPONENT SELECTION AND PCB IMPLEMETATION.....	66
5.2 EXPERIMENTAL SETTING FOR TESTING.....	68
5.3 INITIAL TESTING .....	71
5.4 ESR OF INDUCTORS AND ITS SIGNIFICANCE IN CLASS E RF PA DESIGNS .....	73
5.5 CHANGES IN TESTING AND NEW RESULTS .....	77
5.6 POWER LOSS MECHANISM ANALYSIS.....	83
5.6.1 Losses from Transistor.....	84
5.6.2 Losses from Circuit Lumped Elements.....	86
5.6.3 Losses from Unwanted Harmonics.....	88
5.6.4 Losses from DC Power Supply.....	89
<b>CHAPTER 6</b> .....	<b>90</b>
<b>CONCLUSION</b> .....	<b>90</b>
6.1 CONCLUSION .....	90
6.2 FUTURE WORK.....	90
<b>BIBLIOGRAPHY</b> .....	<b>92</b>
<b>APPENDIX</b> .....	<b>94</b>
A.1 DRAIN CURRENT & VOLTAGE WAVEFORMS OF 17 LINEAR DESIGNS IN ADS BEFORE CIRCUIT OPTIMIZATION .....	94
A.2 DRAIN CURRENT & VOLTAGE WAVEFORMS OF 17 LINEAR DESIGNS IN ADS AFTER CIRCUIT OPTIMIZATION .....	96
A.3 DRAIN CURRENT & VOLTAGE WAVEFORMS OF 15 NONLINEAR DESIGNS IN ADS AFTER CIRCUTI OPTIMIZATION .....	98
A.4 MATLAB CODES FOR CIRCUIT ELEMENT CALCULATIONS USING LINEAR METHOD.....	100
A.5 MATLAB CODES FOR CIRCUIT ELEMENT CALCULATIONS USING ONLINEAR METHOD.....	101

## List of Figures

Figure 1.1 Waveforms for Ideal PAs: (a) Class A, (b) Class B, (c) Class AB and (d) Class C [3].....	6
Figure 2.1 Common Configurations of Power Amplifiers: (a) Single-ended; (b) Complementary (aka, push-pull).....	9
Figure 2.2 The Circuit Schematic of Class E PA Composed of a Single-Pole Switch and A Load Network Developed by Mr. Nathan Sokal [4].....	10
Figure 2.3 Ideal Switch (or Drain) Voltage and Current Waveforms in Class E to Achieve 100 % Efficiency [4].....	11
Figure 2.4 Drain Voltage and Current Waveforms of a Practical Class E PA.....	14
Figure 2.5 Block Diagram of Class E RF Power Amplifier Prototype Proposed..	15
Figure 2.6 Waveform of an Ideal Driver.....	16
Figure 2.7 Waveform of a Trapezoidal Driver.....	16
Figure 2.8 Waveform for a Sinusoidal Driver.....	16
Figure 2.9 Major Current Flows in a Class E PA when Switch is ON.....	20
Figure 2.10 Major Current Flows in a Class E PA when Switch is OFF.....	21
Figure 2.11 Schematic of Load Network when Switch is ON.....	23
Figure 2.12 Schematic of Load Network when Switch is OFF.....	23
Figure 2.13 L-Section Matching Networks for Two Resistive Impedances: (a) L-Section to Match a Low Resistance to a High Resistance; (b) L-Section to Match a High Resistance to a Low Resistance.....	25
Figure 3.1 Circuit Schematic of Class E RF PA Using Linear Design Analysis Method.....	29
Figure 3.2 Configuration of Class A RF Power Amplifier Used in Thesis Work..	31
Figure 3.3 Preamplifier for 10 MHz Design.....	32
Figure 3.4 $V_{DS}$ vs. $I_{DS}$ of MRF134 for $V_{GS}$ from 2.0 V to 4.6 V.....	34
Figure 3.5 DC-IV Curves for an Ideal MOSFET.....	35
Figure 3.6 Gate Voltage Swing for 10 MHz Class E Linear Design Using MRF134.....	36
Figure 3.7 Measuring $V_{input}$ & $I_{input}$ in ADS.....	38
Figure 3.8 Matching Networks: (a) Input Matching for 10 MHz Case; (b) Output Matching for 150 MHz Case.....	47
Figure 3.9 Tank Circuit for 2 <sup>nd</sup> and 3 <sup>rd</sup> HarmonicSuppressions with Output Matching and Load Resistance for 150 MHz Case.....	48
Figure 3.10 Tuning Methods to Achieve Optimum Drain Voltage Waveform.....	49
Figure 3.11 Drain Voltage Waveform of 100 kHz Case.....	49
Figure 3.12 Drain Current and Voltage Waveforms in Time Domain for: (a) 10 MHz Case after Optimization; (b) 150 MHz Case after Optimization.....	51
Figure 3.13 Complete 150 MHz Design in Simulation Using Linear Analysis....	53
Figure 4.1 Large Signal Equivalent Circuit of MOSFET Transistors.....	56

Figure 4.2 Drain Current and Voltage Waveforms for Nonlinear Designs after Circuit Optimization: (a) 10 MHz; (b) 150 MHz.....	63
Figure 4.3 Load Current and Voltage Waveforms for: (a) 10 MHz Linear; (b) 10 MHz Nonlinear; (c) 150 MHz Linear; (d) 150 MHz Nonlinear.....	64
Figure 5.1 PCB Layout for Class A RF Power Amplifier Design.....	67
Figure 5.2 PCB Layout for Class E RF Power Amplifier Design at 10 MHz.....	67
Figure 5.3 PCB Layout for Class E RF Power Amplifier Design at 150 MHz.....	67
Figure 5.4 PCB Board for Class A PA.....	68
Figure 5.5 PCB Board for 150 MHz Class E RF PA.....	68
Figure 5.6 Block Diagram of Experimental Setting.....	69
Figure 5.7 Actual Lab Experimental Setting.....	70
Figure 5.8 Lumped-Element Models of CoilCraft RF Inductors for Series other than 1812FS, 0805LS, 0603LS and 0402AF.....	73
Figure 5.9 Lumped-Element Models of Coilcraft RF Inductors for Series 1812FS, 0805LS, 0603LS and 0402AF.....	74
Figure 5.10 S(1,1) of 100 nH RF Inductor in 1008HQ Series of Coilcraft.....	75
Figure 5.11 S(1,1) of 15 $\mu$ H RF Inductor in 1812FS Series of Coilcraft.....	75
Figure 5.12 150 MHz Class A RF Preamplifier.....	78
Figure 5.13 Linear 150 MHz Design Resulting in Best Measurements.....	79
Figure 5.14 Drain Current and Voltage Waveforms of Best Design for $P_{in} = 0.44$ W.....	81
Figure 5.15 Output Voltage Waveform of 20 dB 50 W Attenuator for Best Design at 150 MHz.....	81
Figure 5.16 Drain Voltage Waveform for Best Design after Attenuation at 150 MHz.....	82
Figure 5.17 Simulated Drain Voltage Waveform for Best Design at 150 MHz....	82
Figure 5.18 Output Capacitance and On Resistance of a MOSFET Transistor....	85
Figure A.1.1 Drain Current & Voltage Waveforms of Linear Designs before Circuit Optimization for $f_o$ Values of 100 kHz, 1 MHz, 10 MHz, 20 MHz, 30 MHz, 40 MHz, 50 MHz and 60 MHz.....	94
Figure A.1.2 Drain Current & Voltage Waveforms of Linear Designs before Circuit Optimization for $f_o$ Values of 70 MHz, 80 MHz, 90 MHz, 100 MHz, 110 MHz, 120 MHz, 130 MHz and 140 MHz.....	95
Figure A.1.3 Drain Current & Voltage Waveforms of Linear Design before Circuit Optimization for $f_o = 150$ MHz.....	95
Figure A.2.1 Drain Current & Voltage Waveforms of Linear Designs after Circuit Optimization for $f_o$ Values of 100 kHz, 1 MHz, 10 MHz, 20 MHz, 30 MHz, 40 MHz, 50 MHz and 60 MHz.....	96
Figure A.2.2 Drain Current & Voltage Waveforms of Linear Designs after Circuit Optimization for $f_o$ Values of 70 MHz, 80 MHz, 90 MHz, 100 MHz, 110 MHz, 120 MHz, 130 MHz and 140 MHz.....	97

Figure A.2.3 Drain Current & Voltage Waveforms of Linear Design after Circuit Optimization for $f_0 = 150$ MHz.....	97
Figure A.3.1 Drain Current & Voltage Waveforms of Nonlinear Designs after Circuit Optimization for $f_0$ Values of 10 MHz, 20 MHz, 30 MHz, 40 MHz, 50 MHz, 60 MHz, 70 MHz and 80 MHz.....	98
Figure A.3.2 Drain Current & Voltage Waveforms of Nonlinear Designs after Circuit Optimization for $f_0$ Values of 90 MHz, 100 MHz, 110 MHz, 120 MHz, 130 MHz and 140 MHz.....	99
Figure A.3.3 Drain Current & Voltage Waveforms of Nonlinear Designs after Circuit Optimization for $f_0 = 150$ MHz.....	99

## List of Tables

Table 1.1 Summary of Transconductance PA's Characteristics.....	6
Table 2.1 FET Transistor Selection [7].....	18
Table 3.1 Calculation Results of 17 Cases Using linear Design Analysis.....	44
Table 3.2 Simulation Results of 17 Cases Using Linear Design Analysis.....	45
Table 3.3 Optimization Results of 17 Cases Using Linear Design Analysis in ADS Simulations.....	52
Table 4.1 Calculation Results of 15 Cases Using Nonlinear Analysis.....	61
Table 4.2 Optimization Results of 15 Cases Using Nonlinear Analysis in ADS Simulations.....	65
Table 5.1 Initial Testing Conditions.....	71
Table 5.2 Measurements and Results of Initial Testing.....	71
Table 5.3 Simulation Results of Initial Testing Cases with Real Inductor.....	72
Table 5.4 ESRs of 100 nH RF Inductor in 1008HQ Series of Coilcraft.....	76
Table 5.5 ESRs of 15 $\mu$ H RF Inductor in 1812FS Series of Coilcraft.....	76
Table 5.6 Testing Results of 150 MHz Class A Preamplifier in Figure 5.12.....	78
Table 5.7 Inductor Types and $DCR_{max}$ in Circuit of Figure 5.13.....	79
Table 5.8 Best Testing Results Associated with Design in Figure 5.13.....	80
Table 5.9 Simulation Results of Best Design in Lab.....	80

## **Chapter 1: Introduction**

### **1.1 Motivations**

Currently, whether the global warming is a natural phenomenon of the planet we are living or it is mainly caused by human activities is under furious debate. However, it is indisputable that global sea level is rising, which is primarily resulted from the melting of ice sheets and glaciers at the polar region. How well we can model the rapid changes of these vast ice caps determines how accurately we can predict the global sea level rising, which in turn can affect the lives of a considerable amount of people living in costal and its related areas. It is the mission of the Center for Remote Sensing of Ice Sheets (CReSIS) to “develop new technologies and computer models to measure and predict the response of sea level change to the mass balance of ice sheets in Greenland and Antarctica”, so that to contribute into the protection of the safety and the well being of people in this world.

The science and technology teams at CReSIS are working hard and collaboratively to design and develop sophisticated sensors, such as seismic sensors and radars, and their carriers, such as the unpiloted airborne vehicles (UAVs) and rovers, as well as better ice sheet models to understand, analyze and synthesize the current observations and measurements from polar regions.

The new sensors being invented here not only should provide better resolution and deeper sounding of the ice sheet; most importantly, they should be much

smaller in size in order to be carried by UAVs and rovers, which have strict constraint for their load size. Thus, miniaturization of sensors, especially radar systems, is essential in achieving CReSIS's mission. By doing so, every component of a radar system, such as power amplifiers, D.C. supplies, receivers and transmitters, must be miniaturized one by one.

### **1.2 Reasons for Need of High Efficiency Power Amplifiers**

High efficiency power amplifiers are needed when the DC power supply is limited, such as the battery-operated hand-held phones in contemporary communication systems, the space-based systems at which the continuous large supply is excessively expensive and not practical, and those at which the weights and sizes are significant design constraints so that those big and powerful supplies are not applicable; for example, the radar system being designed at CReSIS that will be carried by the UAV for the field experiment in the near future. All of these systems require their PAs to perform their jobs much more efficiently so that by using a small power supply, less power will be wasted in the amplification process; in other words, more power can be used.

In addition, DC power supplies are expensive. More efficient PAs require less DC supply to generate the same amount of output power than less efficient PAs. On the other hand, less DC supply implies smaller supply size needed.

Regarding power amplifiers themselves, less efficient PAs will generate more heat during amplifying. If the heat can not be totally absorbed by the associated

heat sink, it can deviate or degrade the device performance, and even damage the device. Furthermore, in those size-limited systems, sufficient cooling carried out by heat sink is not practical.

One of the ultimate technology goals of CReSIS is to miniaturize the radar systems so that by 2010, they can be in the size of a chip. The current systems designed and used in CReSIS usually weigh around 200 lb and up to 2 ft<sup>3</sup> in size. Thus, a prototype design of a high efficiency RF power amplifier no bigger than 10in X 10in X 4in is required as the first step in the system miniaturization process because it demands less expensive and smaller size DC supplies, guaranteeing better performances and occupying smaller space as well.

### **1.3 Reasons for Class E Power Amplifiers**

#### **1.3.1 PA Classifications:**

Currently, there are Class A, B, AB, C, D, E, F, and so on, power amplifiers. The classification is determined by the amplifier's DC bias condition, conduction angle, output terminations at fundamental and harmonics. This classification is ambiguous because many times there is no clear boundary to define the class of a power amplifier as there is not an abrupt change in the mode of operation; sometimes, a PA can fall into two or more classes, and other times, a class operation can be changed to another one when the operation conditions vary.

Dr. Sanggeun Jeon proposed a new classification of PA operations in his Ph.D. dissertation [1]. He uses two broader categories to classify power amplifiers:

transconductance amplifiers with Class A, B, AB and C, and switching mode amplifiers including Class D, E and F, based on the property that either a PA is linear or it is nonlinear.

### **1.3.2 Transconductance Amplifiers for Linearity**

Transconductance amplifiers are linear operations that can correctly produce the amplitude and phase of the input signal at the output terminal. In other words, the reproduced amplitude is linearly propositional to that of the input and the phase difference between input and output signal waveforms remain the same during the amplification process.

Among the transconductance amplifier family, Class A is the most linear mode of operation, Class B the second, Class AB the next, and Class C the least linear. The linearity degrades for the sake of improving efficiency. Below is the brief description for each class of transconductance amplifiers [2].

#### **Class A**

Class A power amplifiers show the relatively highest output power, gain and linearity than any other class mode of operation. On the contrary, its efficiency is the worst. It is fully conductive as the transistor is never turned off. Thus, it has a  $360^\circ$  conduction angle to allow for the always coexistence of drain/collector voltage and current, resulting in huge power dissipation in the transistor.

#### **Class B**

Class B PAs have less transistor power dissipation than Class A because its

gate/base bias is adjusted for drain/collector current cutoff. Therefore, it is conductive a half time in each RF period with  $180^\circ$  conduction angle. Power amplifiers in this class suffer from the crossover distortion, which happens when the input signal level is low.

### **Class AB**

Class AB PAs have the advantages of both class A and B PAs. It is more linear than Class B and more efficiency than Class A. In addition, Class AB solves the crossover distortion associated with Class B. Its conduction angle is more than  $180^\circ$ .

### **Class C**

Class C PAs are less well defined but they are characterized by their conduction angle of less than  $180^\circ$ . They are still linear, but not as linear as the above three classes. There is usually no bias voltage provided except by the drive signal, and the highest efficiency Class C PAs can reach is 90%, ideally. They are the most efficient class mode of operation among the transconductance PAs described.

### **Characteristic Summaries**

The characteristics of the Class A, B, AB, and C power amplifiers are summarized in the Table 1.1, followed by the plots for the drain current and voltage waveforms for the ideal PAs using MOSFET transistors.

**Table 1.1: Summary of Transconductance PAs' Characteristics**

Operation Class Mode	Conduction Angle	Maximum Efficiency	Usual Circuit Topology
A	$360^\circ$	$<50\%$	Single-Ended
B	$180^\circ$	$<78.5\%$	Push-Pull
AB	$>180^\circ$	$<78.5\%$	Push-Pull
C	$<180^\circ$	$<90\%$	Single-Ended

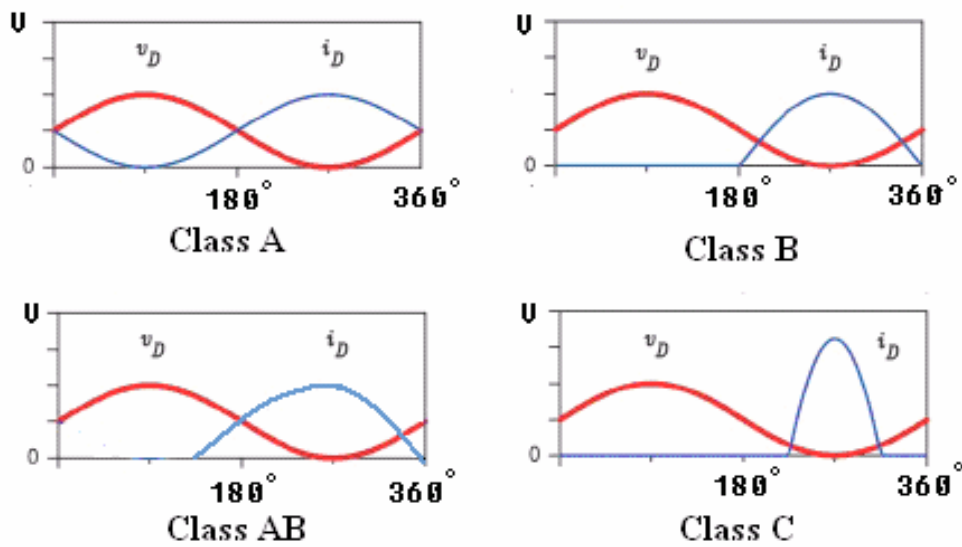


**Figure 1.1: Waveforms for Ideal PAs : (a) Class A, (b) Class B, (c) Class AB and (d) Class C [3]**

In Figure 1.1,  $v_D$  and  $i_D$  are the drain voltage and current if a MOS transistor is used;  $v_C$  and  $i_C$  will be substituted for the design with BJT transistors.

### 1.3.3 Switch Mode Operation for High Efficiency

Comparing to the conventional linear classes operation of PA, the amplifiers with displacement of peak drain/collector voltage and current can achieve a much higher efficiency. This phenomenon only happens when the transistor behaves as an ideal switch which only allows either current or voltage peak to occur at one

time. In such switching mode, power dissipation in the transistor can be totally eliminated, and hence, achieving 100% efficiency, theoretically.

Unlike the linear PAs, switching mode operation requires that the output voltage and current of the amplifier to be the transient response of a specially designed output matching network to the time variant switch and a constant DC power supply. In addition, switching implies that the output current and voltage are discontinuous so that they have many higher order harmonic components. Thus, a proper filtering scheme must be used to suppress the harmonics in order to obtain high efficiency since they also dissipate power.

#### **1.3.4 Class E and Its Advantages over other Classes of Power Amplifiers**

Class E is a switching mode power amplifier. The concept was first proposed and explored by Dr. Gerald Ewig in 1964 in his famous PhD dissertation “High-Efficiency Radio-Frequency Power Amplifiers”. Later, Nathan and Alan Sokal further developed the concept in 1975; Alan Sokal even patented it through the article “Class-E New Class of High-Efficiency Tuned Single-ended Switching Power Amplifiers”.

The most important advantage of class E power amplifiers is their ability to provide high efficiency. Contrary to linear mode classes, class E can operate with power loss smaller by a factor of 2.3 [4] at the same operating frequency to provide the same amount of output power by using the same transistor. Then, class E PA are relatively easy to design with a small size, light weight and relative

intolerance to circuit variation, which fulfill the requirement for system miniaturization. Furthermore, class E power amplifier can be designed to operate either at a specific frequency, i.e., narrow-band operation, or at a wide frequency band, depending on the demand.

Currently, the design for class E operation up to Ku band has been accomplished and engineers are struggling to push this up frequency limit even higher.

#### **1.4 Organization**

This thesis is organized into six chapters. The fundamental concepts and the need for the development of a Class E RF power amplifier prototype have been discussed in this Chapter. Chapter 2 presents the basic Class E amplifier design ideas, including its operation theories, circuit composition and functions. The next two chapters, Chapter 3 and 4 address two design methods, linear and nonlinear with respect to the output capacitance of the transistor, from the analysis to theoretical designs in ADS simulations. Chapter 5 describes laboratory testing and the corresponding results of the prototype using both design methods. The concluding chapter summarizes the thesis work and contains some recommendations for further research.

## Chapter 2: Basic Class E Ideas

### 2.1 Common Class E RF Power Amplifier Configurations

There are two commonly used configurations of power amplifiers. They are single-ended and complementary (also known as push-pull) illustrated as

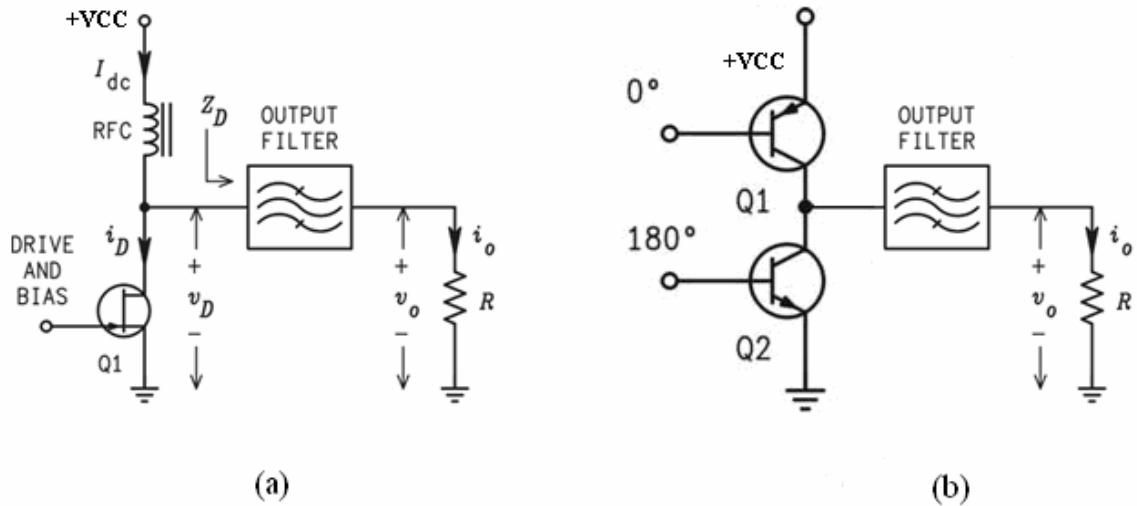


**Figure 2.1: Common Configurations of Power Amplifiers: (a) Single-ended; (b) Complementary (aka, push-pull)**

A single-ended power amplifier has only one transistor, one load, one DC power supply and one output filter network which is the major part of the device responsible for its performance and functions. Compared to it, a push-pull mode PA has two complementary transistors; thus, there will be a P-channel FET with its drain connected to the DC power supply, its source to the drain of another N-channel FET, whose source is grounded, and the rest PA circuit connected to the intersection of the two FETs. They are arranged symmetrically. This is usually called a CMOS configuration. Similarly, the PA composed of BJT transistors in complementary mode will be configured by a PNP BJT connected to the DC

supply and then followed by a NPN BJT, as illustrated in (b) of Figure 2.1.

In this thesis, the single-ended configuration is used since the current standard CMOS technology can not yield high efficiency power amplifiers because their low breakdown voltage and strongly nonlinear parasitic drain-to-bulk output capacitance make this type of PAs difficult to be implemented [5].

## 2.2 Optimum and Suboptimum Class E Operations

In Mr. Sokal's article [4], he defines Class E power amplifier as a tuned power amplifier composed of a single-pole switch and a load network. The load network contains a series resonant LC circuit, a DC drain supply, and a drain shunt capacitor. The load is simply a resistance. Preceding the load network is the switch, which can either be a BJT or a FET. Ahead of the switch is the driver circuit. The class E power amplifier developed by Mr. Sokal has the famous circuit schematic as in Figure 2.2 below.

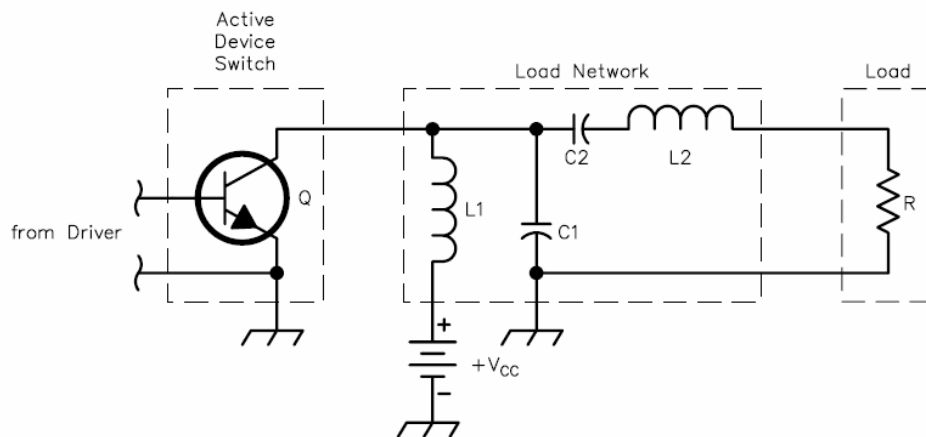


**Figure 2.2: The Circuit Schematic of Class E PA Composed of a Single-Pole Switch and a Load Network Developed by Mr. Nathan Sokal [4]**

In order to achieve a high efficiency, the peak of the current and voltage

waveforms for the switch must be displaced in the time. When the switch is turned on, the current flows through it with no voltage drop across. On the opposite, there will be a voltage induced when the switch is off, blocking any current flow. Thus, the two waveforms behave like two pulse trains, both with fall and rise sections occupying 50% of the RF period, ideally. It is required that the rise section of one waveform occurs when the other one is in its fall to avoid peaking simultaneously. Since the voltage and current of the switch are the same as these of the transistor drain, respectively, drain voltage and drain current will be used from this point forward in the thesis. Figure 2.3 shows the ideal waveforms for 100% efficiency.

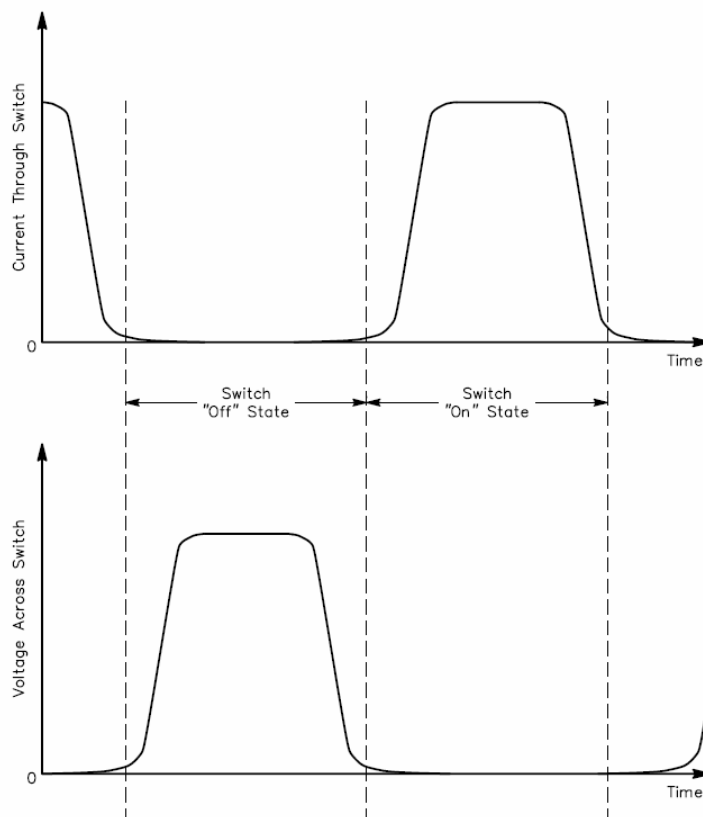


**Figure 2.3: Ideal Switch (or Drain) Voltage and Current Waveforms in Class E to Achieve 100% Efficiency [4]**

Figure 2.3 reveals five conditions that must be realized for a high efficiency operation.

- 1) The peak drain voltage and current do not exist simultaneously.
- 2) At the end of the rise section of the drain current waveform, it must decrease to zero before the rise section of the voltage waveform can start. In other words, the current reaches zero at the end of the ON interval right before the switch is turned off. The beginning of the rise section of the voltage waveform should be delayed until after the switch is turned off.
- 3) The slope of the current waveform at the end of its rise section must be zero to avoid power dissipation due to the existence of both current and voltage.

The similar conditions apply to the drain voltage waveform at the end of its rise section.

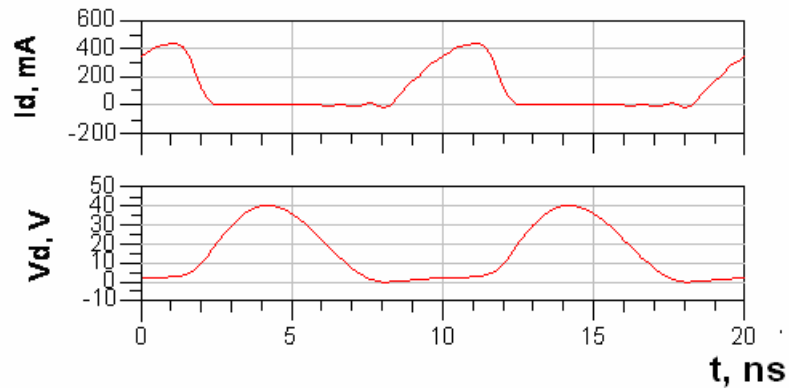
- 4) It must return to zero at the end of the switch OFF interval (right before the switch is turned on) before the rise of the current waveform can start. The starting point of the rise section of the current waveform should be postponed until after the transistor is turned on.
- 5) Its slope is zero at that moment to avoid power dissipation due to the simultaneous imposition of current and voltage.

All the above five conditions are meant to eliminate the power dissipation of the transistor as much as possible during the class E operation so that to increase

the efficiency. The realization of condition 1 reduces the majority power loss. Condition 2 & 3 and 4 & 5 are aimed to decrease the power dissipation during the ON to OFF and OFF to ON transitions of the switching process. They prevent the energy loss from the coexistence of substantial current and voltage during the transitions. Even though the power dissipation during the transition intervals is small compared to that from the coexistence of peak voltage and current, it still can decrease the efficiency dramatically, thus, degrade the class E performance.

The condition 2 and 3 are known as Zero Current Switching (ZCS) and Zero Slope Current Switching (ZsCS), respectively, from the concepts of switching regulator. Similarly, condition 4 and 5 are called Zero Voltage Switching (ZVS) and Zero Slope Voltage Switching (ZsVS).

Practically, ZCS and ZsCS are very difficult to implement for frequencies greater than a few decades of MHz. Therefore, switching condition set ZCS & ZsCS and that for ZVS & ZsVS can not be achieved at the same time for high frequencies. On the contrary, the latter set is much easier to design and implement. Thus, the typical drain voltage and current waveforms for a practical class E power amplifier look like the traces shown in Figure 2.4.



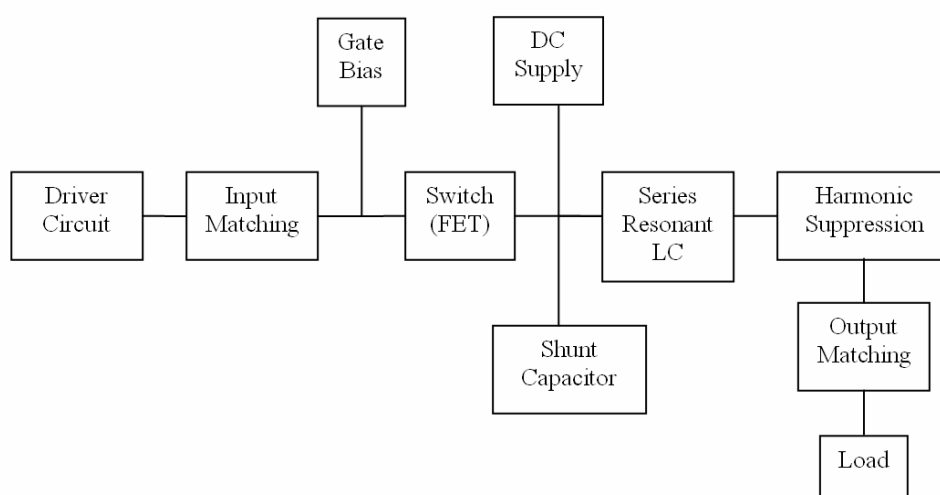
**Figure 2.4: Drain Voltage and Current Waveforms of a Practical Class E PA**

Figure 2.4 reveals a class E PA which realizes ZVS and ZsVS simultaneously, but not ZCS and ZsCS. Thus, it can not reach 100% efficiency. However, its efficiency is still very high because current flows through the switch when its voltage is almost totally zero; most importantly, the peak drain current and peak voltage are displaced in time.

Mr. Frederick H. Raab defined the class E PAs that meet all five conditions as the optimum Class E [6]. He also proposed the definition of suboptimum Class E, which is a class E power amplifier composed of a switch and a load network as in Figure 2.2, however, not meeting those conditions. This allows a mistuned or not optimized power amplifier to be classified as a class E. Similar to switching condition set ZCS & ZsCS, in practice, optimum class E power amplifier is not realizable for frequencies greater than a few tens of MHz. Yet, suboptimum class E power amplifiers are designable and implementable.

## 2.3 Basic Circuit Schematic

In this thesis work, the prototype of the RF class E power amplifier proposed consists of the circuit elements synthesized in the design block diagram below. The composition and design of each block are explained in the following section.



**Figure 2.5: Block Diagram of Class E RF Power Amplifier Prototype Proposed**

## 2.4 Class E circuit Composition and Function

### 2.4.1 Driver

What drives the MOSFET used in class E is the voltage across the input capacitance of the transistor, which is also the gate voltage. Due to the fact that the gate DC current is always zero, the gate voltage does not dissipate power, thus, no power loss.

The ideal driver for class E PAs is a pulse train with rectangular waveform shape because it has the shortest transition interval between fall and rise sections among all the waveforms; hence, it has the lowest power loss during transitions.

However, it is not realizable in practice. Thus, a trapezoidal waveform is the best choice for frequencies below 50 MHz. For higher frequencies, a sine wave can be used as a usable approximation to the trapezoids. Inevitably, there will be transition power loss. But the sine wave driver can generate a relatively high efficiency and satisfactory performance.

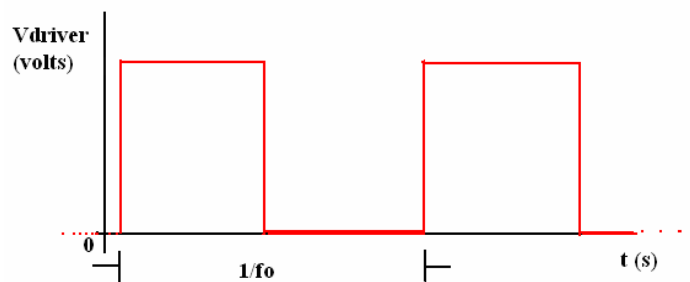


Figure 2.6: Waveform of an Ideal Driver

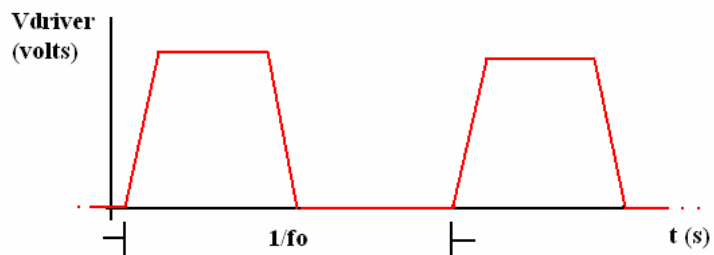


Figure 2.7: Waveform of a Trapezoidal Driver

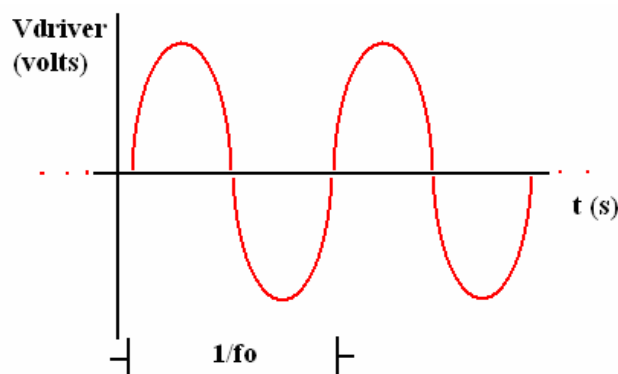


Figure 2.8: Waveform of a Sinusoidal Driver

### 2.4.2 Input Matching

Input matching is required to reduce the reflection due to mismatch between the impedance of the RF input source, the standard  $50\ \Omega$ , and the impedance at the right of  $50\ \Omega$  when looking into the rest of the PA circuit. Let us define the RF power available from the source to be  $P_{AV}$ , and the power entering the power amplifier as  $P_{del}$ .

Since the power amplifier is always a part of a complex system, in which it is always preceded and followed by some other devices with specific output power. It is better to have the conjugate match between the RF power available from the generator, or the output power from the device preceding the PA ( $P_{AV}$ ), and the actual power entering the PA circuit ( $P_{del}$ ), for the purpose of accurately analyzing the PA and the system's performance, such as efficiency and gain.

### 2.4.3 Gate Bias

Since the gate voltage variations will drive the switch on and off, the gate bias is important in supplying this swing. For a BJT acting as the switch in class E, the transistor operates in cutoff and active region for OFF and ON interval, respectively, each for a half RF switching period. The gate bias should be the DC offset of the voltage waveform, which swings among the values needed for cutoff and active, each for half time. For a FET switch, the transistor operates in cutoff and saturation regions when the switch is in the OFF and ON stage, respectively. Similarly, the gate bias should be the DC level of the swing which makes the

transistor to go cutoff or deep saturation.

#### 2.4.4 Switch

Because the DC gate current is always zero of any MOSFET, the gate bias circuit of a FET is easier to design than that of a BJT. Simply, the gate bias can be a voltage divider composed of the resistors. Thus, FET is used as the switch in this thesis work. Table 2.1 gives a summation of FETs that can be used in class E PA design.

**Table 2.1: FET Transistor Selection [7]**

Transistor	Drain BV (V)	Status	Frequency	Major Applications	Manufacturers
RF Power FET	65	Reliable for commercial use	1 MHz – 400 MHz	VHF power amplifier & oscillator	Motorola
GaAs MeSFET	16-22, 60	Very reliable.	1 GHz – 30 GHz	Radar, satellite, military	Triquint, Eudyna, Excelics
SiC MeSFET	100	3 years old, Unproven reliability	500 MHz – 2.3 GHz	Base Station	Cree
GaN MeSFET	160	Holy Grail. Still in research stage.	1 GHz – 30 GHz	Replacement for GaAs	Cree, Triquint
Si LDMOS (FET)	65	Reliable for commercial use	500 MHz – 2 GHz	Base station	Cree, Freescale, Philips, Polyfet
Si VDMOS (FET)	65 – 1200	Reliable for commercial use	1MHz – 500 MHz	HF & FM broadcast, MRI	Polyfet, APT, IXYS

Based on the requirements for frequency and applications, a specific type of FET will be chosen for a specific design. In addition, power output is important in transistor selection, too, which is limited by the transistor's drain breakdown

voltage and maximum current rating. These two parameters are determined during the manufacturing process and are stated in the datasheet explicitly.

#### **2.4.5 DC Supply**

In class E power amplifier operation, the drain voltage will swing up to three times of its DC supply voltage, sometimes even to reach or exceed the breakdown voltage, resulting in the damage to the transistor and the amplifier circuit. Thus, for the safe operation purpose, it is better that drain DC supply is less than a third of the breakdown voltage, and greater than the gate DC bias.

#### **2.4.6 RF Chocks**

In class E design, there are two inductors connecting between the DC power supply and the drain, and the bias voltage at the gate and the switch, respectively. They act as short circuits at the DC and open circuits at the operating or the higher frequencies. Thus, they block the RF signals going to the switch; in other words, they only allow a constant D.C. current flowing from the DC power to the transistor. Therefore, they are called RF chocks as their function is to “chock” (or block) RF signals.

#### **2.4.7 Load Network**

The load network of Class E prototype proposed by this thesis is composed of a drain shunt capacitance, a series resonant LC circuit, LC tank circuits for low order harmonic suppressions, and an output matching network.

##### **1) Drain Shunt Capacitance**

The drain shunt capacitance,  $C_{shunt}$ , delays the starting point of the voltage rise section while the current is at the end of its fall section during the ON to OFF transition. It ensures that at the moment when the switch is turned OFF, the voltage across the switch still remains relatively small as it was still at the end of the fall section of the drain voltage, until after the drain current has reached zero. Thus, its purpose is to shape the drain voltage and current waveforms during the ON to OFF transition to make certain that there is as little power dissipation by the switch as possible. The current flows for ON and OFF intervals around the switch are explained below with the help of Figure 2.9 and 2.10.

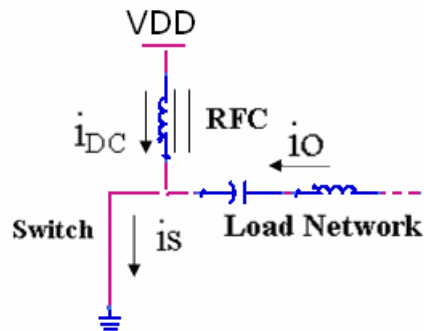


**Figure 2.9: Major Current Flows in a Class E PA when Switch is ON**

When the switch is ON, there is no current flowing through  $C_{shunt}$ , or the voltage drop across it. The relation among the currents going through the RF chock on the drain DC supply path ( $i_{DC}$ ), the switch ( $i_S$ ) and the rest of the load network ( $i_O$ ) is

$$i_S = i_{DC} + i_O \quad (2.1)$$

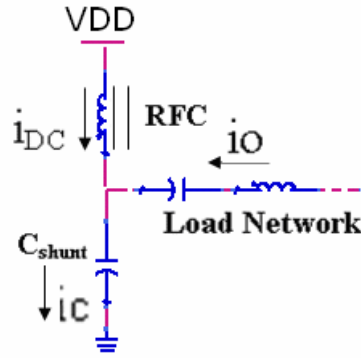


**Figure 2.10: Major Current Flows in a Class E PA when Switch is OFF**

On the other hand, when the switch is OFF,  $i_s$  becomes zero. All of the current that flows through the switch when it is ON now flows through the drain shunt capacitor, charging it up. Thus, the new current relation is

$$i_C = i_{DC} + i_O \quad (2.2)$$

At the switch OFF interval, the voltage across  $C_{shunt}$  is the same as the transistor drain voltage, or the switch voltage. Thus,  $V_S$ ,  $V_D$  and  $V_{Cshunt}$  are used interchangeably in this thesis.

When the switch is turned on again,  $C_{shunt}$  is shorted immediately, causing it to be discharged.

The drain shunt capacitance is mainly composed of the output capacitance of the transistor and an external linear capacitance,  $C_{ex,l}$ , in parallel with it. The rest small portion of the composition comes from the transistor mounting capacitance, the RF choke parasitic capacitance, and other stray capacitances. Since this portion is very small, it is usually ignored in the design.

The required external linear capacitance decreases as the operation frequency

increases. Thus, at high frequencies,  $C_{\text{shunt}}$  is often partially or, sometimes completely, absorbed by the transistor's output capacitance,  $C_{\text{out}}$ . At that case,  $C_{\text{shunt}}$  will not be connected in the circuit of the design.  $C_{\text{out}}$  alone provides enough drain shunt capacitance for the optimal Class E operation.

## 2) Series Resonant $L_O C_O$ Circuit

The series resonant  $L_O C_O$  circuit resonates at a slightly smaller frequency than the PA's operating frequency,  $f_o$ . Typically,  $L_O$  consists of two inductors,  $L_r$  and  $L_e$  with  $L_r$  as the dominant composite.  $L_r$  together with  $C_O$  resonates at  $f_o$ , guaranteeing a substantially sinusoidal load current; and  $L_e$  is the excess inductance makes sure that ZVS and ZsVS conditions are met to eliminate the energy loss. In addition, it causes a phase shift between the sinusoidal load current and the fundamental component of the applied drain voltage.

The relationship between  $C_O$ ,  $L_O$ ,  $L_r$ ,  $L_e$  and  $C_{\text{shunt}}$  can be explained as following:

$$L_O = L_r + L_e \quad (2.3)$$

When the switch is closed, the drain shunt capacitance is shorted; thus, the series  $L_O C_O$  circuit resonates at  $f_L$ , smaller than the resonate frequency of  $C_O L_r$  and the corresponding schematic of load network is shown in Figure 2.11.

$$f_o = \frac{1}{2\pi\sqrt{C_O L_r}} \quad (2.4)$$

$$f_L = \frac{1}{2\pi\sqrt{C_O L_O}} < f_o \quad (2.5)$$

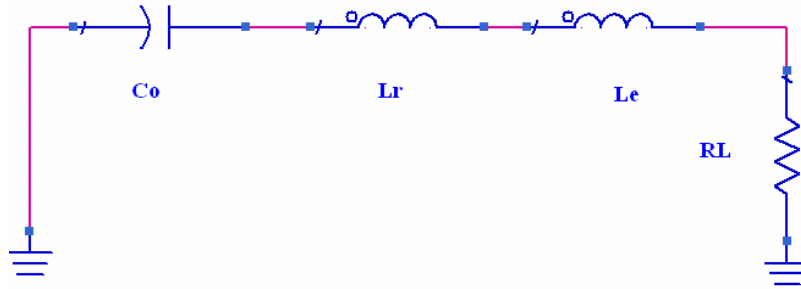


**Figure 2.11: Schematic of Load Network when Switch is ON**

When the switch is open,  $C_{shunt}$  is connected to the series  $L_O C_O$ , changing its resonant frequency to  $f_{c,shunt}$ . Figure 2.12 shows the associated schematic.

$$f_{c,shunt} = \frac{1}{2\pi \sqrt{L_O \frac{C_O C_{shunt}}{C_O + C_{shunt}}}} \quad (2.6)$$

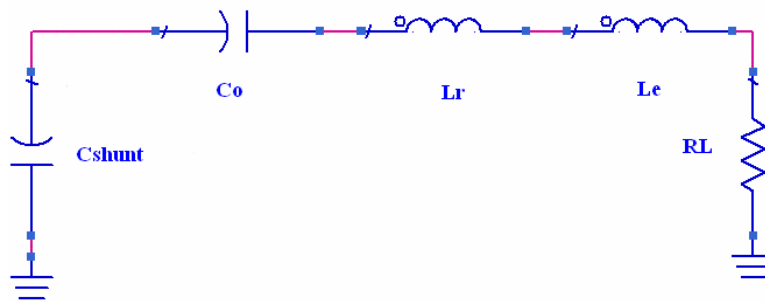


**Figure 2.12: Schematic of Load Network when Switch is OFF**

$f_{c,shunt}$  can be either equal to, or slightly bigger than  $f_o$ , depending on the value of  $L_O$ ,  $C_O$  and  $C_{shunt}$ . But most time,  $f_{c,shunt} > f_o$ .

### 3) Harmonic Suppression Tank Circuits

Harmonic suppression is one part of the Class E PA's circuit to primarily deal with reduction of power loss. It is commonly composed of series LC tank circuit in parallel with the output load. The tank circuit resonates at the desired harmonics, providing at least 45 dB attenuation. In general, the harmonic

attenuation is expressed in dBc, which is the difference in dB between the inter-modulation (IM) power and the fundamental frequency power.

Since the harmonic impedances of a Class E PA are the result of  $C_{\text{shunt}}$  and decrease with frequency, and the third and higher harmonics are of relatively small amplitudes, in most cases, only one LC tank circuit is needed, which resonates at  $2f_0$ . However, sometimes a second tank circuit is implemented for third harmonic if its power level compared to fundamental is smaller than 45 dBc in difference.

#### **4) Output Matching**

Output matching in Class E is usually needed if the required load impedance is other than the standard RF load,  $50 \Omega$ , associated with SMA connectors. Because the matching is done between only two real impedances, the simple L-section lumped elements matching circuit can be used.

The L-section matching network requires only a capacitor and an inductor. There are two configurations and the applications depend on whether the PA's load resistance is bigger or smaller than  $50 \Omega$ . But the design equations are the same. Figure 2.13 plots the design schematics and Equations 2.7 and 2.8 are used to find the circuit component values.

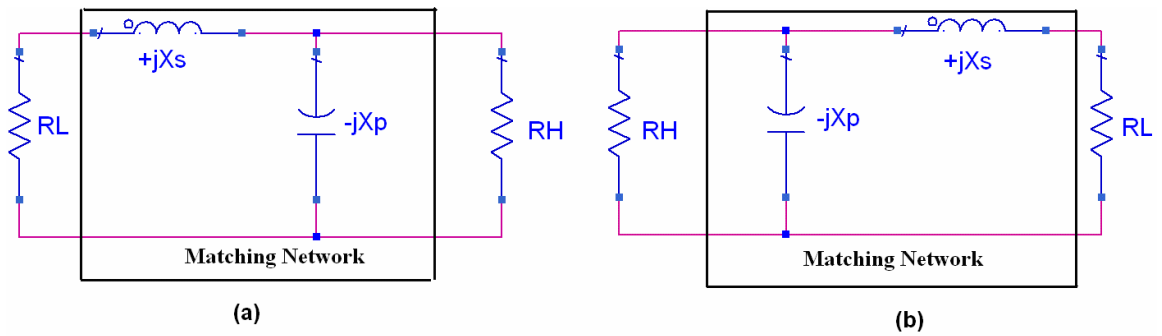


**Figure 2.13: L-Section Matching Networks for Two Resistive Impedances: (a) L-Section to Match a Low Resistance to a High Resistance; (b) L-Section to Match a High Resistance to a Low Resistance**

$$\frac{X_S}{R_L} = Q_L = \frac{R_H}{X_P} \quad (2.7)$$

$$\frac{R_H}{R_L} = Q_L^2 + 1 \quad (2.8)$$

Where,  $Q_L$  is the loaded quality factor of LC, which has to be small compared with the unloaded Q factor of the components.  $X_S$  is the series inductance and  $X_P$  is the parallel capacitance of the matching network.  $R_H$  and  $R_L$  are the high and low resistances to be matched; one will be  $50 \Omega$  and the other one will be the Class E PA's required load resistance.

#### 2.4.8 Load

A resistive load is implemented in Class E PA at the output terminal. Besides the resistance from the design equations, which will be addressed in the next chapter, the load must include all of the parasitic resistances, the equivalent series resistance (ESR) of the inductors at the operating frequency in the circuit for high frequency operation. ESR resistances change with respect to the frequency; they increase as operating frequency increases, but not in a linear way. Being able to

accurately model the behavior and predict the values of ESR in the circuit can prevent additional energy loss because similar to regular resistors, ESRs dissipate power when current is flowing through them.

## **Chapter 3: Class E PA Circuit Design Analysis with Linear Drain Shunt Output Capacitance**

Mr. Nathan Sokal and Mr. Alan Sokal are the very first people who explored the concepts of Class E RF power amplifier in the middle 70's. They analyzed the circuit of this type power amplifier exclusively and provided very useful and valuable analysis equations. Most importantly, they assumed the transistor output capacitance is linear. Thus, the name, Linear Design Method or Linear Design Analysis, is used throughout the thesis to refer to the method proposed by two Mr. Sokal. This circuit analyzing method is applicable for operation frequency below 900 MHz. The design equations [4] will be re-stated in the next section with some modifications to fit the design in this thesis work.

### **3.1 Linear Design Analysis for Class E PA Operations**

In Mr. Nathan Sokal's famous article "Class E RF Power Amplifiers" [4], he gave 5 equations for determining the component values of a class-E amplifier using BJT transistors. The corresponding equations for Class E design using FET transistors are below.

$$V_{DD} = \left( \frac{BV_{DSV}}{3.56} \right) SF \quad (3.1)$$

Equation 3.1 gives the voltage supply to be used.  $V_{DD}$  is the drain supply voltage,  $BV_{DSV}$  is the breakdown voltage of the FET to be used, and SF is the safety factor.

$$R_L = \left( \frac{V_{DD}^2}{P_{out}} \right) 0.576801 \left( 1.001245 - \frac{0.414395}{Q_L} - \frac{0.402444}{Q_L^2} \right) \quad (3.2)$$

Equation 3.2 gives the value of resistance for the load that is to be used.  $V_{DD}$  is the supply voltage given by Equation 3.1.  $P_{out}$  is the output power desired.  $Q_L$  is the loaded quality factor of the series  $L_0C_0$  resonant circuit.

$$C_{shunt} = \frac{1}{34.2219 f_o R_L} \left( 0.99866 + \frac{0.91424}{Q_L} - \frac{1.03175}{Q_L^2} \right) + \frac{0.6}{(2\pi f_o)^2 L_1} \quad (3.3)$$

Equation 3.3 gives the value of  $C_{shunt}$ , which is the drain shunt capacitance. According to Mr. Sokal, this  $C_{shunt}$  should also include any output capacitance associated with the transistor.  $f_o$  is the center/operating frequency.  $R_L$  is the resistance calculated from Equation 3.2.  $Q_L$  is the loaded quality factor.  $L_1$  is the RF chock at the drain. Mr. Sokal did not give explicit equations about how to calculate this inductance. Instead, he proposed that the values of RFC can be chosen as long as its impedance at  $f_o$  and higher frequencies is big enough that we can assume there is an open circuit. Then, any AC signal and AC power will be blocked by  $L_1$  and there is only a constant DC current flowing in the drain power supply path.

$$C_o = \frac{1}{2\pi f_o R_L} \left( \frac{1}{Q_L - 0.104823} \right) \left( 1.00121 + \frac{1.01468}{Q_L - 1.7879} \right) - \frac{0.2}{(2\pi f_o)^2 L_1} \quad (3.4)$$

Equation 3.4 gives the value of  $C_o$ , the capacitance in the series  $L_0C_0$  resonant circuit.  $f_o$  is again the operating frequency.  $R_L$  is the load resistance from Equation 3.2.  $Q_L$  is the loaded quality factor.  $L_1$  is the DC feed RF choke.

$$L_o = \frac{Q_L R_L}{2\pi f_o} \quad (3.5)$$

Equation 3.5 gives the value of  $L_o$ , the total inductance in the series resonant circuit.  $f_o$  is the operating frequency.  $R_L$  is the resistance from Equation 3.2.  $Q_L$  is the loaded quality factor.

Using the notations for the calculations above, the schematic for the main part of Class E power amplifier from Mr. Sokal's design analysis can be shown as in Figure 3.1 below, which is just the modified version of the schematic in Figure 2.2 in Chapter 2.

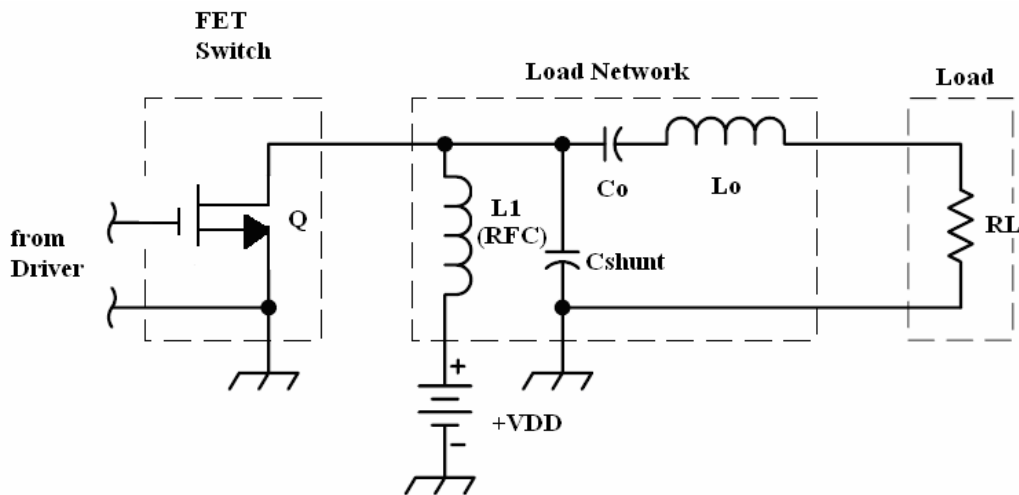


**Figure 3.1: Circuit Schematic of Class E RF PA Using Linear Design Analysis Method**

Those design equations are used to calculate load resistance  $R_L$ , the drain shunt capacitor  $C_{shunt}$ , and  $L_o$  and  $C_o$  in the resonant circuit for a desired operating frequency  $f_o$ , loaded quality factor  $Q_L$ , output power  $P_{out}$ , input power from the source generator  $P_{in}$ , drain power supply  $V_{DD}$  and RF Choke at drain  $L_1$ .

### **3.2 Circuit Design by Using Linear Method**

For this thesis work, the Class E power amplifiers for operating frequencies of 100 kHz, 1 MHz, 10 MHz and those with a factor of 10 increments afterwards till 150 MHz are designed by using linear method and simulated in Advanced Design System (ADS) from Agilent Technologies. Thus, there are total 17 theoretical designs. However, only these two at 10 MHz and 150 MHz are actually implemented in the laboratory; the detail will be addressed in the Chapter 5.

#### **3.2.1 General Circuit Parameter Selections for Theoretical Design in ADS**

##### **Driver**

For all the 17 cases, a sinusoidal waveform at the designated operating frequency is employed in simulation. In addition, a preamplifier generating a trapezoidal waveform is designed and used as the driver for 10 MHz case. Similarly, a preamplifier outputting a saw shape waveform is used to drive the 150 MHz Class E power amplifier.

Basically, the preamplifier is a modified Class A RF power amplifier using another FET transistor. Its circuit configuration is very similar to that of a class E, but much simpler; there is a sine input, a gate bias, a drain DC power supply and an output load as indicated in Figure 3.2.

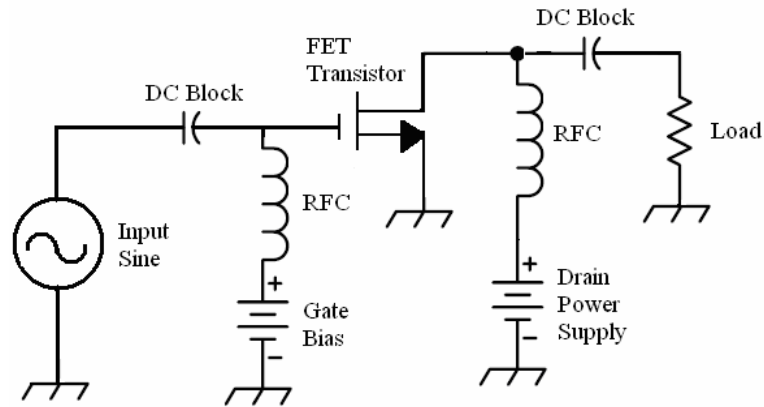


**Figure 3.2: Configuration of Class A RF Power Amplifier Used in Thesis Work**

Theoretically, a Class A RF power amplifier accepts a sinusoidal input and outputs another sinusoid at the same frequency but with much greater amplitude and their phase difference remains constant during the entire amplification process. Thus, the transistor must operate in the saturation region of a FET only and its input must be small enough that it will not be able to drive the transistor into cutoff.

However, in order to have a trapezoidal waveform at the output of an amplifier in generic Class A configuration, the input signal should be big enough to drive the transistor as a switch, which operates between the saturation and cutoff regions. Hence, it requires the FET gate bias to be around its threshold for turning on as well. The preamplifier designed for the 10 MHz case is shown in Figure 3.3.

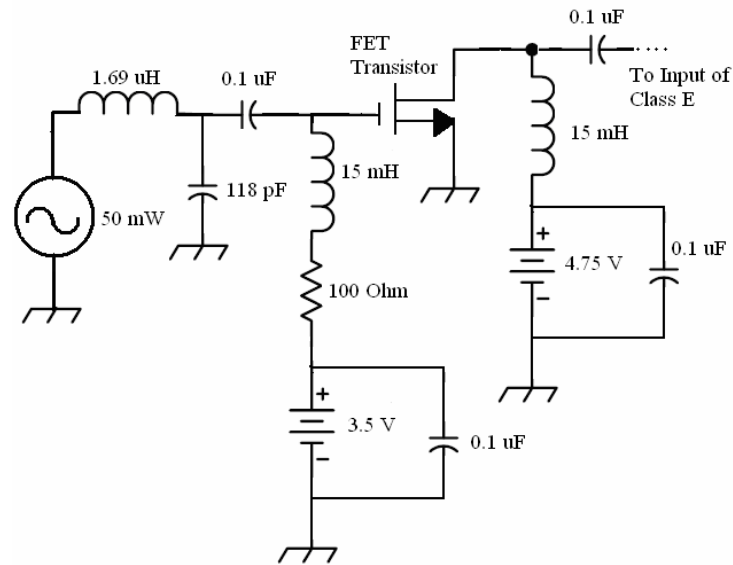


**Figure 3.3: Preamplifier for 10 MHz Design**

In Figure 3.3, 3.5 V and 4.75 V are the gate bias and drain DC power supply, respectively; the L-network composing of a 1.69  $\mu\text{H}$  inductor and a 118 pF capacitor is the input matching network to match the actual power delivered to the preamplifier to the power from the generator, which is 50 mW. The series 0.1  $\mu\text{F}$  capacitors are for DC blocking and those parallel ones are for bypassing. The series RL configuration and the bypass capacitor at the gate bias together ensure the low frequency stability of the device.

The preamplifier for the 150 MHz case has the same circuit configuration as that in Figure 3.3, but with different component values. Furthermore, when the frequency is increased from 10 MHz to 150 MHz, even though the transistor is still driven to operate between cutoff and saturation, a trapezoidal waveform is not generated any more; instead, a saw waveform resulted because the switching becomes non-ideal as frequency increases.

## Switch

RF power FET, MRF134, is chosen for this thesis work because of its high drain breakdown voltage (65 V), big allowable gate voltage swing ( $\pm 40$  V), and VHF frequency operation band (1 MHz – 400 MHz) [8]. In addition, RF power FET has the advantages of high gain, low noise, simple gate bias, and ability to withstand severely mismatched loads without damage. Furthermore, it can yield a wide range of output power with a low power DC control signal. By correctly changing its gate bias DC voltage, MRF134 can supply an output power from its maximum rating value down to zero.

ADS has both the Spice and S-parameter models of MRF134 transistor. Thus, the designer can simulate and evaluate the theoretical design thoroughly before actually building the circuit. The simulation results can be used as the check points for the experimental measurements as well. MRF134 has a simple footprint, and easy to be implemented on the printed circuit board (PCB). However, it has two major drawbacks compared to other RF power FETs. Its size is big 0.81" X 0.81" (width X length), and it can only output 9 watts maximally when the operation conditions and the design are correct. Nevertheless, its characteristics are sufficient for the prototype design of Class E RF PAs.

### 1) The DC-IV Curves of MRF134

The MRF134 transistor has the following drain-to-source voltage ( $V_{DS}$ ) verses drain-to-source current ( $I_{DS}$ ) characteristics for several values of gate-to-

source DC voltages.

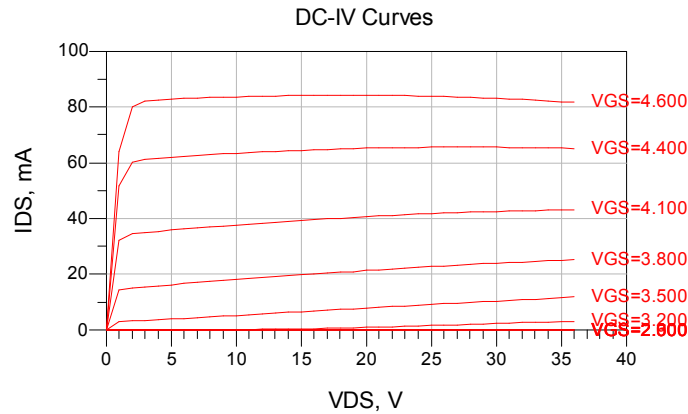


**Figure 3.4:  $V_{DS}$  vs.  $I_{DS}$  of MRF134 for  $V_{GS}$  from 2.0 V to 4.6 V**

We call the curves in Figure 3.4 as DC-IV curves. Figure 3.4 is generated by using the root model of MRF134 on the ADS. 0V to 36 V with a 1 V increment is input to the drain as the  $V_{DS}$  and 2.0 V to 4.6 V with 0.3 V increment to the gate as the  $V_{GS}$ . Under such voltage input ranges, Figure 3.4 indicates that when the  $V_{DS}$  is greater than 2.5 V and  $V_{GS}$  exceeds 3.5 V, there is a relatively constant current flowing from drain to source for a constant  $V_{GS}$  and the transistor is saturated. The triode mode of MRF134 is very brief; it only happens for the  $V_{DS}$  values between 0 V and 2.5 V and for  $V_{GS}$  greater than the threshold.

The DV-IV curves for an ideal MOSFET transistor should have absolutely constant  $I_{DS}$  for a fixed  $V_{GS}$  value and  $I_{DS}$  is totally independent of  $V_{DS}$  in saturation region as in the figure below because the channel pinch-off occurs.

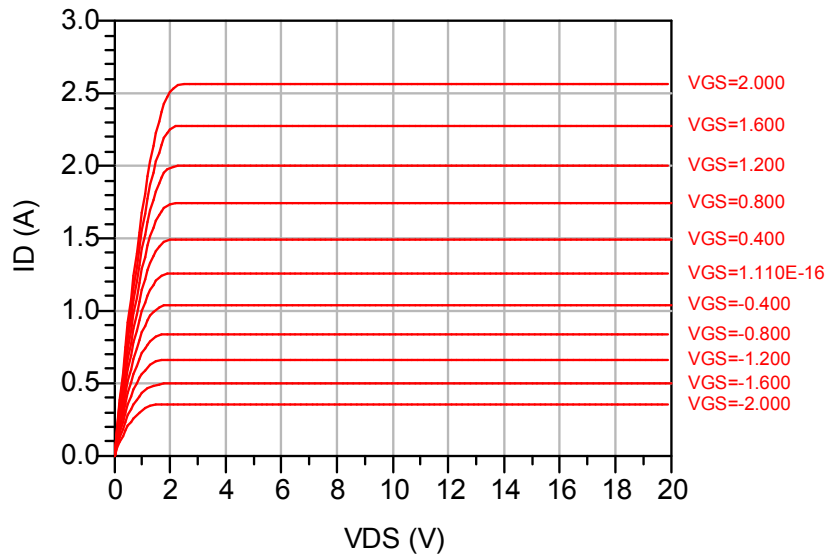


**Figure 3.5: DC-IV Curves for an Ideal MOSFET**

Ideal DC-IV characteristics do not exist due to the fact there is no ideal MOSFET. In general,  $I_{DS}$  has some dependence on  $V_{DS}$  in saturation mode because of the Channel Length Modulation associated with MOSFET transistors;  $I_{DS}$  increases with the increase in  $V_{DS}$  slightly. Thus, those horizontal lines in Figure 3.4 will incline toward left a little bit as in Figure 3.5, which is created by employing a practical MRF134 model.

The DV-IV curves are totally independent of the operating frequency. Hence the same curves are used for all 17 design cases.

### **Gate Bias**

As exhibited in Figure 3.4 and [8], the typical gate threshold voltage, the critical value to turn the transistor MRF134 on, is 3.5 V. In order to guarantee that the switch is OFF when it is not ON, either 3 V, a value below the threshold a little bit, or 3.5 V is used as the gate DC bias for the designs. Thus, the gate voltage

swings between the values that drive the transistor into cut off and saturation region each for half of the RF switching period.

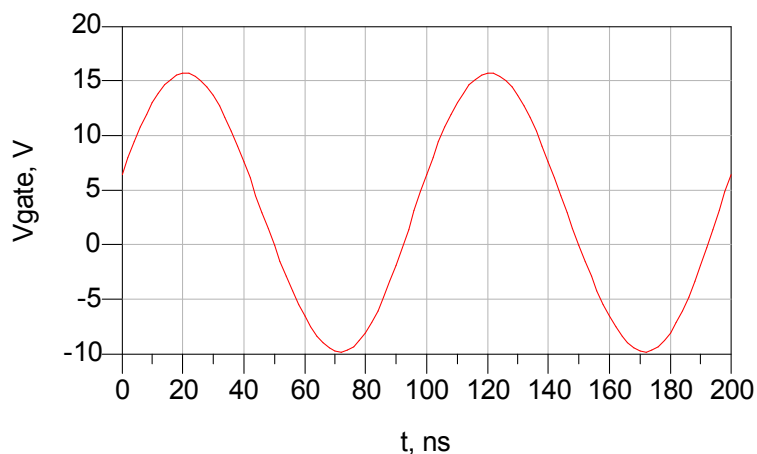


**Figure 3.6: Gate Voltage Swing for 10 MHz Class E Linear Design Using MRF134**

When 3 V is used at the gate and 100 mW as the input power to a Class E RF PA design at 10 MHz, the corresponding gate voltage swing is in Figure 3.6, which has a DC offset around 3 V. Thus, the transistor is on and off for 50% of the time individually.

### **DC Supply**

Using Equation 3.1, the theoretical drain DC supply voltage with the safety factor equal to 1.0 is 18.26 V. Using a third of the breakdown voltage of the transistor MRF134, it should be less than 21.67 V. The power suppliers in the lab at CReSIS can provide maximum 25 V. Thus, any value that is equal to or below 25 V and does not generate a drain voltage swinging close to breakdown when operating with other circuit elements in PA, can be used as the drain DC power supply. In fact, higher DC voltage supply provides higher output power if

designed correctly.

For 17 operating frequency cases, DC voltages within 15 V to 23 V are used as the supply voltage for different designs.

### **RF Chokes**

There is no explicit equation proposed by Mr. Sokal for the values of RF chokes. However, it is advisable to use big inductances so that the inductors can operate as open circuits at  $f_0$ , ideally. Thus, in ADS simulation, 1mH is used for design cases with  $f_0$  up to 60 MHz, 0.1 mH for 60 MHz and 70 MHz cases, and 50  $\mu$ H for  $f_0$  from 80 MHz to 150 MHz. Then, the impedances of those RF chokes are at least 47 k $\Omega$ , big enough to prevent current flows through it.

However, it is not feasible to use big value inductances in practice because they invertibly have series equivalent resistances which change with respect to frequency; therefore, they impact the design results dramatically. This will be addressed in Chapter 5 later.

### **Input Matching**

ADS is able to tell the values of the current flowing through and the voltage across any circuit component and at any node by using current and voltage probes, respectively. When putting those two at the beginning of the power amplifier circuit right after the source, or the power generator, the power delivered to the power amplifier circuit from the generator,  $P_{del}$ , can be calculated as:

$$P_{del} = \frac{|V_{input}| * |I_{input}|}{2} \quad (3.6)$$

Where,  $V_{input}$  and  $I_{input}$  are the AC input voltage and current respectively and  $||$  is the magnitude calculation symbol.

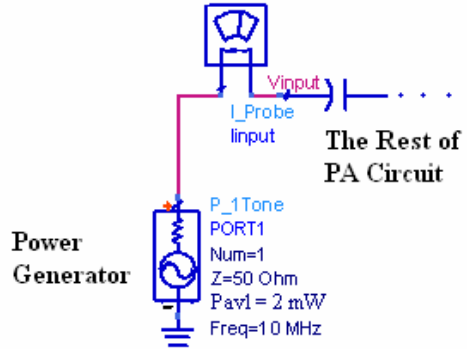


Figure 3.7: Measuring  $V_{input}$  &  $I_{input}$  in ADS

Once the  $P_{del}$  is obtained, and with  $P_{AVL}$  (the power available from the source generator) set by the designer, the impedance ratio between the source resistance,  $R_S$ , which is a standard  $50 \Omega$ , and the resistance looking at the input of the PA circuit,  $R_{in}$ , will simply be the square root of the ratio of  $P_{AVL}$  to  $P_{del}$ . Consequently, the value of  $R_{in}$  can be acquired easily as

$$R_{in} = R_S * \sqrt{\frac{P_{del}}{P_{AVL}}} \quad (3.7)$$

Then, the input matching network can be design by using Equation 2.7 and 2.8 with either configuration in Figure 2.13. Once  $P_{del}$  is matched with  $P_{AVL}$ , they are equal to each other and  $P_{in}$  is used to denote the input power when this match occurs.

$$P_{del} = P_{AVL} |_{matched} = P_{in} \quad (3.8)$$

## Load

For all 17 cases, the calculations for the circuit element values are done by using the operating conditions:  $P_{\text{out}} = 5 \text{ W}$ ,  $Q_L = 5$ ,  $V_{\text{DD}} = 15 \text{ V}$  and  $V_{\text{GG}} = 3 \text{ V}$ . Thus, according to Equation 3.2, the resultant load resistance,  $R_L$ , which is only dependent of  $P_{\text{out}}$ ,  $Q_L$  and  $V_{\text{DD}}$ , is the same for all cases, which is  $23.225 \Omega$ .

## Load Network

The drain shunt capacitance,  $C_{\text{shunt}}$ , and  $C_O$  and  $L_O$  in the series resonant circuit, can be obtained by using Equation 3.3, 3.4 and 3.5, respectively.

The tank circuits for 2<sup>nd</sup> and sometimes 3<sup>rd</sup> harmonic suppression are obtained by using

$$(2\pi n f)^2 L_{\text{tank},n} C_{\text{tank},n} = 1 \quad (3.9)$$

Where,  $n$  represents the order of the harmonics. After the value of either  $L_{\text{tank},n}$  or  $C_{\text{tank},n}$  is chosen, the other one can be calculated using Equation 3.8. The tank circuits are series LC resonant at the  $n_{\text{th}}$  harmonic frequency. It is recommended to pick big inductors which result in sharp resonance, thus, great harmonic attenuation.

The output matching is done easily for these 17 cases because both resistances for matching are known; they are  $50 \Omega$  for the standard RF connector and  $23.225 \Omega$  load resistance as calculated using linear analysis. Then, the matching design will be followed by the method addressed in Chapter 2.

### 3.2.2 Performance Evaluating Parameters for Class E RF Power Amplifiers

There are five important parameters used to evaluate the performance of a Class E RF power amplifier. They are DC power from the power supply, output power, power gain, efficiency and the 2<sup>nd</sup> and 3<sup>rd</sup> harmonic attenuations. Even though the desired output power,  $P_{out}$ , is used in Equation 3.2 for the calculation of  $R_L$ , it is in general not the output power generated after all the component values have been decided, which is much more important than former.

#### DC Power

According to the design block diagram in Figure 2.5, there are two DC voltage supplies used in the PA circuit, the gate bias and the drain DC supply. However, the nature of the FET transistor requires no current flow at the gate. Hence, there is no power supplied to the circuit by the gate bias. Using the probes in ADS at the drain, the corresponding DC current and voltage can be measured and thereof the DC power,  $P_{DC}$  which is the same as the drain supply power  $P_{DD}$ , can be obtained as

$$P_{DC} = I_{DC} * V_{DD} = P_{DD} \quad (3.10)$$

#### Output Power (i.e., Load Power)

When the current and voltage probes are used at the load of a PA design in ADS, the output power,  $P_{out}$ , can be found easily.

$$P_{out} = \frac{|V_{load}| * |I_{load}|}{2} \quad (3.11)$$

Where,  $V_{load}$  and  $I_{load}$  are the AC input voltage and current respectively and  $||$  is the magnitude calculation symbol.

### Power Gain

Once the output power is found and the input power from the source generator is known, the power gain,  $G$ , of a Class E power amplifier is the ratio between these two values as

$$G = \frac{P_{out}}{P_{in}} \quad (3.12)$$

Almost all the time, the power gain is expressed in dB scale as a convention

$$G = 10 \log_{10} \left( \frac{P_{out}}{P_{in}} \right) \quad (3.13)$$

### Efficiency

In general, the efficiency of any amplifier is called the power-conversion efficiency and defined as the ratio between the output power to the supply power

$$\eta = \frac{OutputPower(P_{out})}{SupplyPower(P_s)} \quad (3.14)$$

In class E design, Equation 3.14 will be altered specifically by using drain supply power as the denominator and the load power as the numerator. It then becomes the definition of the drain efficiency for a FET class E power amplifier.

The modified equation is

$$\eta_d = \frac{LoadPower}{DrainSupplyPower} = \frac{P_{out}}{P_{DD}} = \frac{P_{out}}{P_{DC}} \quad (3.15)$$

Due to the existence of harmonics and the filtering circuits to attenuate them,

the RF fundamental power is a very good approximation for  $P_{out}$ .

In addition, power-added efficiency, PAE, is used most of the time to evaluate the performance of class E PAs along with  $\eta_d$ . Unlike drain efficiency, PAE takes into account of the RF input source power,  $P_{in}$ , as well.

$$PAE = \frac{P_{out} - P_{in}}{P_{DC}} \quad (3.16)$$

According to Equation 3.16, a power amplifier with a greater  $P_{in}$  will have a smaller PAE and a smaller power gain than the one with a smaller  $P_{in}$ , for the same amount of output power. But their  $\eta_d$  will be the same.

Similar to PAE, the overall efficiency,  $\eta_{all}$ , also accounts for  $P_{in}$ . It is the ratio of the output power to the sum of the DC and the RF input power.

$$\eta_{all} = \frac{P_{out}}{P_{DC} + P_{in}} \quad (3.17)$$

Again, high  $\eta_{all}$  requires a small  $P_{in}$  if the DC and output power are fixed.

## 2<sup>nd</sup> and 3<sup>rd</sup> Harmonic Attenuation

ADS has embedded functions to calculate the load voltage at  $n^{\text{th}}$  harmonic and at the fundamental frequency. The harmonic attenuation can be obtained by taking the ratio between the fundamental load and  $n_{\text{th}}$  harmonic voltages and the result is expressed in dBc as

$$n_{\text{th,att}} = -20 \log_{10} \left( \frac{V_f}{V_{n,har}} \right) \quad (3.18)$$

Where,  $n_{\text{th,att}}$  is the attenuation for  $n^{\text{th}}$  harmonic,  $V_f$  is the fundamental load

voltage and  $V_{n,\text{har}}$  is the  $n^{\text{th}}$  load harmonic voltage.

### **3.2.3 ADS Simulation for 17 Cases with Calculated Circuit Elements Using Linear Design Method**

Using Equation 3.2, 3.3, 3.4 and 3.5 to calculate  $R_L$ ,  $C_{\text{shunt}}$ ,  $C_O$  and  $L_O$  values for each  $f_0$  with the conditions  $Q_L =$ ,  $V_{DD} = 15$  V,  $V_{GG} = 3$  V,  $P_{\text{in}} = 100$  mW,  $L_1$  values chosen as explained in Subsection 3.2.1, and desired  $P_{\text{out}} = 5$  W, the calculation and simulation results, i.e., DC power, output power, power gain, efficiencies, and 2<sup>nd</sup> and/or 3<sup>rd</sup> harmonic attenuations, for 17 cases of Class E RF power amplifiers with the configuration in Figure 3.1, which has no input and output matching networks and no tank circuits for harmonics, are summarized in the Table 3.1 and 3.2, respectively. Because the load resistance for all the cases is 23.225  $\Omega$ , it is not listed in the table. In addition, the power delivered to the PA circuit from the source generator,  $P_{\text{del}}$ , and the DC current measured at the drain DC supply path in ADS,  $I_{S\_H}$ , are also listed in the table.

**Table 3.1: Calculation Results of 17 Cases Using Linear Design Analysis**

<b>f<sub>o</sub> (MHz)</b>	<b>C<sub>shunt</sub> (pF)</b>	<b>C<sub>O</sub> (pF)</b>	<b>L<sub>O</sub> (μH)</b>
0.1	14.45X10 <sup>3</sup>	18.40X10 <sup>3</sup>	184.82
1	1.44X10 <sup>3</sup>	1.84X10 <sup>3</sup>	18.48
10	143.61	184.33	1.85
20	71.732	92.19	0.924
30	47.84	61.45	0.616
40	35.87	46.09	0.462
50	28.70	36.87	0.370
60	23.91	30.73	0.308
70	20.53	26.33	0.264
80	17.98	23.03	0.231
90	15.98	20.47	0.205
100	14.38	18.43	0.185
110	13.07	16.75	0.168
120	11.98	15.36	0.154
130	11.05	14.18	0.142
140	10.26	13.17	0.132
150	9.58	12.29	0.123

Table 3.1 reveals that  $C_{shunt}$  decreases as frequency increases and its decreasing rate is the same as the increasing rate of  $f_o$ . The same phenomena occur to  $C_O$  and  $L_O$ . The analytical equation of  $C_{shunt}$ , Equation 3.3, has two terms, both of them are inversely proportional to  $f_o^n$ , where  $n$  is the power factor. However, the second term is much smaller than the first; therefore, the value of  $C_{shunt}$  is inversely proportional to the first power of  $f_o$ , so is  $C_O$  in Equation 3.4 and  $L_O$  in Equation 3.5.

**Table 3.2: Simulation Results of 17 Cases Using Linear Design Analysis**

<b>f<sub>o</sub> (MHz)</b>	<b>P<sub>del</sub> (mW)</b>	<b>I<sub>S H</sub> (mA)</b>	<b>P<sub>DC</sub> (W)</b>	<b>P<sub>out</sub> (W)</b>	<b>η<sub>d</sub> (%)</b>	<b>PAE (%)</b>	<b>G (dB)</b>	<b>2<sup>nd</sup> (dBc)</b>	<b>3<sup>rd</sup> (dBc)</b>
0.1	2	183	2.75	1.75	63.54	59.90	12.42	-17.86	-42.28
1	2	183	2.75	1.76	63.94	60.306	12.45	-17.78	-42.26
10	22	197	2.96	1.87	63.13	59.75	12.71	-18.97	-45.56
20	45	188	2.82	1.91	67.70	64.15	12.80	-20.45	-41.71
30	68	186	2.80	1.93	68.90	65.32	12.85	-21.54	-41.24
40	90	183	2.75	1.92	69.64	66.01	12.82	-22.52	-40.99
50	116	198	2.97	1.98	66.79	63.42	12.97	-23.09	-43.22
60	129	175	2.63	1.85	70.46	66.65	12.67	-24.22	-40.93
70	146	170	2.55	1.80	70.56	66.64	12.55	-25.00	-41.10
80	159	165	2.48	1.75	70.58	66.55	12.43	-25.69	-41.34
90	170	160	2.40	1.69	70.50	66.34	12.29	-26.36	-41.69
100	178	155	2.33	1.63	70.25	65.95	12.13	-27.00	-42.20
110	184	150	2.25	1.57	69.91	65.45	11.96	-27.56	-42.84
120	187	145	2.17	1.51	69.44	64.83	11.78	-28.03	-43.61
130	189	140	2.09	1.44	68.80	64.03	11.59	-28.42	-44.60
140	188	135	2.02	1.37	67.96	63.01	11.38	-28.75	-45.84
150	186	130	1.95	1.31	66.86	61.75	11.16	-28.99	-47.39

Note: 2<sup>nd</sup> and 3<sup>rd</sup> in column 9 and 10 are the 2<sup>nd</sup> and 3<sup>rd</sup> harmonic attenuations, respectively, with respect to the fundamental power measured at the load in ADS.

Even though there is an inverse proportional relationship between  $f_o$  and the circuit component values, there is no such conspicuous relations between the operating frequency and the performance evaluating parameters.

The drain voltage verses time and drain current verses time plots of all 17 cases are attached at the Appendix A.1. From these plots, several observations can be made. 1) Most obviously, as  $f_o$  increases, the current and voltage waveforms deviated from the ideal shapes; they smear out more so that the transitions for both ON to OFF and OFF to ON need more time to perform. This indicates that it is getting hard to switch between ON and OFF promptly for the transistor as frequency goes up. 2) As  $f_o$  increases, the voltage waveform peaks lower and the current goes down below 0 more; 3) as  $f_o$  increases, the current waveform changes toward a sinusoid more. Thus, circuit optimization is needed in order to make the designs change toward optimum operations.

### **3.2.4 Design Optimization**

There are two ways to optimize the designs employed in this thesis. First, the matching networks for both input and output and the tank circuits for harmonic suppression are added to the design in the previous sections, aiming at increasing the efficiency. Then, the circuit values are tuned to achieve ideal drain voltage waveform for optimum operation.

### **Additions of Matching Networks and Tank Circuits**

For all 17 cases,  $P_{del}$  values are listed in Table 3.2. They are different for

different  $f_0$  cases. Then, the matching network for input is done using the method explained in Subsection 3.2.1. On the contrary, all 17 cases have the same  $R_L$ , which is  $23.225 \Omega$  due to design conditions. But the values of the LC matching network are different for each case because, again, their operating frequencies are not the same. The output matching networks are designed in compliance with the method addressed also in Subsection 3.2.1. Output matching is used to increase the load power, consequentially, increasing the efficiencies.

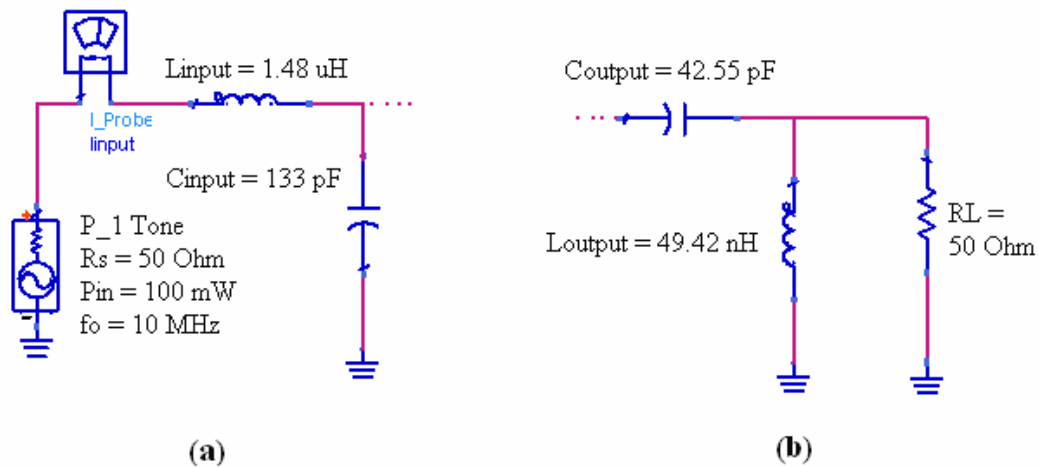


**Figure 3.8: Matching Networks: (a) Input Matching for 10 MHz Case; (b) Output Matching for 150 MHz Case**

The tank circuit design is quite easy as addressed in Subsection 3.2.1. It is in the configuration of a LC series combination in parallel with the output matching network, which is in parallel with the  $50 \Omega$  load. Its schematic used in the designs is shown in Figure 3.9.

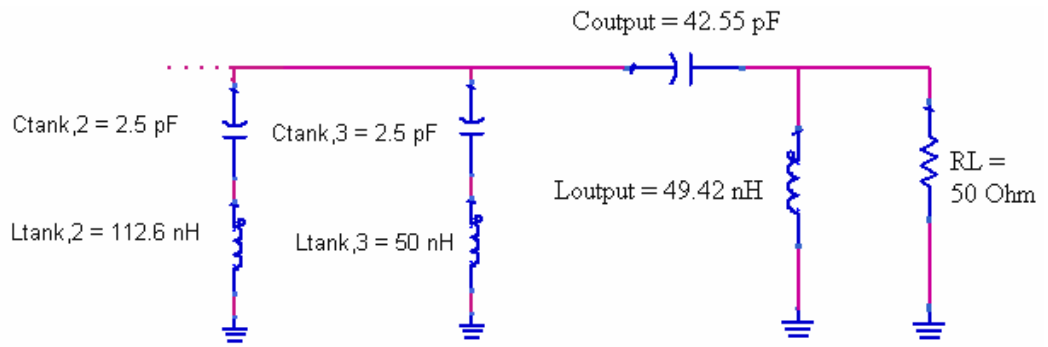
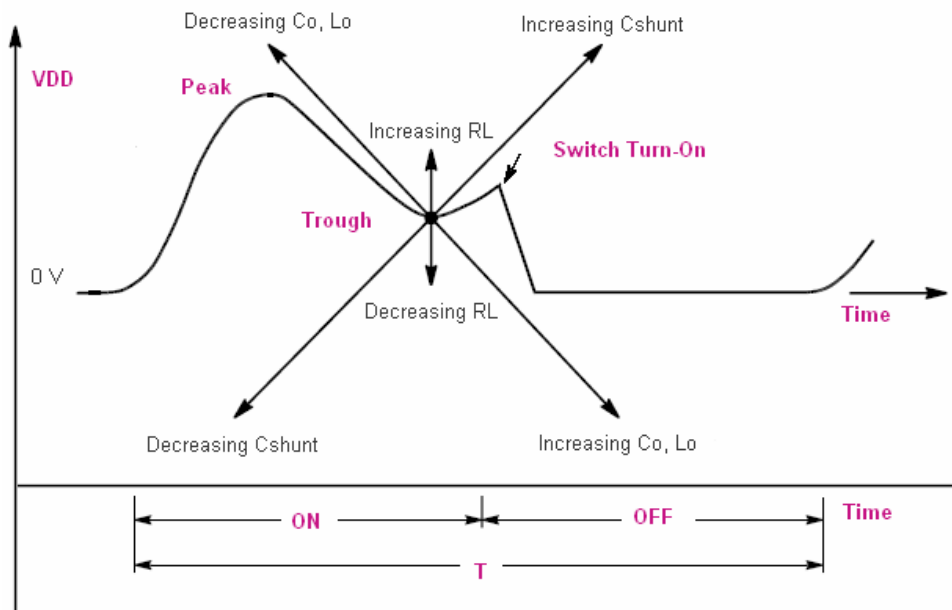


**Figure 3.9: Tank Circuit for 2<sup>nd</sup> and 3<sup>rd</sup> HarmonicSuppressions with Output Matching and Load Resistance for 150 MHz Case**

### Circuit Tuning

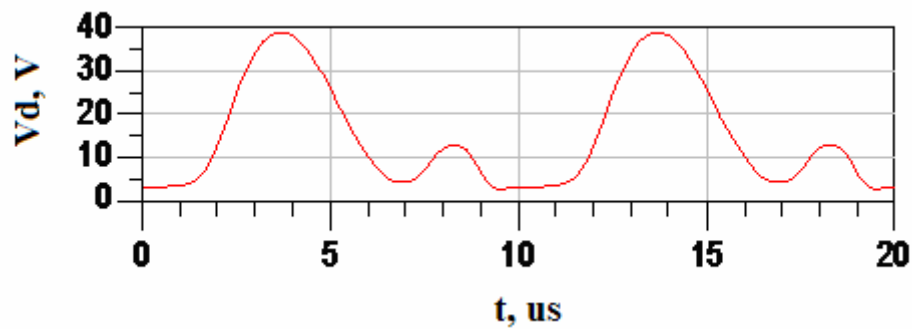
Both [4] and [9] address the method to tune the circuit values of Class E RF power amplifier so that its drain voltage waveform can resemble the ideal one more and therefore the circuit can function toward the optimum performance more. The tuning is mainly focus on the values of  $C_{shunt}$ ,  $C_O$ ,  $L_O$  and  $R_L$  because they affect the waveform shape directly. In addition, the drain supply voltage, the gate bias, the component values in the matching circuits, and those in the tank circuits are also tuned for further improvements in both efficiency and waveform shapes.

Figure 3.10 shows the tuning mechanism for  $C_{shunt}$ ,  $C_O$ ,  $L_O$  and  $R_L$ .



**Figure 3.10: Tuning Methods to Achieve Optimum Drain Voltage Waveform**

The drain voltage waveforms resulted from the simulations of all 17 cases with circuit component values from calculations directly have very similar shape, all look like the one in Figure 3.11.



**Figure 3.11: Drain Voltage Waveform of 100 kHz Case**

Waveform in Figure 3.11 very resembles the one in Figure 3.10. Thus, the following tuning process is employed in order to make the drain voltage more like the optimum one. First of all, the  $C_{shunt}$  and  $C_O$  values are increased gradually in

proportions so that the small peak near the transition will become smaller and smaller and eventually disappears. Then, the  $C_{shunt}$  value is decreased by the amount of  $C_{oss}$  as stated in the Datasheet of the MRF134 transistor [8] to account for its output capacitance. This brings in only a slight change in the waveform. Subsequently, the values of  $L_O$  and  $R_L$  are changed according to the method in Figure 3.10 and the drain DC supply voltage as well as the RFC values is also tuned for higher load output power. Consequently, the output matching network values are varied slightly for better waveform shape. The optimization simulation results are summarized in the next section.

### **3.2.5 Results from Optimization Using Linear Method**

The optimization methods in the previous subsection both increase the efficiency and improve the drain voltage waveform for all 17 cases more or less. The tuning process stops when changing the circuit values any further will not increase the efficiency, nor improve the waveform shape any more. The drain waveforms of both voltage and current for 10 MHz and 150 MHz after circuit optimization are shown in Figure 3.12. Others are listed in Appendix A.2.

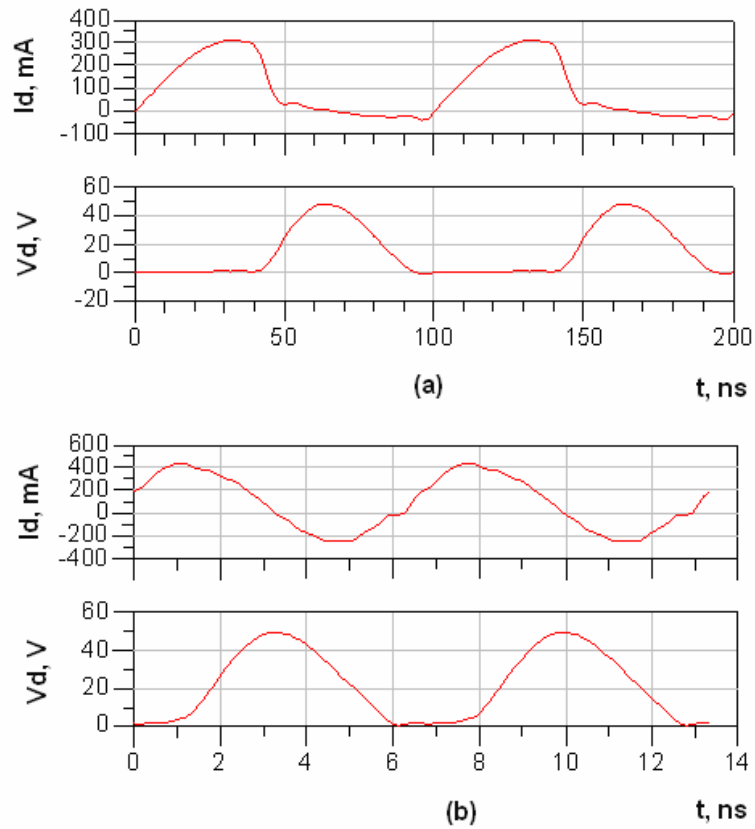


**Figure 3.12: Drain Current and Voltage Waveforms in Time Domain for: (a) 10 MHz Case after Optimization; (b) 150 MHz Case after Optimization**

Even though the waveforms for high frequency, such as 150 MHz, do not resemble the ideals one as in Figure 2.3, especially the drain current which has one third of its period going below zero instead of staying at zero, the efficiency is improved dramatically after optimization. Table 3.3 summarizes the simulation results after optimization for all 17 cases.

**Table 3.3: Optimization Results of 17 Cases Using Linear Design Analysis in ADS Simulations**

$f_o$ (MHz)	$I_{S_H}$ (mA)	$P_{DC}$ (W)	$P_{out}$ (W)	$\eta_d$ (%)	PAE (%)	G (dB)	2 <sup>nd</sup> (dBc)	3 <sup>rd</sup> (dBc)
0.1	109	1.63	1.35	82.44	76.32	11.29	-56.00	-115.34
1	145	2.17	1.73	79.49	74.89	12.37	-57.43	-84.23
10	96	1.44	1.24	86.42	80.79	10.94	-57.80	-48.46
20	121	1.81	1.45	80.20	74.68	11.62	-55.07	-94.22
30	127	1.91	1.52	79.58	74.35	11.82	-53.00	-93.8
40	113	1.69	1.35	79.96	74.05	11.30	-46.57	-62.79
50	111	1.66	1.34	80.53	74.51	11.26	-62.30	-82.20
60	97	1.46	1.18	81.30	74.43	10.73	-53.48	-141.51
70	84	1.26	1.04	82.24	74.32	10.17	-59.43	-82.71
80	109	1.63	1.31	80.24	74.10	11.16	-58.29	-114.43
90	83	1.25	1.03	82.39	74.36	10.13	-52.34	-60.31
100	88	1.32	1.08	82.18	74.60	10.35	-58.74	-126.77
110	82	1.22	1.00	82.14	73.96	10.02	-59.24	-129.59
120	89	1.78	1.44	80.86	75.24	11.58	-69.84	-77.80
130	74	1.56	1.27	81.51	75.09	11.03	-67.52	-67.10
140	73	1.67	1.34	80.25	74.27	11.28	-62.44	-67.32
150	87	1.91	1.55	81.13	75.90	11.91	-84.59	-87.48

Note: 2<sup>nd</sup> and 3<sup>rd</sup> in column 8 and 9 are the 2<sup>nd</sup> and 3<sup>rd</sup> harmonic attenuations, respectively, with respect to the fundamental power measured at the load in ADS.

Table 3.3 reveals that all 17 cases have drain efficiency,  $\eta_d$ , either above 80% or very close to 80% and PAE around 75%. Their major harmonics, 2<sup>nd</sup> and 3<sup>rd</sup> harmonics are at least 45 dBc below the fundamental power. They have very different output powers but all of them have power gain above 10 dB. However, it is harder to get higher efficiency and takes more time to tune the circuit as frequency increases.

Figure 3.13 below is the circuit schematic for 150 MHz case after optimization with the simulation results in Table 3.3. It has the input matching, the gate bias, the drain shunt capacitor, the drain power supply, the  $C_O L_O$  series resonant circuit, the tank circuits for 2<sup>nd</sup> and 3<sup>rd</sup> harmonic suppressions, the output matching and the standard 50  $\Omega$  load. The schematic in Figure 3.13 is in compliance with block diagram for the proposed prototype of Class E RF power amplifier in Figure 2.5.

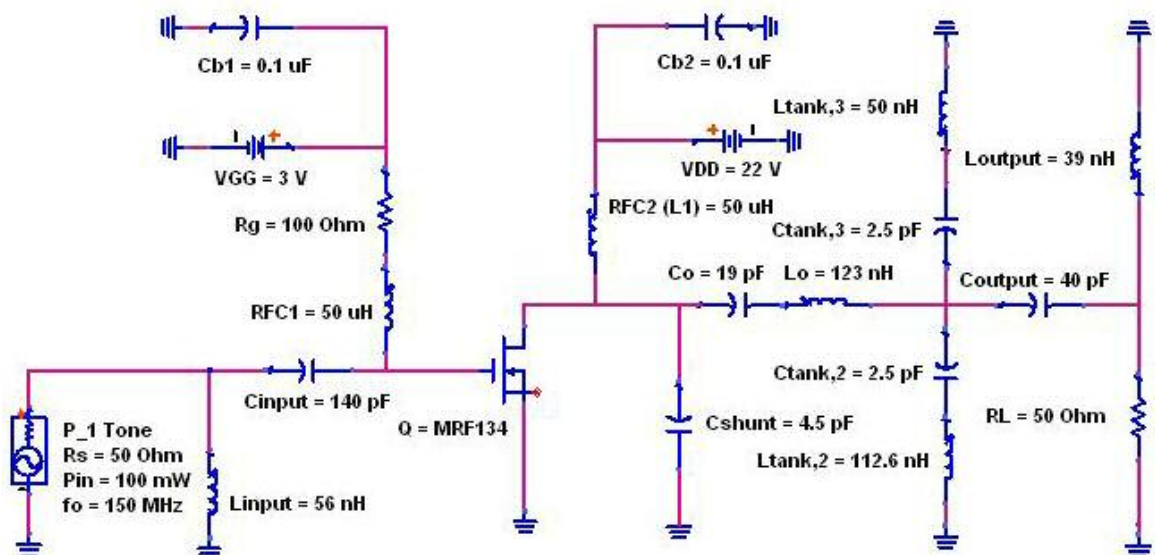


Figure 3.13: Complete 150 MHz Design in Simulation Using Linear Analysis

## **Chapter 4: Class E PA Circuit Design Analysis with Nonlinear Drain Shunt Output Capacitance**

The exact drain shunt capacitance is required for Class E RF power amplifiers to achieve their optimum performances. In Chapter 3,  $C_{shunt}$  is used for this capacitance, which is composed of both external linear capacitance,  $C_{ex,l}$ , and any output capacitance,  $C_{out}$ , from the transistor. This output capacitance is assumed to be linear in the analysis and designs in Chapter 3. However, for most FET transistors,  $C_{out}$  is nonlinear and it becomes more dominant in  $C_{shunt}$  as operating frequency increases and eventually it makes up the entire drain shunt capacitance required for operation. Thus, being able to accurately model the nonlinear capacitance is important for Class E RF power amplifiers, especially those operating in high frequencies. In this chapter, the analysis equations for nonlinear design using MRF134 transistor are derived and the simulation results in ADS for designs with operating frequencies from 10 MHz to 150 MHz with a 10 MHz increment are presented for the comparisons with the linear designs in Chapter 3.

### **4.1 Analysis Equations for Class E Nonlinear Design using MRF134**

Chudobiak is the person who derived the first set of design equations describing the Class E amplifier with a nonlinear shunt capacitance. In his paper [10], he used 0.5 duty cycle and  $m = 0.5$  for the grading coefficient of the nonlinear shunt capacitance, which according to his paper is the external drain shunt capacitance. However, his equations are abstract and inapplicable for

practical designs using power MOSFET, such as MRF134 used in this thesis work.

[11] presents an expression for the nonlinear shunt capacitance which uses data given in most power MOSFET manufacturer's datasheets, called equivalent linear shunt capacitance. It also gives a design procedure of a Class E amplifier with a nonlinear shunt capacitance using the equivalent linear shunt capacitance. However, the procedure proposed in this paper is based on the assumption that the output capacitance of the transistor is the only shunt capacitance; there is no linear external capacitance. It also assumes that the operation has 100% efficiency and uses 50% duty cycle input signals. In this section, the design equations for the Class E RF power amplifiers, whose drain shunt capacitance is composed of both nonlinear  $C_{out}$  and linear  $C_{ex,l}$ , by using MRF134 transistor are derived from [11], and the same assumptions are kept for equation deviations.

Most manufacturers of power MOSFET provide the transistor input, output and reverse transfer capacitances with the notations  $C_{iss}$ ,  $C_{oss}$  (the same as  $C_{out}$  in this thesis), and  $C_{rss}$ , respectively, for the specific measurement conditions, usually

$$V_{DS} = 25 \text{ V}$$

$$V_{GS} = 0 \text{ V}$$

$$f_o = 1 \text{ MHz}$$

It is important to provide the large signal equivalent circuit of a power MOSFET for the understanding of the definitions of these three capacitances.

Any practical MOSFET transistor has the following large signal equivalent

circuit to account for parasitic components [12].

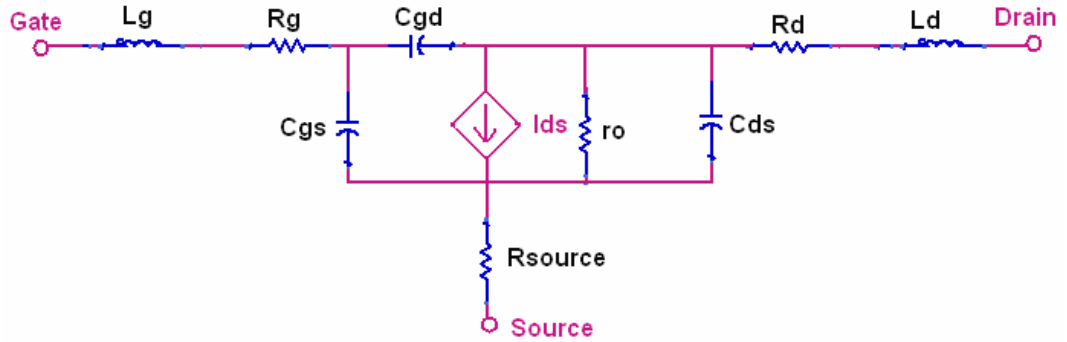


**Figure 4.1: Large Signal Equivalent Circuit of MOSFET Transistors**

In Figure 4.1,  $L_g$  and  $R_g$  are gate parasitic inductance and resistance; similarly,  $R_d$  and  $L_d$  are drain parasitic inductance and resistance and  $R_{source}$  is source parasitic resistance.  $r_o$  is output resistance from channel length modulation.  $C_{gd}$  is gate-to-drain capacitance, which forms the feedback path between those two terminals.  $C_{gs}$  is shunt gate-to-source capacitance and  $C_{ds}$  is shunt drain-to-source capacitance. The following equalities hold for those parasitic capacitances.

$$C_{oss} = C_{ds} + C_{gd} = C_{out} \quad (4.1)$$

$$C_{rss} = C_{gd} \quad (4.2)$$

$$C_{iss} = C_{gs} + C_{gd} \quad (4.3)$$

In Class E amplifier designs, the parasitic components at the gate side,  $L_g$ ,  $R_g$ , and  $C_{iss}$  are taken care by the input matching network.  $C_{rss}$  (i.e.,  $C_{gd}$ ) is much smaller than  $C_{oss}$  so that it can be ignored in the design. It is  $C_{oss}$  that must be considered seriously because its major constituent,  $C_{ds}$ , is transistor  $C_{out}$  at any specific operating conditions.

Transistor MRF134 has 9.7 pF for  $C_{oss}$  of, 7 pF for  $C_{iss}$  and 2.3 pF for  $C_{rss}$ ; all of them are measured at  $V_{DS} = 28$  V instead of 25 V [8]. Because the drain-to-source capacitance,  $C_{ds}$ , changes with respect to the AC drain-to-source voltage,  $V_{ds}$ , in a nonlinear manner, the design equations for MRF134 are slightly different from those in [10].

$$C_{ds} = \frac{C_{jo}}{\left(1 + \frac{v_s}{V_{bi}}\right)^m} \quad (4.4)$$

Equation 4.4 is the classic nonlinear drain-to-source parasitic capacitance derived by Chudobiak [10], in which  $v_s$  is the DC drain-to-source voltage, same as  $V_{DD}$  used in this thesis;  $C_{jo}$  is the capacitance at zero drain supply voltage;  $V_{bi}$  is the built-in potential which ranges from 0.5 V to 0.9 V for MOSFET transistors and  $m$  is the grading coefficient of the diode junction, assumed to be 0.5 in [10]. The modified version of Equation 4.4 is below to fit for the measurement conditions specified in the datasheet of MRF134.

$$C_{ds} = C_{28} = \frac{C_{jo}}{\sqrt{1 + \frac{28}{V_{bi}}}} \quad (4.5)$$

The first circuit element that can be obtained is the load resistance,  $R_L$ , when using the nonlinear method.

$$R_L = \frac{8V_{DD}^2}{(\pi^2 + 4)P_{out}} \quad (4.6)$$

Equation 4.6 calculates the value of load resistance for specified drain DC

supply voltage and desired output power. Once  $R_L$  is known, the linear  $C_{out}$  required for finding the nonlinear value can be obtained as

$$C_{out\_linear} = \frac{8}{2\pi^2 f_o (\pi^2 + 4) R_L} \quad (4.7)$$

And the nonlinear output capacitance  $C_{out}$  is

$$C_{out} = C_{out\_linear} (0.0781 + \sqrt{0.0061 + 0.0239V_{DD}}) \quad (4.8)$$

Equation 4.8 is derived for  $V_{bi} = 0.7$  V. The linear external capacitance will then be the difference between the  $C_{shunt}$  from Mr. Sokal's analysis and  $C_{out}$  in Equation 4.8 above.

$$C_{ex,l} = C_{shunt} - C_{out} \quad (4.9)$$

In addition, the value of  $L_O$  can be found if  $R_L$  and  $Q_L$ , the loaded quality factor, are both known.

$$L_O = \frac{R_L Q_L}{2\pi f_o} \quad (4.10)$$

In Chapter 3, the values of RF chokes are picked randomly as long as they act as open circuits at  $f_o$ . In nonlinear analysis, their values are fixed and directly and inversely proportional to the load resistance and the operating frequency, respectively.

$$RFC = 2\left(\frac{\pi^2}{4} + 1\right) \frac{R_L}{f_o} \quad (4.11)$$

The equation to find the value  $C_O$  in the series resonant circuit is simple as in Equation 4.12.

$$C_o = \frac{1}{2\pi f_o (R_L Q_L - X)} \quad (4.12)$$

Where, X is the excess reactance in the series  $L_o C_o$  resonant circuit. When  $L_o$  and  $f_o$  are known, X is simply the difference between  $L_o$  and the inductance which combining with  $C_o$  resonates at  $f_o$ .

$$X = 2\pi f_o \left( L_o - \frac{1}{(2\pi f_o)^2 C_o} \right) \quad (4.13)$$

Equation 4.13 and 4.14 together can not be used to solve  $C_o$ . Thus, another expression for X independent of  $C_o$  must be known. [11] has a derivation of X other than Equation 4.13. The results are summarized here.

$$X = R_L \tan(\varphi_1 - \varphi) \quad (4.14)$$

Where,  $\varphi$  is the phase difference between input and output signals of a Class E RF PA. It is a constant with the value of -0.567 rad under the assumptions of 100% efficiency and 50% duty cycle operation.  $\varphi_1$  is a complicated expression in terms of  $R_L$ ,  $f_o$ ,  $C_{jo}$ , and  $V_{bi}$ , which is assumed to be 0.7 V. It is in the unit of radians.

$$\varphi_1 = \tan^{-1} \frac{2[2\pi f_o V_{bi} C_{jo} R_L (6\pi^2 - 48)(\pi^2 + 4) + 8\pi V_{DD}]}{12(2\pi)^2 f_o V_{bi} C_{jo} R_L (\pi^2 + 4) + 8V_{DD} (5\pi^2 - 32)} \quad (4.15)$$

The combination  $2\pi f_o C_{jo} R_L$  in Equation 4.15 can be found as

$$2\pi f_o C_{jo} R_L = \frac{12V_{bi} + \sqrt{6V_{bi} (24V_{bi} - 24\pi^2 V_{DD} + \pi^4 V_{DD}) + 9\pi^2 (\pi^2 + 4)V_{bi} V_{DD}}}{3\pi (\pi^2 + 4)V_{bi}} \quad (4.16)$$

Thus, Equation 4.15 simplifies  $\varphi_1$  expression in Equation 4.14 in terms of  $V_{DD}$

and  $V_{bi}$  only.

## 4.2 Circuit Design by Using Nonlinear Analysis

The nonlinear analysis taking account of both nonlinear output capacitance of the transistor and the linear external drain capacitance is commonly used in the contemporary designs, especially those operating at frequencies greater than 900 MHz, at which the nonlinear output capacitance is comparable to the linear external one so that the latter will not be connected in the design at all.

Once the values of supply voltage  $V_{DD}$ , the loaded quality factor of series resonant circuit  $Q_L$ , the operating frequency  $f_o$ , and the desired output power  $P_{out}$  are specified for a particular design using MRF134 transistor, the corresponding circuit component values for  $R_L$ , RFC,  $C_O$ ,  $L_O$  and drain shunt capacitances for both internal nonlinear  $C_{out}$  and external linear  $C_{ex,l}$  can be found using the design equations in the previous section for the assumption  $V_{bi} = 0.7$  V, 100% efficiency, i.e., ideal operation, and 50% duty cycle.

Fifteen cases of design with operating frequencies from 10 MHz to 150 MHz with 10 MHz increment are simulated in ADS using the nonlinear analysis. Except their respective  $f_o$ , all of them have the same operating conditions of  $V_{DD} = 20$  V,  $V_{GG} = 3$  V,  $P_{out} = 2.6$  W,  $P_{in} = 100$  mW,  $Q_L = 10$ , and  $V_{bi} = 0.7$  V. Due to same values of  $V_{DD}$  and  $P_{out}$ , they have same  $R_L$  according to Equation 4.6. Other circuit element values are different because of different  $f_o$  since all other elements,  $C_{out}$ ,  $C_{out\_linear}$ ,  $C_O$ ,  $L_O$  and RFC, are all frequency dependent corresponding to

Equation 4.7 to 4.12.

Similar to the linear method in Chapter 3, waveforms become more and more non-ideal as operating frequency increases and drain current waveforms go down below zero more. Unlike the linear designs which have PAEs all above 60% and almost all  $\eta_d$  above 65% with the circuit values from calculations directly, the efficiencies drop a lot for nonlinear designs without circuit optimization. Thus, optimization is applied to all 15 nonlinear cases for higher efficiencies and better drain voltage and current waveforms.

**Table 4.1: Calculation Results of 15 Cases Using Nonlinear Analysis**

$f_o$ (MHz)	$C_{out}$ (pF)	$C_{shunt}$ (pF)	$C_o$ (pF)	$L_o$ ( $\mu$ H)	RFC ( $\mu$ H)
10	25.48	39.82	20.61	14.12	61.54
20	12.74	19.91	10.31	7.06	30.77
30	8.49	13.27	6.78	4.71	20.51
40	6.37	9.95	5.15	3.53	15.39
50	5.10	7.96	4.12	2.82	12.31
60	4.25	6.64	3.44	2.35	10.26
70	3.64	5.69	2.94	2.02	8.79
80	3.19	4.98	2.58	1.77	7.69
90	2.83	4.42	2.29	1.57	6.84
100	2.55	3.98	2.06	1.41	6.15
110	2.32	3.62	1.87	1.28	5.59
120	2.12	3.32	1.72	1.18	5.13
130	1.96	3.06	1.59	1.09	4.73
140	1.82	2.84	1.47	1.01	4.40
150	1.70	2.65	1.37	0.94	4.10

Similarly to linear designs, Table 4.1 exhibits that the values of  $C_{out}$  are inversely proportional to  $f_o$ , so are values of  $C_{shunt}$ ,  $C_o$ ,  $L_o$  and RFC. This phenomenon is in accordance with their individual design Equations in section 4.1. Table 4.1 has lower capacitor values but higher inductor values than Table 3.1 due to that the two sets of designs are at different operating conditions. However, if

these conditions are kept the same, the same thing also occurs. This can be verified by plotting in conditions in Matlab codes in Appendix A.4 and A.5 for circuit value calculations of both analysis methods.

In addition, Table 4.1 shows that the capacitor values are smaller than those used for the method in Chapter 3 for the same  $f_o$ , but inductor values are much bigger. This is caused by the higher  $Q_L$  value in design. In Chapter 3,  $Q_L = 5$  is used and it is 10 in the design method of this chapter, which is the lowest allowable loaded quality factor value for  $L_O C_O$  resonant circuit in order to have a sinusoidal waveform at the load output with the same frequency as  $f_o$  for each case. Higher inductance brings difficulties in circuit implementation and function, which will be addressed in the next chapter.

### **4.3 Optimization for 15 Cases by Using Nonlinear Method**

The same optimization method as addressed in Chapter 3 is used to increase the efficiency and improve the waveform shapes for nonlinear designs. Again, it takes more time to tune the circuit values for higher frequencies. Even though the efficiencies raise a lot, the waveforms, especially the drain current waveforms, still differ from the ideal one significantly for high frequencies. They just do not stay at zero during ON state.

The drain current and voltage waveforms for both 10 MHz and 150 MHz nonlinear cases after optimization are shown in Figure 4.2 and the complete simulation results after optimization for all 15 cases are listed in Table 4.2.

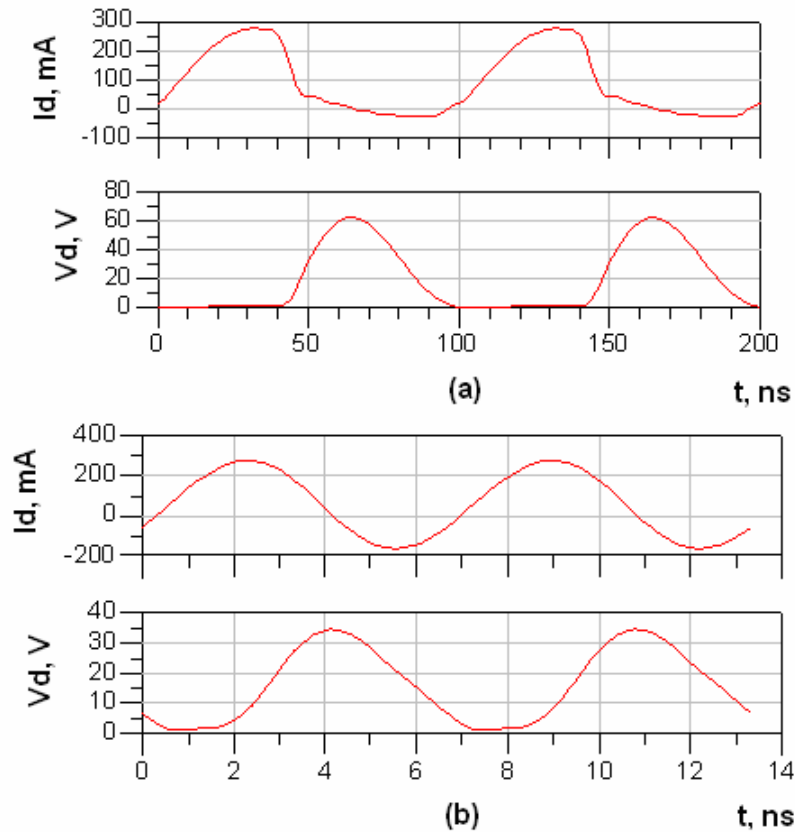


**Figure 4.2: Drain Current and Voltage Waveforms for Nonlinear Designs after Circuit Optimization: (a) 10 MHz; (b) 150 MHz**

Waveforms in Figure 4.2 are very similar to those in Figure 3.12. There is even the same change tendency for both analysis methods for  $f_0$  changes from 10 MHz to 150 MHz.

Even though a different method is used compared to the one in Chapter 3 and hence the corresponding circuit component values are totally different for the same  $f_0$ , the output waveforms are all sinusoid at the frequency equal to  $f_0$  for both nonlinear and linear methods. This is guaranteed by the design of the  $L_0C_0$  series resonant circuit at the load network. Figure 4.3 shows the output voltage and current waveforms for 10 MHz and 150 MHz using both analysis methods.

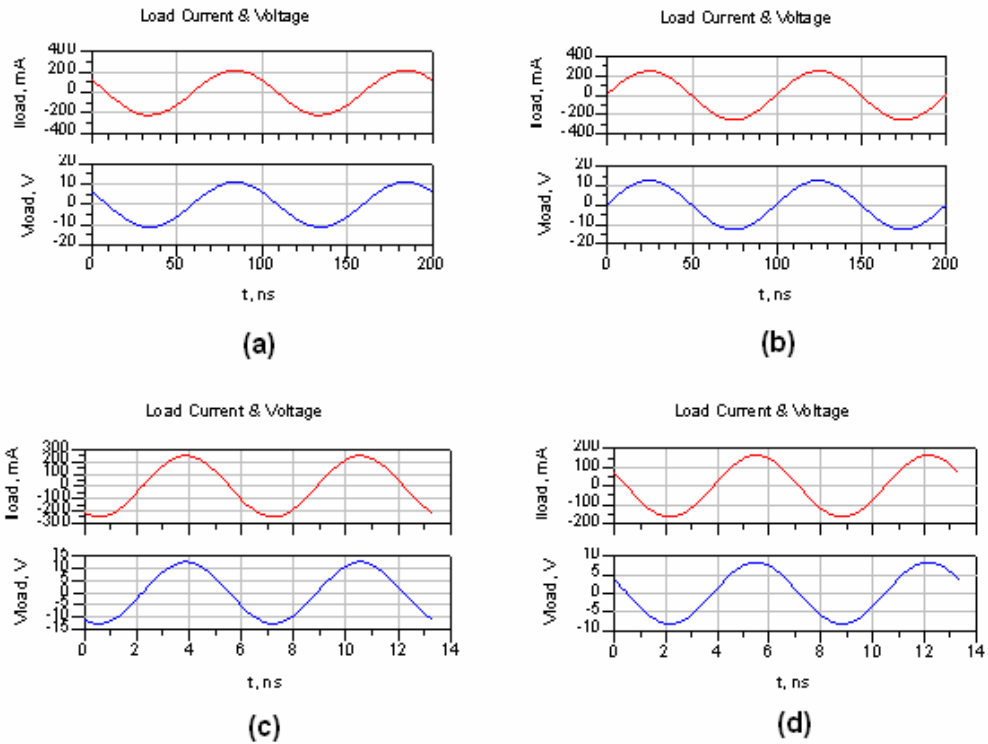


**Figure 4.3: Load Current and Voltage Waveforms for: (a) 10 MHz Linear; (b) 10 MHz Nonlinear; (c) 150 MHz Linear; (d) 150 MHz Nonlinear**

Table 4.2 shows that drain efficiencies for 15 cases after optimization are all above 77.5%, with 150 MHz having the lowest value; for  $f_0$  less than 40 MHz,  $\eta_d$  is even either very close or greater than 90%. This is not the case in the linear design as in Table 3.3 in Chapter 3, whose 17 cases have  $\eta_d \geq 80\%$ . In addition, the PAE for nonlinear cases are all above 70% and again the lowest value, 71.14%, is associated with 150 MHz. In this aspect, linear methods result in  $PAE \geq 74\%$ ; thus, it is a little bit more efficient overall.

**Table 4.2: Optimization Results of 15 Cases Using Nonlinear Analysis in ADS Simulations**

$f_o$ (MHz)	$I_{S_H}$ (mA)	$P_{in}$ (mW)	$P_{DC}$ (W)	$P_{out}$ (W)	$\eta_d$ (%)	PAE (%)	G (dB)	2 <sup>nd</sup> (dBc)	3 <sup>rd</sup> (dBc)
10	58	100	1.17	1.08	92.21	84.93	10.32	-44.95	-74.03
20	43	50	0.86	0.80	93.05	87.25	12.06	-44.83	-72.09
30	45	50	0.90	0.83	91.31	85.88	12.17	-45.44	-73.20
40	51	50	1.03	0.91	89.78	84.84	12.60	-48.50	-71.99
50	62	50	1.24	1.07	86.29	82.27	13.32	-51.48	-72.95
60	65	50	1.31	1.11	84.76	80.94	13.45	-113.84	-50.98
70	66	100	1.31	1.14	86.63	79.01	10.56	-80.49	-49.89
80	58	50	1.16	0.97	83.62	79.30	12.87	-119.63	-49.86
90	53	50	1.07	0.89	83.10	78.42	12.49	-85.41	-52.57
100	79	100	1.59	1.33	83.71	77.42	11.24	-83.71	-50.61
110	70	100	1.4	1.17	83.71	76.57	10.69	-131.35	-51.18
120	50	50	0.84	0.68	80.47	74.54	11.33	-68.90	-53.12
130	51	50	0.82	0.65	79.65	73.52	11.14	-79.61	-53.10
140	91	100	1.82	1.43	78.41	73.25	11.54	-89.46	-54.03
150	49	50	0.78	0.60	77.57	71.14	10.81	-76.17	-54.92

Note: 2<sup>nd</sup> and 3<sup>rd</sup> in column 9 and 10 are the 2<sup>nd</sup> and 3<sup>rd</sup> harmonic attenuations, respectively, with respect to the fundamental power measured at the load in ADS.

## **Chapter 5: Design Implementation and Testing**

### **5.1 Component Selection and PCB Implementation**

For the theoretical designs in Chapter 3 and 4, only the transistor model is fixed, which is MRF134 from Motorola; all other circuit components, such as inductors, resistors and capacitances, are all ideal one in simulation. For the actual design at the lab, both resistors and capacitors are 0805 size surface mount components from Digi-key. Sizes of 0805, 1206, 1008 and 1812 are used for inductors and only those from CoirCraft are employed. They are from series 0805HQ, 0805 HT, 1008HT, 1008HQ, 1008CS, 1008HS, 1206CS, and 1812FS.

There are three kinds of PCB boards fabricated, Class A, Class E for 10 MHz and for 150 MHz designs. The layouts are generated in Altium Designer using Protel software. All of them are two layer boards with signal (i.e. power) layout on the top and ground layout on the bottom. The sizes for Class A, Class E at 10 MHz and 150 MHz are listed below.

Class A: 3300 mil X 1400 mil (i.e., 3.3 in X 1.4 in)

Class E at 10 MHz: 2500 mil X 1500 mil (i.e., 2.5 in X 1.5 in)

Class E at 150 MHz: 2900 mil X 1600 mil (i.e., 2.9 in X 1.6 in)

The final layouts are shown in Figure 5.1, 5.2 and 5.3.

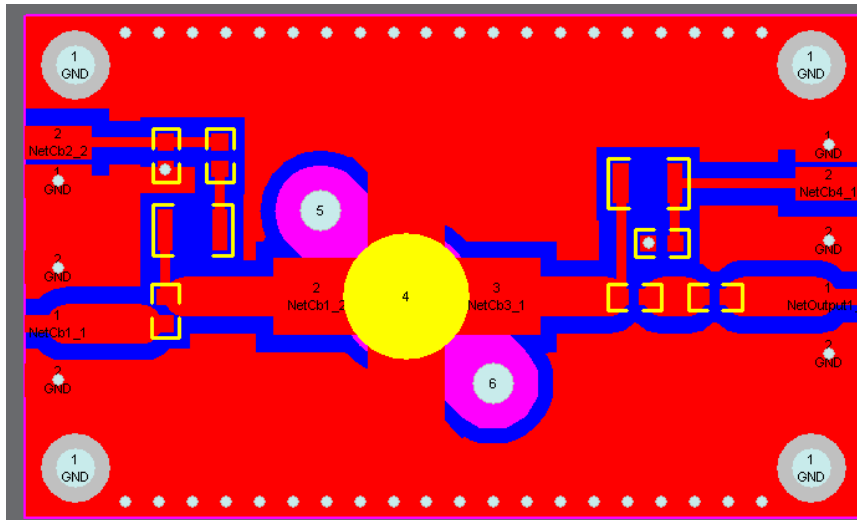


Figure 5.1: PCB Layout for Class A RF Power Amplifier Design

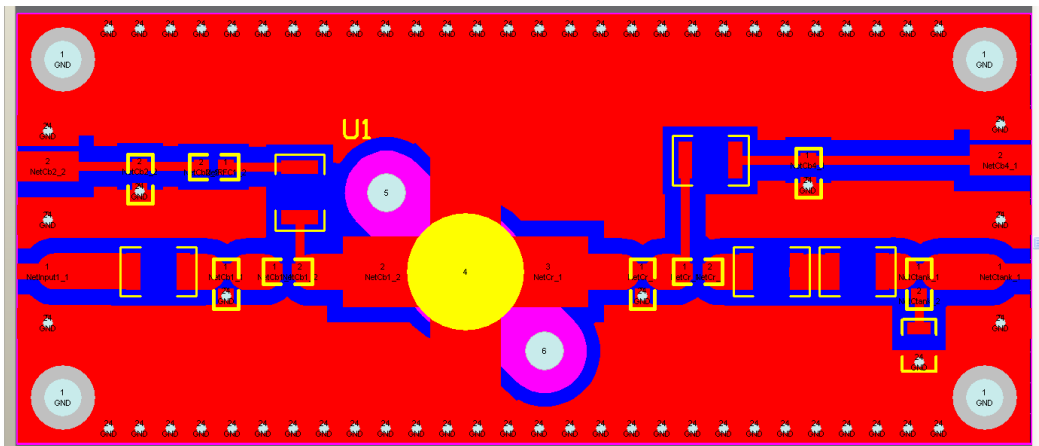


Figure 5.2: PCB Layout for Class E RF Power Amplifier Design at 10 MHz

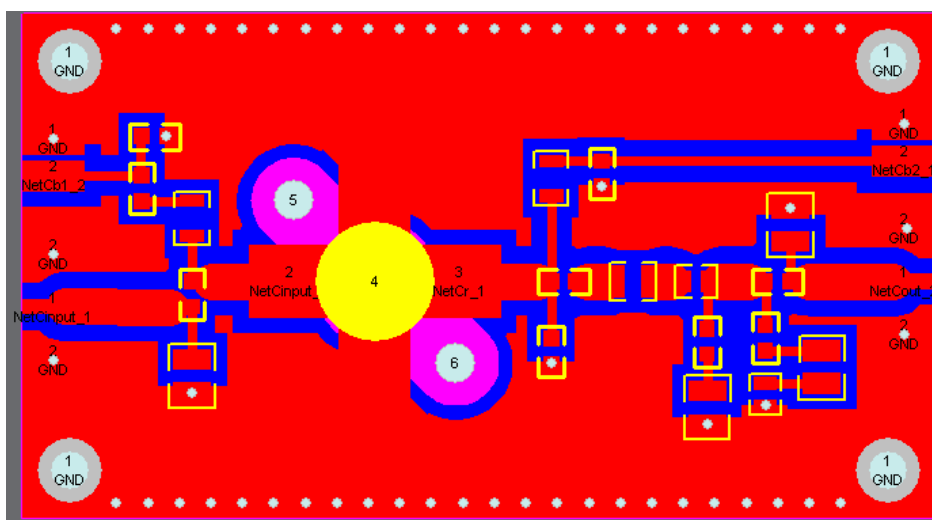
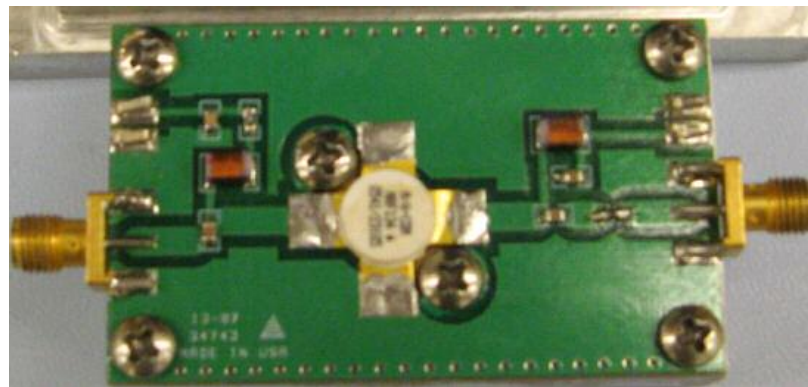
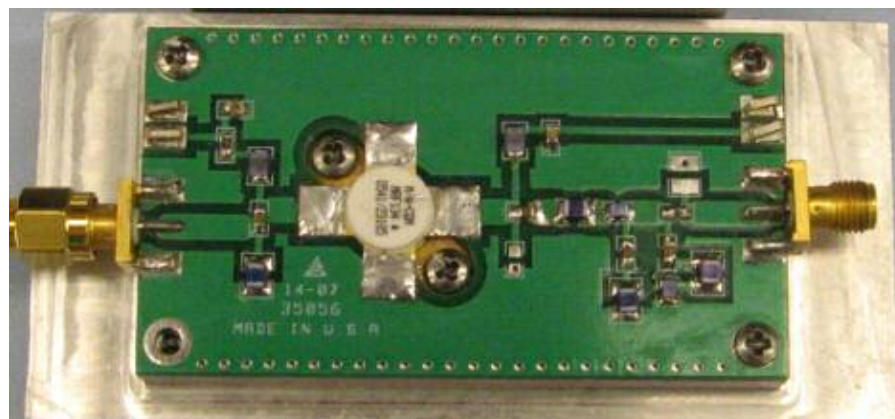


Figure 5.3: PCB Layout for Class E RF Power Amplifier Design at 150 MHz

The boards are manufactured by Proto-Express in California with the place where the transistor sits is milled out. There is an aluminum pad attached to each board, functioning as heat sink for the transistor. The heat sinks are created at CReSIS' mechanical lab by Mr. Dennis Sundermeyer. The circuit components are soldered onto the boards using soldering irons. The boards are then ready for testing. The final boards for Class A and 150 MHz Class E designs are shown in the pictures below.



**Figure 5.4: PCB Board for Class A PA**



**Figure 5.5: PCB Board for 150 MHz Class E RF PA**

## **5.2 Experimental Setting for Testing**

The designs are tested with the experimental setting as in the following block

diagram.

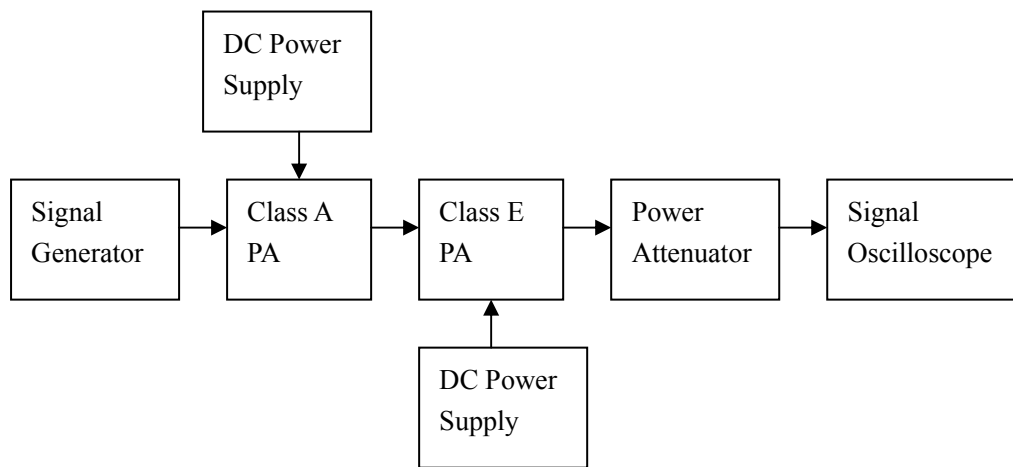


**Figure 5.6: Block Diagram of Experimental Setting**

The 6060A Synthesized RF Signal Generator is used to output either a 10MHz or 150 MHz signal with the usable amplitude in the range of 14 dBm to 19 dBm as the input to a Class A power amplifier, which is solely designed for the usage of this thesis work because all signal generators at the CReSIS's lab can provide a sinusoidal signal no greater than 20 dBm in amplitude. The Class A PA amplifies the signal, and outputs a new one with the same frequency. Its output range from 200 mW to 500 mW is used as desired input range for the following Class E PA, which amplifies the signal further. The resultant larger signal is first passed through a 20 dB 50 Watts power attenuator and then displayed by a signal oscilloscope, which is a LeCroy Wave Master 8600 A 6 GHz Oscilloscope. The attenuator is required since all oscilloscopes at the lab can only stand  $\pm 4$  V peak to peak signal at 50  $\Omega$  coupling. Last, two DC power supplies, Agilent E3630A Triple Output DC Power Supplies, are employed to support the two power

amplifiers respectively. The actual lab setting is shown in the picture below.

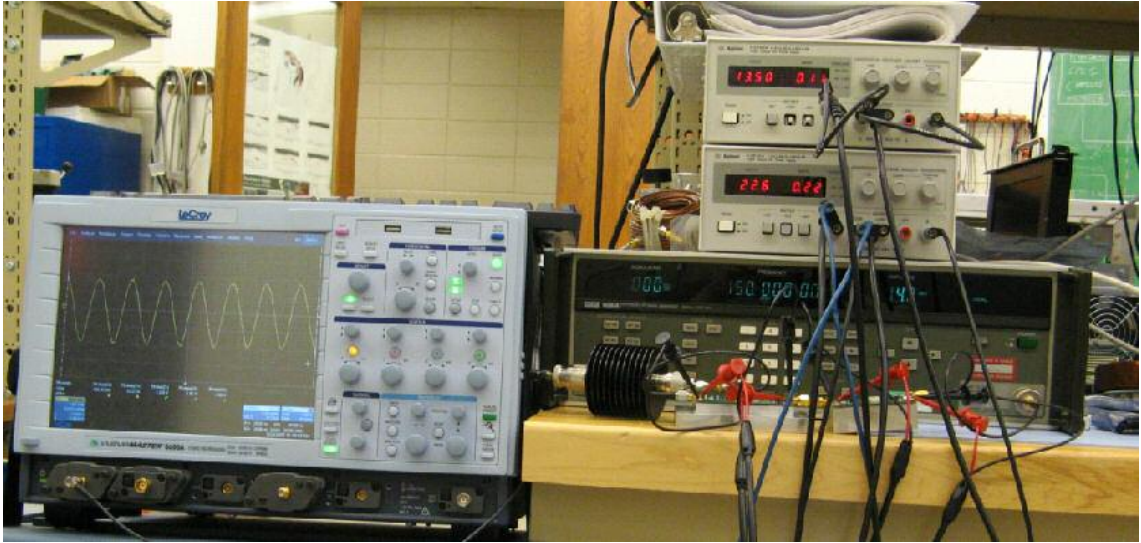


**Figure 5.7: Actual Lab Experimental Setting**

The frequency and the RMS voltage of the output signal from the power attenuator are measured by the oscilloscope and the voltage waveform shape is also captured. Since  $50 \Omega$  DC coupling is used throughout the testing system, the actual output power of the Class E RF power amplifier,  $P_{out,act}$ , is calculated as

$$P_{out,act} = \frac{(10VRMS_{out,att})^2}{50} \quad (5.1)$$

Where  $VRMS_{out,att}$  is the output voltage in RMS form at the output of the power attenuator. Because the attenuation is 20 dB in power, there is a factor of 10 reductions in voltage correspondingly. Thus,  $VRMS_{out,att}$  must multiply by 10 in order to find the RMS voltage at the output of the amplifier. Then,  $P_{out,act}$  is found using popular Ohm's Law as in Equation 5.1, in which the denominator is the load resistance, the standard  $50 \Omega$  associated with the RF SMA connectors.

### 5.3 Initial Testing

Initially, Class A PA is not used in the testing so that the signal generator provides the input to the Class E PA directly. Class E PA at 10 MHz and 150 MHz both using linear and the latter one using nonlinear are tested. The theoretical designs require 100 mW (20 dBm) for both 10 MHz linear and nonlinear cases and 50 mW (17 dBm) for 150 MHz nonlinear design. However, the signal generator used can only output signals with amplitude up to 19 dBm. Thus, it is used instead of 20 dBm. The testing conditions for each design and the results are summarized in Table 5.1 and 5.2.

**Table 5.1: Initial Testing Conditions**

Design Type	Input Power (dBm)	Gate Bias (V)	Drain Supply (V)
10 MHz Linear	20	3	15
150 MHz Linear	20	3	22
150 MHz Nonlinear	17	3	20

**Table 5.2: Measurements and Results of Initial Testing**

Design Type	Output Frequency (MHz)	Measured $I_D$ (mA)	$V_{RMS_{out,att}}$ (V)	$P_{out,att}$ (W)	Drain Efficiency (%)
10 MHz Linear	10	60	0.408	0.333	37
150 MHz Linear	150	115	0.616	0.759	30
150 MHz Nonlinear	150	93	0.540	0.583	31.34

The initial testing results are way different from those theoretical values in Chapter 3 and 4. Not only the output power is much smaller, the drain efficiency

is also much lower. There are two major reasons for these big discrepancies. The equivalent series resistance (ESR) of the inductors on the boards are not considered into the designs in Chapter 3 and 4 and the amplifier input signals have too small amplitude to drive the switch on and off, especially for high frequency operation.

When using the real inductor models from the CoilCraft in the simulations for the three cases listed about, the theoretical results are summarized in Table 5.3.

**Table 5.3: Simulation Results of Initial Testing Cases with Real Inductor**

<b>Design Type</b>	<b>Simulated <math>I_D</math> (mA)</b>	<b><math>P_{out}</math> (W)</b>	<b>Drain Efficiency (%)</b>
10 MHz Linear	110	0.621	37.72
150 MHz Linear	87	1.201	62.512
150 MHz Nonlinear	77	0.61	39.788

Comparing values in Table 5.3 with Table 5.2, the drain efficiencies for 10 MHz linear and 150 MHz nonlinear cases are very similar but it is different for linear 150 MHz. This is because the inductor values at 10 MHz are much bigger than those at 150 MHz, thus, the associated ESRs are much bigger. In addition,  $L_O$  in 150 MHz nonlinear case is almost 1  $\mu$ H, whose ESR is comparable to the 50  $\Omega$  load resistance at that frequency. In simulation, the linear 150 MHz has much higher  $\eta_d$ . The possible cause is the insufficient input power used to drive the transistor; the impact from its ESRs are small because its inductor values are all less than 390 nH. These two reasons will be addressed in the following two

sections.

#### 5.4 ESR of Inductors and Its Significance in Class E RF PA Designs

Most manufacture's datasheet of inductors only provides the maximum ESR at DC, named as  $DCR_{max}$ . In fact, ESR increases as frequency goes up and very dramatically for high inductance and it is at its minimum value at DC. ADS is able to simulate the frequency-dependant behavior of Coilcraft RF surface mount inductors from 1 MHz to the upper frequency limit specified on the datasheet by using the lumped-element (SPICE) models provided by Coilcraft.

There are two kinds of lumped-element models for the inductors used on the designs. Among the inductor series mentioned in section 5.1, the 1812FS series has a different model than all other ones. Figure 5.8 and 5.9 show the model schematics [13] and [14].

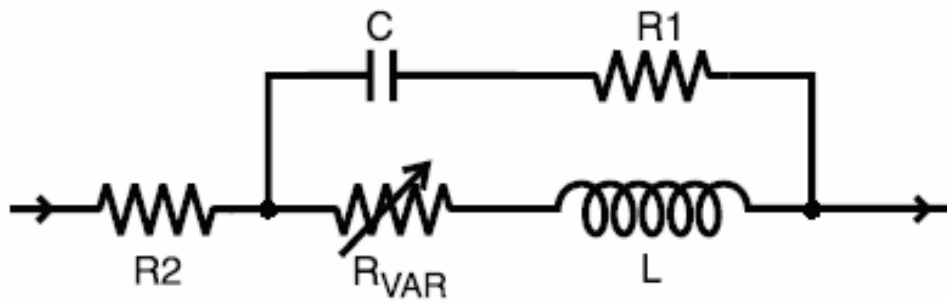


**Figure 5.8: Lumped-Element Models of CoilCraft RF Inductors for Series other than 1812FS, 0805LS, 0603LS and 0402AF.**

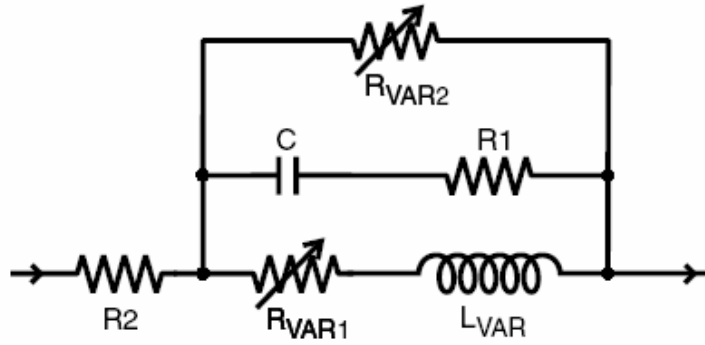


**Figure 5.9: Lumped-Element Models of CoilCraft RF Inductors with Series 1812FS, 0805LS, 0603LS and 0402AF.**

In Figure 5.8 and 5.9,  $R_{VAR}$  and  $R_{VAR1}$ ,  $R_{VAR2}$  are frequency-dependent resistances related to the skin effect for both models and they are calculated from

$$R_{VAR} = k\sqrt{f} \quad (5.2)$$

$$R_{VAR1} = k1\sqrt{f} \quad (5.3)$$

$$R_{VAR2} = k2\sqrt{f} \quad (5.4)$$

In Figure 5.9,  $L_{VAR}$  is the frequency-dependent inductance and is calculated from

$$L_{VAR} = k3 - k4 \log(k5f) \quad (5.5)$$

All values of  $k$ ,  $k1$ ,  $k2$ ,  $k3$ ,  $k4$ ,  $k5$ ,  $R1$ ,  $R2$ ,  $C$  and  $L$ , as well as the upper limit of the operating frequencies for each inductor model are provided by the Coilcraft. Then, using the schematics in Figure 5.8 and 5.9 and those variables and constants in ADS, the ESR value for a specific frequency of an actual Coilcraft inductor can be found by connecting the two open ports each with a  $50 \Omega$  terminator and then plotting the S-parameters on Smith Chart.

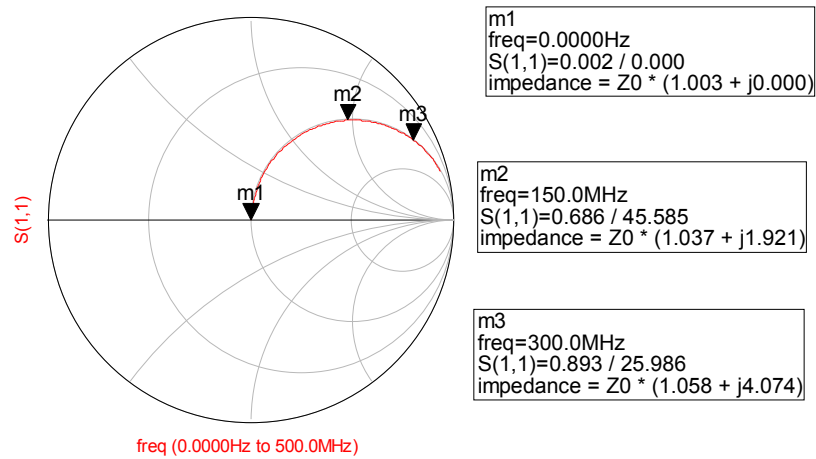


Figure 5.10: S(1,1) of 100 nH RF Inductor in 1008HQ Series of CoilCraft

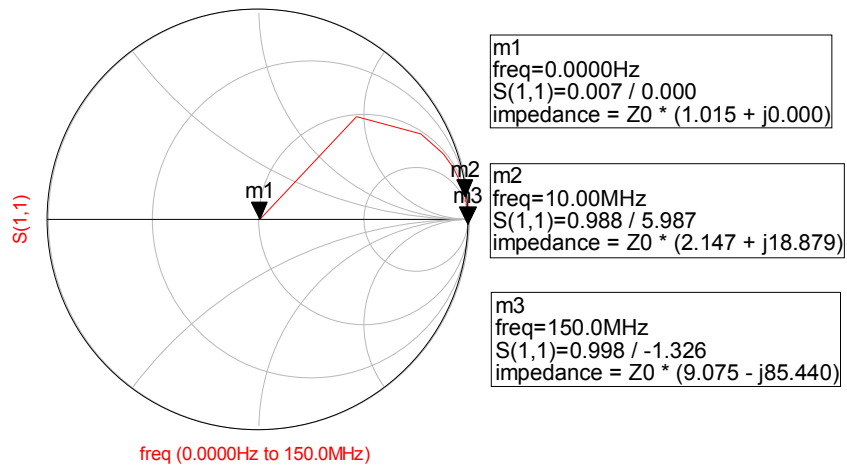


Figure 5.11: S(1,1) of 15 μH RF Inductor in 1812FS Series of CoilCraft

Figure 5.10 and 5.11 are the S(1,1) plots in the Smith Chart format for 100 nH and 15 μH from 1008HQ and 1812FS series of CoilCraft, respectively. As a matter of fact, the circuits in Figure 5.8 and 5.9 are reciprocal; S(1,1) plot is the same as S(2,2) so is S(1,2) to S(2,1). This should be expected due to the fact inductors have no polarities. ADS provides Impedance for markers at any frequency, freq, in the form of

$$impedance = Z0(R \pm jX) \quad (5.6)$$

Where,  $Z_0$  is the  $50 \Omega$  and the difference between the product of  $Z_0$  and  $R$  and  $R$  gives the ESR at that frequency as

$$ESR_{freq} = Z_0 R - Z_0 \quad (5.7)$$

Thus, the ESR values for frequencies at the marker places in Figure 5.10 and 5.11 calculated using Equation 5.7 are summarized in Table 5.4 and 5.5.

**Table 5.4: ESRs of 100 nH RF Inductor in 1008HQ Series of CoilCraft**

Frequency (MHz)	ESR ( $\Omega$ )
0	0.15
150	1.85
300	2.90

**Table 5.5: ESRs of 15  $\mu$ H RF Inductor in 1812FS Series of CoilCraft**

Frequency (MHz)	ESR ( $\Omega$ )
0	0.75
10	57.35
150	403.75

According to the datasheet, the values of  $DCR_{max}$  are  $0.16 \Omega$  and  $0.75 \Omega$ , which are very close to values from simulation, and the upper operating frequencies are 1.4 GHz and 100 MHz for 100 nH and 15  $\mu$ H inductors in Table 5.4 and 5.5, respectively. Thus, ESR value at 150 MHz for 15  $\mu$ H from ADS simulation is not valid.

Comparing values in these two tables, the ESR for 15  $\mu$ H increases much more dramatically than 100 nH. For frequency changes from DC to 10 MHz, ESR goes up by a factor more than 50 for 15  $\mu$ H and the increase is only a factor of 12.33 for 100 nH with the frequency varies from DC to 150 MHz. This

phenomenon plays a significant role for low frequency designs with high inductances.

At both 10 MHz linear and nonlinear Class E RF PA designs, inductances higher than 10  $\mu\text{H}$  are used at the  $L_O C_O$  series resonant circuit and several micro Henry is needed for the output matching networks. Consequently, there is huge power dissipation by those ESRs; therefore, the power delivered to the output load will be reduced considerably, which in turns degrades the efficiencies exceptionally when the DC power is kept the same.

However, ESRs do not decrease the efficiencies as much for higher frequency operations such as 150 MHz Class E RF power amplifier design because its required inductor values are all less than 1  $\mu\text{H}$ . The weak input signal causes the 150 MHz designs have very low efficiencies. The modifications in testing will be addressed in next section.

### **5.5 Changes in Testing and New Results**

There are two major changes on both circuits and testing setting made. First of all, the magnitudes of the input signals to the amplifiers are increased from the initial range 14 dBm-19 dBm to 20 dBm-27 dBm. This boosts the efficiencies by more than a factor of 2; thus, the drain efficiencies now can reach higher than 60%. The 6060A Synthesized RF Signal Generator can only output a sinusoidal signal with magnitude up to 19 dBm. Thus, a Class A PA is used to generate the desired input signals as in Figure 5.6. Its schematic is shown in Figure 5.12 and its testing

results at lab are summarized in Table 5.6.

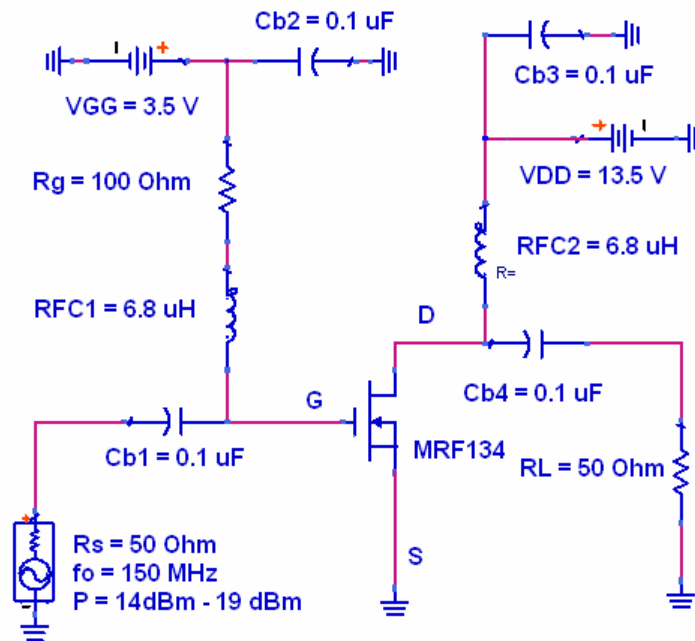


Figure 5.12: 150 MHz Class A RF Preamplifier

Table 5.6: Testing Results of 150 MHz Class A Preamplifier in Figure 5.12

$P_{in}$ (dBm)	$I_D$ (A)	$P_{out}$ (mW)	$G$ (dB)	$\eta_d$ (%)
14	0.11	331	11.2	22.3
15	0.12	387	10.88	23.89
16	0.13	440	10.43	25.07
17	0.14	502	10.04	26.56

After tuning the actual circuit values at the lab slightly, the linear design for the best results at 150 MHz is obtained, whose schematic is in Figure 5.13 with information for the inductors used summarized in Table 5.7.

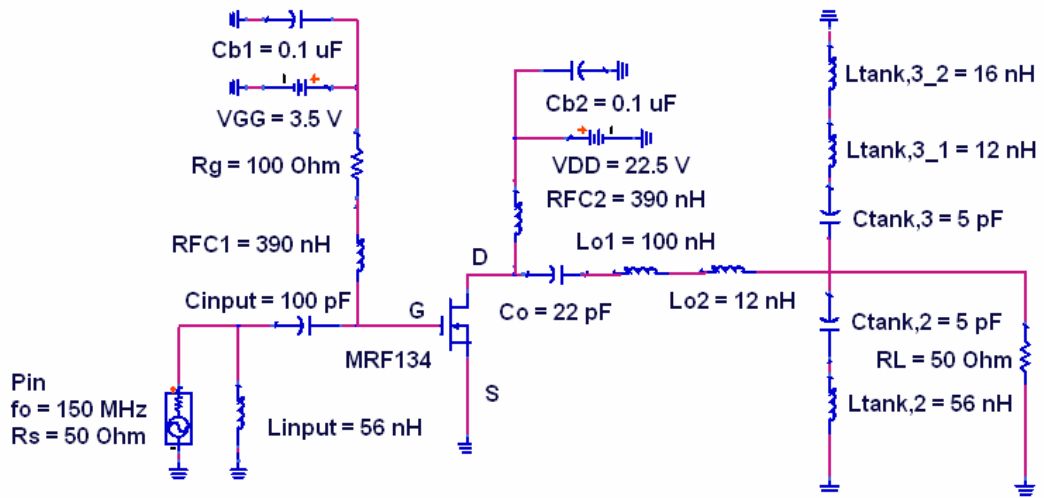


Figure 5.13: Linear 150 MHz Design Resulting in Best Measurements

Table 5.7: Inductor Types and  $DCR_{max}$  in Circuit of Figure 5.13

Inductor Names	Values (nH)	Coilcraft Series #	$DCR_{max}$ ( $\Omega$ )	$ESR_{150MHz}$ ( $\Omega$ )
$L_{input}$	56	1008HQ	0.12	0.95
$RFC_1$	390	1008HS	1.12	5.85
$RFC_2$	390	1008HS	1.12	5.85
$L_{O1}$	100	1008HQ	0.16	1.85
$L_{O2}$	12	0805HQ	0.045	0.35
$L_{tank,2}$	56	1008HQ	0.12	0.95
$L_{tank,3\ 1}$	12	1008HQ	0.06	0.3
$L_{tank,3\ 2}$	16	0805HQ	0.06	0.4

Table 5.7 shows that ESR values for the inductors used in the best design are all less than 6  $\Omega$  at 150 MHz. The biggest values are associated with  $RFC_1$  and  $RFC_2$ , which are 1.12  $\Omega$  at DC and 5.85  $\Omega$  at 150 MHz. However, for RF chokes, only DCR matters. There are two boards for the design in Figure 5.13 created and tested with results in Table 5.8.

**Table 5.8: Best Testing Results Associated with Design in Figure 5.13**

<b>Boards</b>	<b>P<sub>in</sub> (mW)</b>	<b>I<sub>D</sub> (A)</b>	<b>VRMS<sub>out,att</sub> (Vrms)</b>	<b>P<sub>out,act</sub> (W)</b>	<b>η<sub>d</sub> (%)</b>	<b>G (dB)</b>
S1	440	0.24	1.327	3.522	65.22	9.033
S1	331	0.23	1.300	3.380	65.31	10.091
S3	502	0.22	1.312	3.443	69.55	8.379
S3	331	0.22	1.288	3.318	67.03	10.011

According to Table 5.8, the highest drain efficiency achieved is 69.55% but its power gain is smaller than other three cases as a tradeoff. The optimum case will be board S1 which results in a 65.31% of drain efficiency and 10.09 dB of power gain when 0.331 mW is input from Class A. The simulated results are in Table 5.9 below for comparison.

**Table 5.9: Simulation Results of Best Design in Lab**

<b>P<sub>in</sub> (mW)</b>	<b>I<sub>D</sub> (A)</b>	<b>P<sub>out</sub> (W)</b>	<b>η<sub>d</sub> (%)</b>	<b>G (dB)</b>
0.331	0.256	4.119	71.587	10.95
0.440	0.262	4.306	73.029	9.906
0.502	0.265	4.380	73.456	9.407

Comparing Table 5.9 with Table 5.8, the simulation results have higher DC drain current hence output powers are also higher, so are power gain and drain efficiencies. The waveforms from both simulation and testing are listed in Figure 5.14 to 5.16.

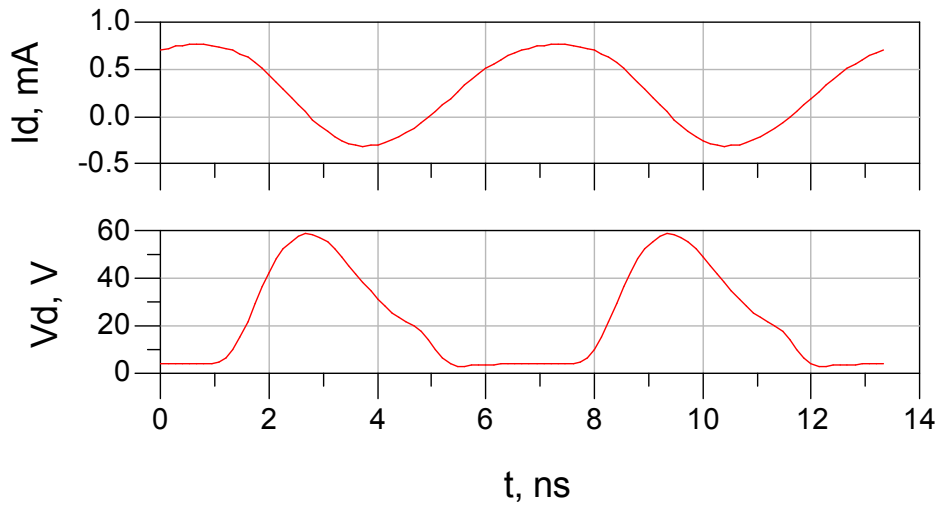


Figure 5.14: Drain Current and Voltage Waveforms of Best Design for  $P_{in} = 0.44$  W

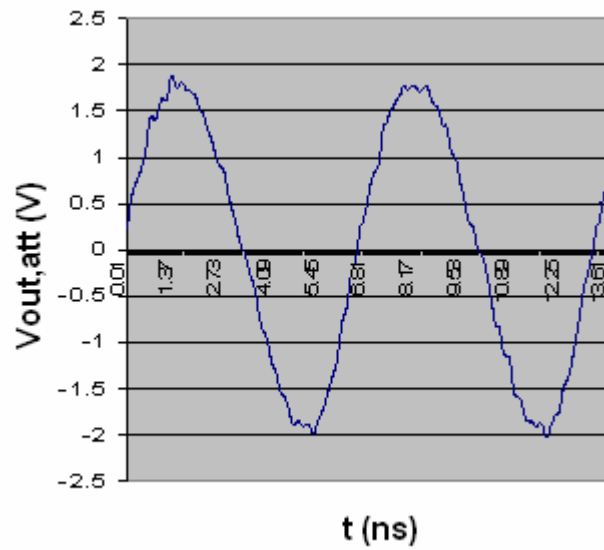
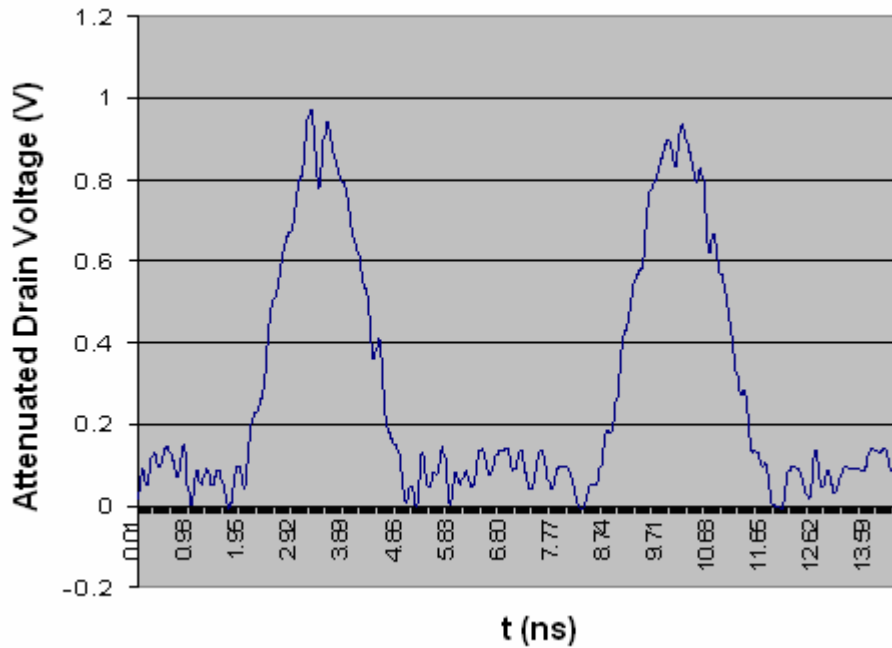
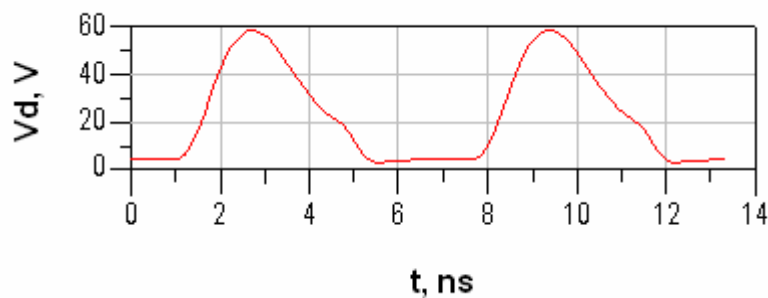


Figure 5.15: Output Voltage Waveform of 20 dB 50 W Attenuator for Best Design at 150 MHz



**Figure 5.16: Drain Voltage Waveform for Best Design after Attenuation at 150 MHz**

Figure 5.15 shows the designed power amplifier using the linear method outputs a sinusoidal signal at the operating frequency 150 MHz. Figure 5.17 indicates that the drain voltage waveform is almost a half sinusoid similar to the theoretical shape in Figure 5.14 from ADS simulation. These two approve that the amplifier designed is of Class E type.



**Figure 5.17: Simulated Drain Voltage Waveform for Best Design at 150 MHz**

Figure 5.17 is the drain waveform for the best design at 150 MHz from the

ADS simulation. Its peak value is around 58 V, which is only about 0.97 V in Figure 5.16. This is because a 30 dB 50 W attenuator is employed for the measurement. Thus, 0.97 V corresponds to 43.4 V, which is the peak for the drain waveform of the actual design. The lower peak value is tightly related to the lower drain DC power due to smaller drain current than theoretical design in ADS.

The efficiencies of 10 MHz linear and nonlinear designs can not be boosted because no surface mount RF inductors in size of 1812 whose ESR values at 10 MHz are lower than 5  $\Omega$  can be found. Similarly, since the nonlinear 150 MHz design also requires an inductor close to 1  $\mu$ H for  $L_O$  in the series resonant circuit, there is no improvement for the efficiencies and output power. For surface mount RF inductors from Coilcraft with values close to 1 $\mu$ H, the ESR is more than 15  $\Omega$  at 150 MHz, drawing a significant amount of power which is supposed to go to the 50  $\Omega$  load. For example, the 1 $\mu$ H inductor of 1008HT series has a DCR of 2.8  $\Omega$  and ESR of 16.3  $\Omega$  at 150 MHz.

## **5.6 Power Loss Mechanism Analysis**

Comparing the simulation results and the measurements for the best design in Section 5.5, the latter has lower efficiencies, power gain, drain DC current, drain DC power, and output power. In fact, all these parameters are related in such a way that for fixed input power of the amplifier, lower DC power will result in lower output power, which in turns cause lower power gain and efficiencies. Even with the simulation results, the drain efficiency is only 72.95 %, lower than the

initial design in Table 3.3 in Chapter 3, which has only ideal circuit components.

Power loss in the device is causing those differences.

Power loss prevents the efficiency of the amplifier less than 100 % since not all of DC supply powers as well as the input power are delivered to the load. There are four major power loss sources associated with Class E amplifiers design. They are losses from transistor, lumped circuit elements, unwanted harmonics, and DC power supply path.

### 5.6.1 Losses from Transistor

The majority part of power loss in a Class E PA design is due to the active device, i.e., the MRF134 transistor in this thesis work. There are two major loss mechanisms on the transistor.

#### a) On Resistance Power Loss ( $R_{on}$ )

Theoretically, the drain current,  $I_D$ , remains constant with the increase in  $V_{DS}$  during the saturation of a MOSFET, causing the slope of the waveform to be zero as in Figure 3.5. This rarely happens in practice; in fact,  $I_D$  changes with  $V_{DS}$  in saturation region, resulting in a constant resistance, which dissipates power when  $I_D$  is flowing through it, altering the slope slightly. This is the Channel Length Modulation of MOSFET transistor addressed in Chapter 3. We call this resistance as on resistance and denote using  $R_{on}$ .

$$R_{on} = \frac{\Delta V_{DS}}{\Delta I_D} \quad (5.8)$$

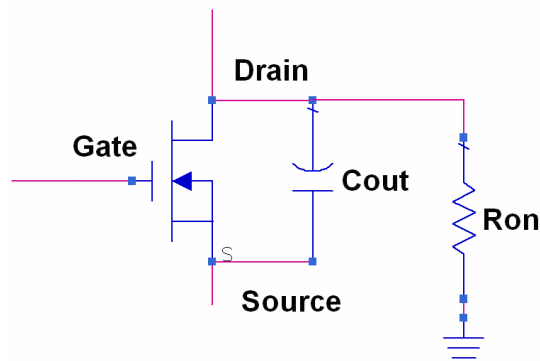


**Figure 5.18: Output Capacitance and On Resistance of a MOSFET Transistor**

According to Equation 5.8,  $R_{on}$  is infinite in ideal case; thus, it will appear as an open circuit.

For MRF134 transistor, its DC-IV curves are shown in Figure 3.4, which indicates that the value of  $R_{on}$  is also very big, hence, the power loss in the device due to the on resistance is very small and can be neglected.

#### b) Switching Loss

As frequency increases, the switch behavior will deviate from the ideal one more and more so that the time needed for switching from NO to OFF state and vice versa becomes greater. Hence, the transition intervals become longer so that the drain current and voltage waveforms start smearing out, especially the current waveform which will change toward a sinusoid with more portion going below zero. The changes associated with the waveforms will bring power dissipations in the transistor; therefore, reducing the efficiencies and output power.

Three points in the class E design are aimed to avoid the loss on the transistor:

- i) Simultaneous drain voltage and current are avoided

- ii) Using a shunt capacitor to hold the drain voltage at zero during the ON to OFF transition of the switch
- iii) The resonant load network plus the excess inductance and the load resistant are designed such that they allow the drain voltage to fall to zero right before the OFF to ON transition.

However, even when the circuit components are lossless, i.e., ideal, there will still be loss due to the discharge of the drain shunt capacitance at the instant the switch turns ON. The discharge can cause the coexistence of substantial drain voltage and current at the OFF to ON transition to induce power dissipation as shown in Figure 5.14. This energy loss can be eliminated or reduced by properly designing and selecting of  $C_{shunt}$ , which must be discharged fully before the switch can be turned ON. .

Also in Figure 5.14, the power loss for the coexistence of drain voltage and current at the ON to OFF transition is more than OFF to ON. This causes the biggest portion of power loss in the designs in this thesis work.

### **5.6.2 Losses from Circuit Lumped Elements**

Lumped circuit elements are lossy, especially inductors with high ESRs. The loss can be reduced by using high Q (unloaded quality factor) components, which in general have lower loss than those with low Q.

High loaded  $Q_L$  is required for series resonant network to make sure that the output current of the amplifier is sinusoidal at the operating frequency. However,

the resonant network with a high  $Q_L$  demands a large inductor, which is often not practical. In addition, large inductor has ESR, which is the winding resistance resulting from the metal wire forming the coils and frequency-dependent as addressed in Section 5.4 of this chapter with the problems it causes to the designs. When current is flowing through the inductor, power is dissipated in the form of heat by the resistance, inducing a loss of inductive quality. How big this loss will be for a specific operating frequency, or, how efficient the inductor's performance will be, depends on its unloaded quality factor,  $Q$ , which is the ratio of inductor's reactance at that frequency to its series resistance as

$$Q = \frac{2\pi f_o L}{ESR} \quad (5.9)$$

As revealed by Equation 5.9, for fixed  $f_o$  and  $L$  values, the higher the  $Q$  factor of an inductor is, the smaller ESR value will be and the more efficient the inductor can perform, and the less loss it will have when current is through and hence, the closer it approaches the ideal behavior.

In class E operation, even though the series resistance of the inductor in the series resonant network can be combined into the load resistance, they form a voltage divider so that the power at the actually load at the output is reduced; correspondingly, the efficiency is reduced. Furthermore, high  $Q_L$  implies a smaller 3-dB operation bandwidth for the desired performance as indicated by the Equation 5.10.

$$Q_L = \frac{f_o}{BW} \quad (5.10)$$

Where, BW is the 3-dB bandwidth. Thus, there is a tradeoff between efficiency and bandwidth.

Even though the best design cases in Section 5.5 have low DCR and ESR inductors, there are still losses from those parasitic resistances that can not be eliminated totally, which account as the secondary power loss mechanism occurring in this thesis work.

### **5.6.3 Losses from Unwanted Harmonics**

In practice, the quality factor (loaded  $Q_L$ ) of the series resonant circuit is below 10. This can not provide sufficient harmonic suppressions, especially for the attenuation of the 2<sup>nd</sup> harmonic, which is the largest harmonic in Class E. Thus, there will be power loss in undesired harmonics if no remedy is made. This associated loss can be minimized by adding series LC tank circuits, which are resonant at the desired harmonic frequencies being eliminated, in parallel with the output load.

The design in this thesis has already included the tank circuit for 2<sup>nd</sup> and 3<sup>rd</sup> harmonic suppressions so that 45 dB attenuation and more are realized for all harmonics. Thus, there is no loss from this category in the designs having been done and tested.

#### **5.6.4 Losses from DC Power Supply**

The actual RF chokes used in this thesis are not ideal at all; they all have non-zero DCRs. When DC current flows through them, power also is dissipated. Obvious, the best way to minimize this loss is to use RF chocks with small values of DCRs. There is a small portion of power loss in this thesis work that is due to non-zero DCR chokes.

## **Chapter 6: Conclusion**

### **6.1 Conclusion**

A Class E RF Power Amplifier prototype is designed and implemented. Two design methods, linear and nonlinear, are studied and 17 and 15 theoretical design cases for each method, respectively, with operating frequency up to 150 MHz are simulated in ADS. All of them have drain efficiencies greater than 77.5%, power-added efficiencies no less than 71%, and input-output power gain more than 10 dB.

Three cases of design, 10 MHz linear, 150 MHz linear and nonlinear are implemented at lab using MRF134 transistor from Motorola. Only the 150 MHz linear design with an actual size 2.9 in X 1.6 in gives the best results, which has 65.31% of drain efficiency and 10.09 dB of power gain with a 0.331 W input power. In addition, the highest drain efficiency observed is 69.55% with the same design when 0.502 W of power is input. The measurements are close to simulation results except the DC drain current observed is lower, which brings in lower  $\eta_d$ ,  $P_{DC}$ ,  $P_{out}$  and G. The other two designs do not realize desired performance and the possible reasons are explained.

In conclusion, the Class E RF power amplifier prototype designed and implemented is functioning desirably and has met the design purposes: small size but high efficiency.

### **6.2 Future Work**

The prototype has been tested extensively in the laboratory with a preceding

Class A power amplifier but still requires testing with other RF devices both preceding and following it, such as another power amplifier or filters, to check how it will function when used inside a system.

It should be noticed that the coexistence of the substantial drain voltage and current at the ON to OFF transition as described in Chapter 5 dissipates the most power in the transistor, resulting in the biggest power loss mechanism on this thesis work. The possible causes for this coexistence have not been found and there are few articles addressing this problem currently. In addition, as frequency increases, the drain current waveform goes below zero level, and the negative current portion becomes bigger and bigger as  $f_0$  goes up more and more. Also, there is no work done to explain this phenomenon. The assumption that it is one property associated with Class E RF power amplifiers has been made in this thesis but no verification has been given. In the future, efforts must be devoted to solve these two questions.

## Bibliography

- [1] Jeon, Sanggeun, Design and stability analysis techniques for switching-mode nonlinear circuits: power amplifiers and oscillators, Ph.D. Dissertation, California Institute of Technology, 2006.
- [2] Sedra, S. Adel and Smith, C. Kenneth, Microelectronic Circuits 4th ed., Oxford University Press, Oxford, NY, 1998.
- [3] F. Rabb, P. Asbeck, S. Cripps, P. Kenington, Z. Popovich, N. Pothecary, J. Sevic, and N. Sokal, RF and microwave power amplifier and transmitter technologies – part 2, High Frequency Electronics, May 2003.
- [4] Sokal, Nathan, Class E RF power amplifiers, QEX, pp. 9-20, Jan/Feb 2001.
- [5] Tsai, King-Chun and Gray, R. Paul, A 1.9GHz 1W CMOS class E power amplifier for wireless communications, Department of Electrical Engineering and Computer Science, The University of California, Berkeley, 1999.
- [6] Raab, H. Frederick, Suboptimum operation of class-E RF power amplifiers, in Proc. RF Technology Expo '89, Santa Clara, CA, Feb. 14-16, 1989, pp. 85-98.
- [7] Brown, Louis, Fundamentals of RF power amplifier design, in CReSIS Presentation, The University of Kansas, Lawrence, KS, June, 2005.
- [8] <http://download.siliconexpert.com/pdfs/transistor/mot/mrf134.pdf>
- [9] Albulet, Mihai, RF Power Amplifier, Scitech Pub Inc, Raleigh, NC, 2001.
- [10] Chudobiak, MJ, The use of parasitic nonlinear capacitors in class E amplifiers, IEEE Trans. Circuits Syst I, Fundam. Theory Appl, vol. 41, no.12,

pp.941-944, Dec. 1994.

- [11] Suetsugu, Tadashi and Kazimierczuk, K. Marian, Comparison of Class-E amplifier with nonlinear and linear shunt capacitance, IEEE Trans. Circuits Syst I, Fundam. Theory Appl, vol. 50, no.8, pp.1089-1097, Aug. 2003.
- [12] C. Fager, J.C. Pedro, N.B. de Carvalho and H. Zirath, Prediction of IMD in LDMOS transistor amplifiers using a new large-signal model, IEEE Trans. Micro Theory Tech, vol.50, no.12, pp.2834-2842, Dec. 2002.
- [13] [http://www.coilcraft.com/pdfs/spice\\_1008ht.pdf](http://www.coilcraft.com/pdfs/spice_1008ht.pdf)
- [14] [http://www.coilcraft.com/pdfs/spice\\_1812fs.pdf](http://www.coilcraft.com/pdfs/spice_1812fs.pdf)

## Appendix

### A.1 Drain Current & Voltage Waveforms of 17 Linear Designs in ADS before Circuit Optimization

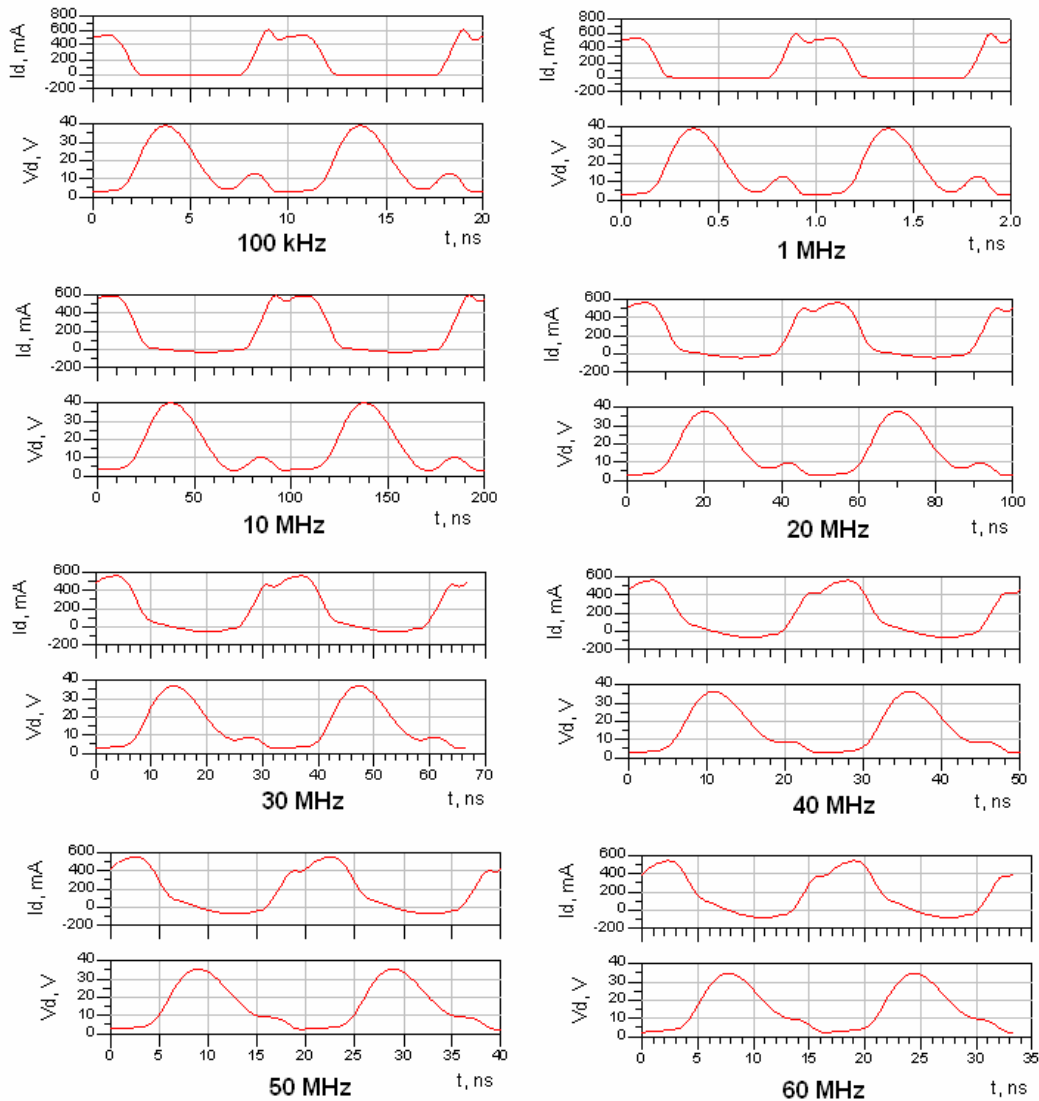


**Figure A.1.1: Drain Current & Voltage Waveforms of Linear Designs before Circuit Optimization for  $f_0$  Values of 100 kHz, 1 MHz, 10 MHz, 20 MHz, 30 MHz, 40 MHz, 50 MHz and 60 MHz.**

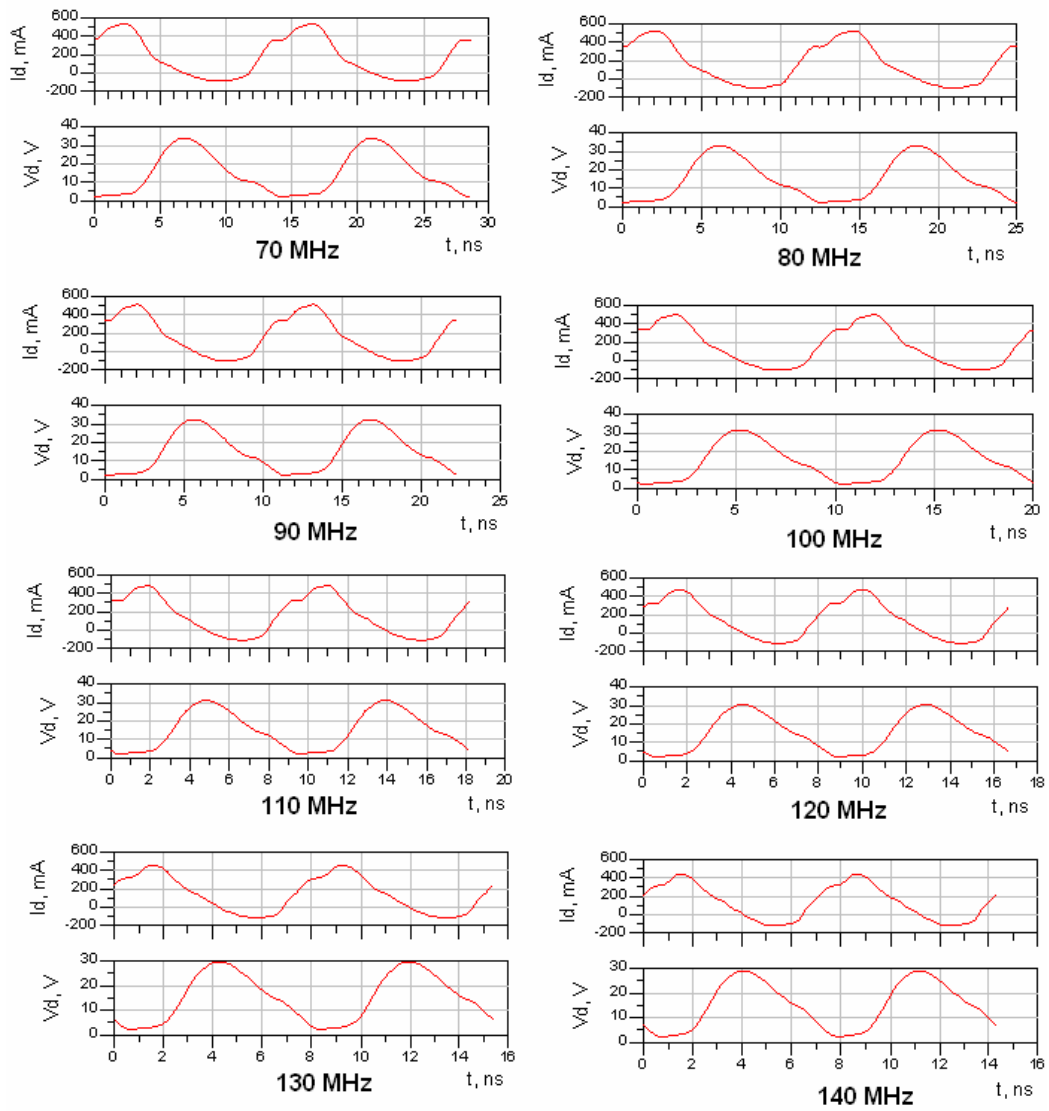


**Figure A.1.2: Drain Current & Voltage Waveforms of Linear Designs before Circuit Optimization for  $f_0$  Values of 70 MHz, 80 MHz, 90 MHz, 100 MHz, 110 MHz, 120 MHz, 130 MHz and 140 MHz.**

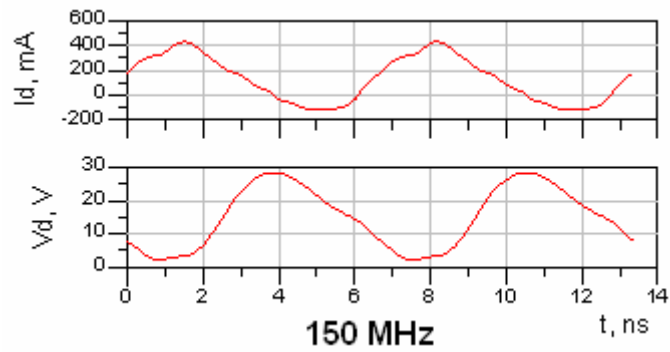


**Figure A.1.3: Drain Current & Voltage Waveforms of Linear Design before Circuit Optimization for  $f_0 = 150$  MHz**

## A.2 Drain Current & Voltage Waveforms of 17 Linear Designs in ADS after Circuit Optimization

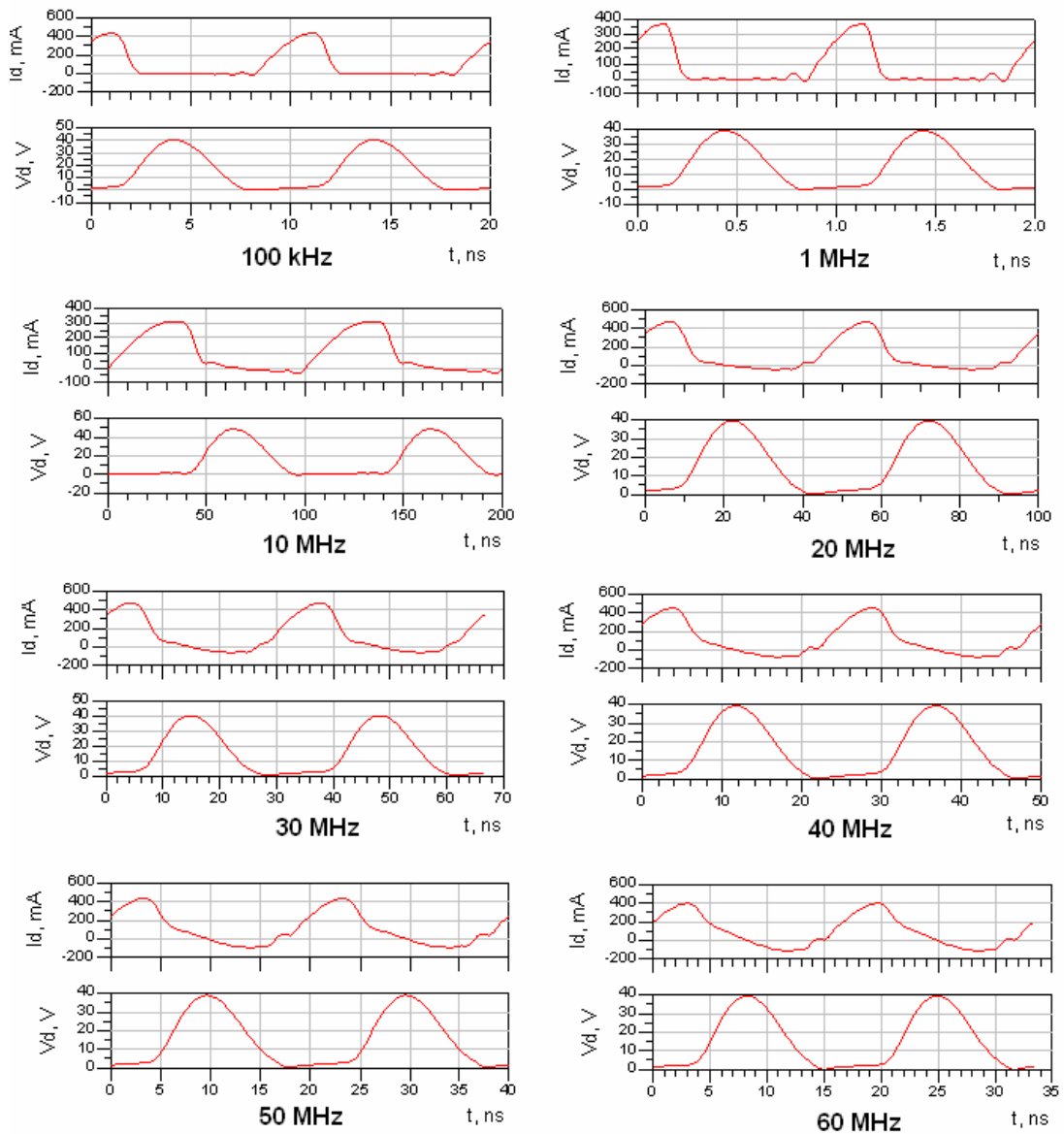


**Figure A.2.1: Drain Current & Voltage Waveforms of Linear Designs after Circuit Optimization for  $f_0$  Values of 100 kHz, 1 MHz, 10 MHz, 20 MHz, 30 MHz, 40 MHz, 50 MHz and 60 MHz.**

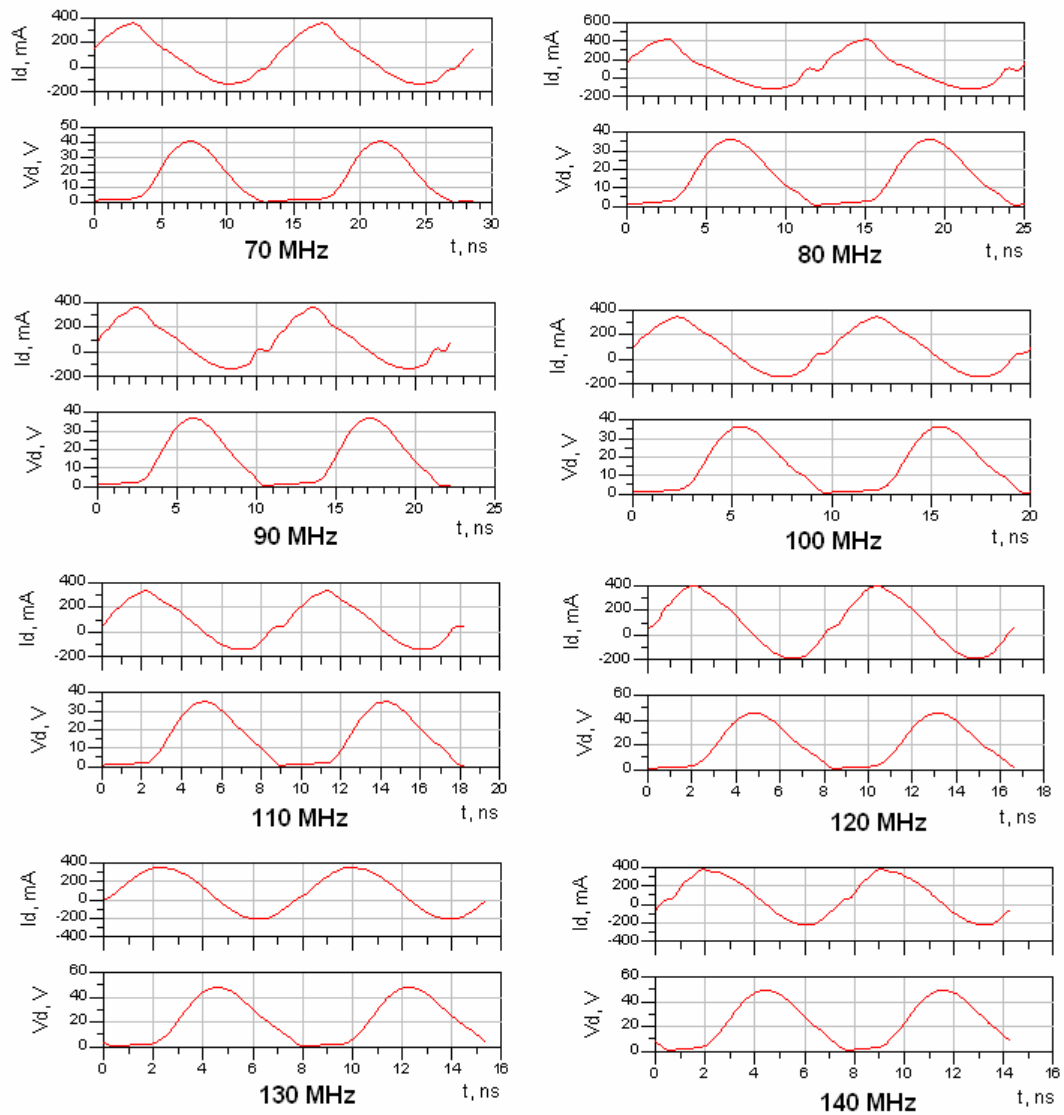


**Figure A.2.2: Drain Current & Voltage Waveforms of Linear Designs after Circuit Optimization for  $f_0$  Values of 70 MHz, 80 MHz, 90 MHz, 100 MHz, 110 MHz, 120 MHz, 130 MHz and 140 MHz.**

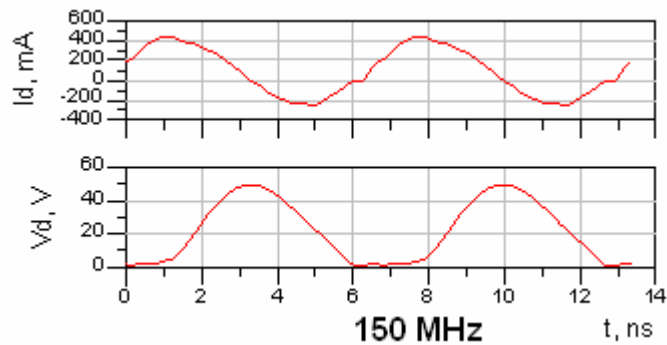


**Figure A.2.3: Drain Current & Voltage Waveforms of Linear Design after Circuit Optimization for  $f_0 = 150$  MHz**

### A.3 Drain Current & Voltage Waveforms of 15 Nonlinear Designs in ADS after Circuit Optimization

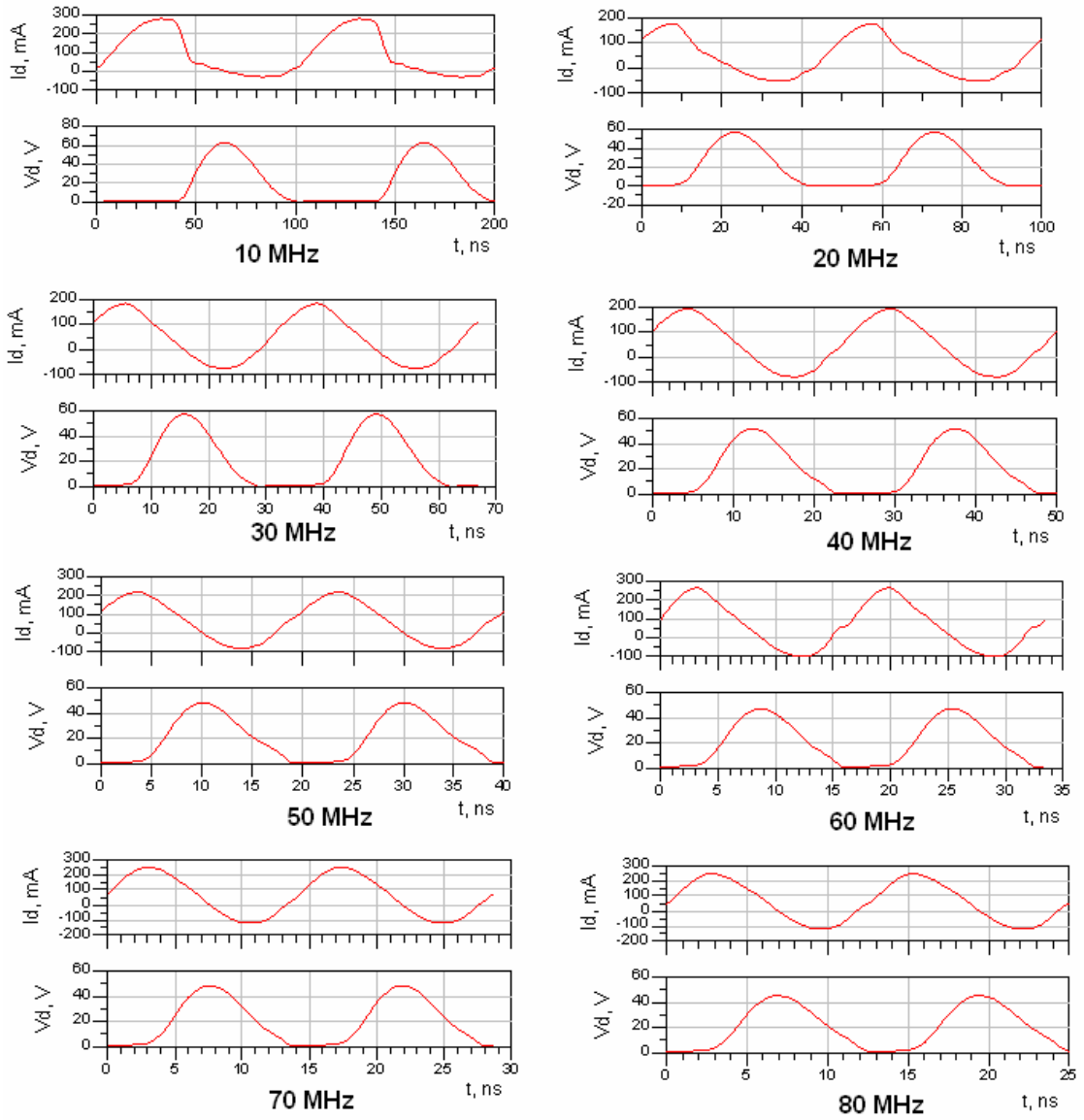


**Figure A.3.1: Drain Current & Voltage Waveforms of Nonlinear Designs after Circuit Optimization for  $f_0$  Values of 10 MHz, 20 MHz, 30 MHz, 40 MHz, 50 MHz, 60 MHz, 70 MHz and 80 MHz.**

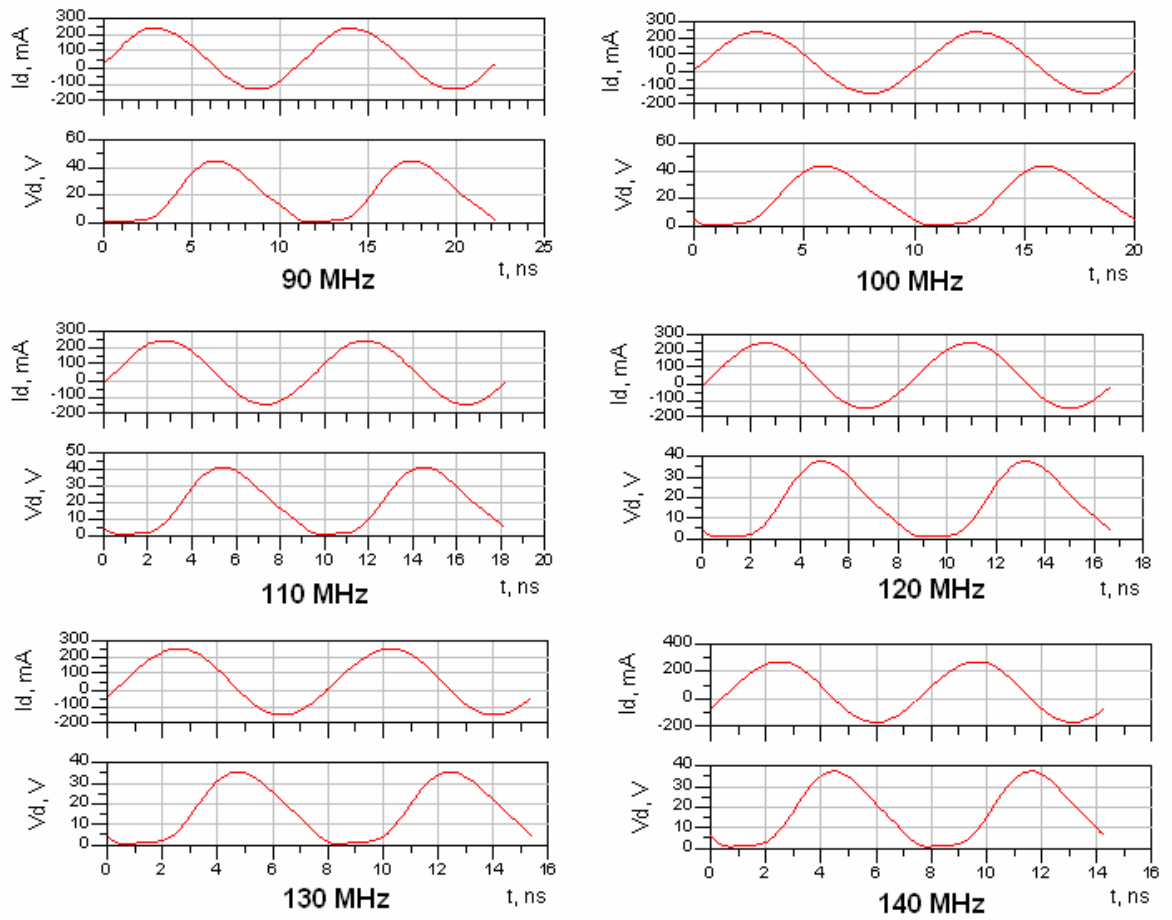


**Figure A.3.2: Drain Current & Voltage Waveforms of Nonlinear Designs after Circuit Optimization for  $f_0$  Values of 90 MHz, 100 MHz, 110 MHz, 120 MHz, 130 MHz, and 140 MHz.**

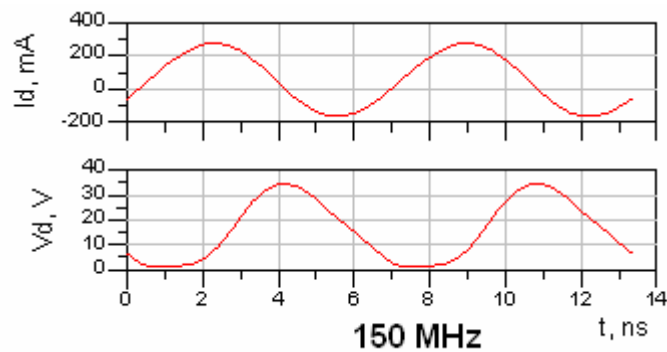


**Figure A.3.3: Drain Current & Voltage Waveforms of Nonlinear Designs after Circuit Optimization for  $f_0 = 150$  MHz**

## A.4 Matlab Codes for Circuit Element Calculations Using Linear Method

```
% Spring 2007

clc;
clear;

fo= 10e6 % operating frequency in MHz
Pout = 5 % desired output power in Watts
QL = 5 % loaded quality factor of CoLo series resonant circuit
L1 = 18e-6 % L1 is the value for RF chocks used in both gate bias
          % and drain dc supply, in micro Henry
VDD = 15 % drain dc supply voltage in Volts

RL = (VDD^2/Pout)*0.576801*(1.001245-0.451759/QL-0.402444/(QL^2))
% calculate the load resistance

Cshunt = (1/(34.2219*fo*RL))*(0.99866+0.91424/QL-
1.03175/(QL^2))+0.6/((2*pi*fo)^2*L1)
% calculate the drain shunt capacitance

Co = (1/(2*pi*fo*RL))*(1/(QL-0.104823))*(1.00121+1.01468/(QL-
1.7879))-0.2/((2*pi*fo)^2*L1)
% calculate the capacitance in CoLo series resonate circuit

Lo = QL*RL/(2*pi*fo)
% calculate the inductance in CoLo series resonate circuit
```

#### A.4 Matlab Codes for Circuit Element Calculations Using Nonlinear Method

```
clc;
clear;

fo = 10e6 % operating frequency in MHz
VDD = 15 % drain DC supply voltage in V
VGG = 3 % gate bias voltage in V
Pout = 5 % desired output in Watts
QL = 5 % loaded quality factor of CoLo series resonant circuit
Vbi = 0.7 % the built-in potential in Volts which typically ranges
        % from 0.5V to 0.9V
Pin = 0.1 % input power in Watts

wo = 2*pi*fo; % operating frequency in radian per second

RL = 8*VDD^2/(pi^2+4)/Pout % calculate the load resistance

C1_linear = 8/(pi*(pi^2+4)*wo*RL) % calculate the linear shunt C,

Cout = (0.0781+sqrt(0.0061+0.0239*VDD))*C1_linear % calculate the
        % equivalent linear shunt C

wCjoRL_top = 12*Vbi+sqrt(6*Vbi*(24*Vbi-
24*pi^2*VDD+pi^4*VDD)+9*pi^2*(pi^2+4)*Vbi*VDD);
wCjoRL_bottom = 3*pi*(pi^2+4)*Vbi;
wCjoRL = wCjoRL_top/wCjoRL_bottom

IDD = 8*VDD/(pi^2+4)*RL

phi_top = ((6*pi^2-48)*Vbi*wCjoRL+pi*IDD*RL)*2;
phi_bottom = 24*pi*Vbi*wCjoRL+(5*pi^2-32)*IDD*RL;
phi_aug = phi_top/phi_bottom;
phi = atan(phi_aug)

phy = -0.567;

X = RL*tan(phi-phy)

Lo = RL*QL/wo % calculate the inductance in series resonant
        % circuit
```

```
Co = 1/(wo*(RL*QL-X)) % calculate the capacitance in series
    % resonant circuit

RFC = 2*(pi^2/4+1)*RL/fo % calculate RF chocks used in both gate
    % bias and drain dc supply
```